TORQUE METERS BASED ON MAGNETIC-STRESS ANISOTROPY

bу

Rudolf J. Ionides, B.Sc.

A thesis submitted to the Faculty of Graduate Studies and Research in partial fulfilment of the requirements for the degree of Master of Engineering.

Department of Electrical Engineering,

McGill University,

Montreal, Quebec.

June, 1964.

ABSTRACT

A theory of operation, design recommendations and performance limits of torque meters, based on magnetic-stress anisotropy, have been established. The theory, based on considerations of total magnetic-crystal energy, successfully explains both the qualitative and quantitative behaviour of these devices. The theory has been checked and the design recommendations have been established by measurement of the behaviour of steel and nickel torque tubes of various wall thicknesses over a range of magnetizing force, frequency and stress. It has been established that sustained accuracies of better than 1% are readily obtained, the limit of accuracy being of the order of 0.1%. Such devices are simple, robust and have an output power sufficient to operate a meter directly.

ACKNOWLEDGEMENTS

The author wishes to record his sincere thanks to Dr. T.H. Barton who suggested the subject matter and provided invaluable guidance and encouragement throughout.

He wishes to extend his gratitude to the Professors and Graduate Students of the Department of Electrical Engineering for their valuable suggestions, to the technicians for their assistance in constructing the experimental apparatus and to the staff of the Computing Centre for their co-operation. Thanks are also due to Mrs. Peggy Hyland for the typing of this thesis.

The author is also indebted to the Canadian Universities
Foundation for the award of the Commonwealth Fellowship
(1962-1964) and to the National Research Council of Canada, whose
interest and financial support made this project possible.

TABLE OF CONTENTS

	Page
ABSTRACT	i
ACKNOWLEDGEMENTS	ii
TABLE OF CONTENTS	iii
CHAPTER I INTRODUCTION	1
CHAPTER II THE MAGNETIC-ANISOTROPY TORQUE METER	6
2.1 Introduction	6
2.2 Construction	6
2.3 Method of Excitation	9
2.4 Principle of Operation	10
CHAPTER III GENERAL SURVEY	. 12
3.1 Choice of Materials	12
3.2 Hysteresis Loop Characteristics	13
3.3 Transfer Characteristic	16
3.4 Output Signal Harmonics	18
3.5 Linearity and Hysteresis	18
3.6 Optimum Stress Level	23
3.7 Torque Tube Wall Thickness	24
3.8 Effect of Eddy Currents	24
3.9 Frequency of Excitation	25
3.10 Output Signal	30
3.11 Nickel-plated Brass Torque Tube	34
3.12 Re-annealing the Nickel Torque Tubes	34
3.13 Effect of Temperature	36
3.14 Locus of Output Signal Vector	36
3.15 Final Transfer Characteristic	36
3.16 Conclusions	42
CHAPTER IV THEORETICAL SURVEY	43
4.1 Domains	43
4.2 Stability of Domain Orientation	43
4.2.1 Crystal Anisotropy Energy	44
4.2.2 Magneto-elastic Energy	44

		Εf	fec	ti	ve	An	is	ot:	r 0	ру	, a	nd	M	a g	ne	to	8	tr	ic	ti	. 01	n	٠, •	45
		St	res	8	Ene	erg	У	•	• •				٠.	٠.			• •				•			45
4.	2.3	Ма	gne	to	sta	ati	c	En	er	8у	•						• •			٠.	•	• •		47
		Dе	mag	ne	t .i.2	in	g	En	er	gу							• •		٠.				•. •	47
		Fí	e1d	E	neı	еду	,			٠.												٠.		47
4.3	Anisc	tr	ору	a	n d	Ma	gn	et	o s	tr	ic	ti	on.	C	on	st	tai	a t	8					48
4.4	Polyc	ry	s t a	11	ine	e M	at	er:	Ĺа	1 s										٠.				49
CHAPTE	R V	T	HEO	RE	T,I (CAL	A	NA]	LY	SI	S	OF	T	ΗE	r	101	RQτ	JΕ	M	ET	E	R		51
5.1	Intro	du	cti	on				• •																51
5.2	Steel	T	or q	ue	Me	te	r															٠.		52
5.3	Cryst	a1	Or	ie	nta	ati	on										• •							61
5.4	Effec	t	o f	Te	mpe	ra	tu	re		٠.												••		63
5.5	Nicke	1	Tor	qu	e l	le t	er	,									• • •							66
5.6	Cryst	a1	Or	ie	nta	ati	on													•. •				74
5.7	Effec	t	οf	Te	mpe	era	tu	re	•								• •					٠.		7 5
5.8	Nicke	1	at	Te	mpe	ra	tu	re	3	80	-1	00	°c						• •		. •			7 5
5.9	Nicke	1	at	Te	mpe	ra	tu	re	3	ab	ov	e	10	o°	c		• •		• •		•	٠.		78
5.10	Corre	1 a	tio	n	o f	Th	еo	rу	w	i t	h	Εx	рe	ri	m e	nt	=	. •	• •		•			78
5.11	Concl	us	ion	8				• •	•												•			80
CHAPTE	R VI	P	RE C	IS	ION	M	EA	SUI	RE:	ME	ΝI	'S					• •	• •	• •					84
6.1	Intro	du	cti	on				• • •													•			84
6.2	Facto	rs	Af	f.e	cti	lng	P	er	Εo	rn	an	ce	:						• •					8 5
6.	2.1	Eχ	cit	at	ior	ı L	ev	e 1										• •	• •			• •		8 5
6.	2.2	Te	mpe	ra	tui	e		• • •									• •							87
6.	2.3	Lo	ad	Re	sis	ta	n c	e	•													• •		87
6.3	Stabi	11	tу	οf	No	rm	a1	Cl	ı a	r a	ct	er	is	ti	cs	3	•					• •		87
6.4	Repro	du	cib	11:	ity	7 a	n d	L	l n	e a	ri	tу	,					• •	• •		•	• •		89
6.	4.1	Po	ssi	ъ1	e S	ou	rc	e s	0	£	Er	ro	r									• •		92
6.5	Conc 1	us	ion	s		•. •		• • •							٠.			• •			•			93
CHAPTE	R VII	C	ONC	LU	SIC	NS		• • •		• •								• •			•		• •	94
CHAPTE	R VII	I.	APP	EN	DIX		DE	SCI	RI	PΤ	IO	N	OF	E	Qυ	II	ME	N2	r	•			• •	96
8.1	Beam	Ar	ran	ge	mer	t	•											• •		•. •	•	٠.		96
8.2	Weigh	t-	pos	it	ior	ı D	e t	ect	0	r	•													98

8	.2.1	Photocell Arrangement 9	9
		Calibration 9	9
8	.2.2	Digital-to-analogue Converter 10	1
		Calibration	1
8.3	Phase	-shifting Network 10	4
8.4	Phase	-sensitive Detector	4
8	.4.1	Effect of Harmonics	8
8	.4.2	Calibration of Detector	0
8	.4.3	Suggestions for Future Work	2
APPENI	DIX A	AUXILIARY EQUIPMENT	3
APPENI	DIX B	THEORETICAL ANALYSIS OF STEEL TORQUE METER. 11	4
APPENI	DIX C	THEORETICAL ANALYSIS OF NICKEL TORQUE METER. 11	7
		Temperature of Specimen below 80°C 11	7
		Temperature of Specimen between 80100°C 12	0
		Temperature of Specimen above $100^{\circ}C$ 12	2
APPENI	DIX D	FORTRAN COMPUTER PROGRAM FOR EVALUATING	
		THE AXIAL INDUCTION 12	3
REFERI	ENCES		8

CHAPTER I

INTRODUCTION

Many ingenious devices have been used to measure the torque transmitted by the shaft of a rotating machine, varying from dynamometers, of the absorption and transmission type, to gauges involving the direct measurement of stress or strain in a section of the shaft.

Absorption dynamometers are generally used as brakes and absorb the total power delivered by the machine being tested. The Prony brake is the most common type, in which the torque developed by the machine to overcome friction is determined by the product of the force preventing rotation of the brake and the lever arm.

Transmission dynamometers can be subdivided into torsion and cradle dynamometers. Torsion dynamometers, involving the measurement of the torsion over a certain shaft length, have among other things the disadvantage of requiring a fairly long measuring length. Slip rings are also necessary in certain designs, thus limiting the sensitivity of the device.

The cradle type dynamometer, generally used in laboratories, presents a convenient method of measuring torque. The dynamometer in this sense, is a machine having a stator and a rotor. The rotor shaft is coupled to the shaft of the machine whose torque is to be measured, while the dynamometer stator is mounted on a bearing system. The stator delivers power to the rotor or receives power from it, and in so doing it tends to turn. This tendency of the stator to turn can be measured at a fixed lever arm distance from the center of rotation of the shaft. Hence the torque reaction between the dynamometer stator and rotor is determined and it is a measure of the dynamometer shaft torque.

This type of dynamometer suffers from low accuracy, mainly due to frictional forces in the bearings. The effect of friction can be minimized by using counter-rotating, pneumatic or hydraulic bearings and in cases where such devices have been employed, accuracies of better than 0.1% have been claimed by various experimenters 1,2,3.

Dynamometers are in general mechanical devices and as such their speed of response is extremely low, making them entirely unsuitable in detecting transient torques.

Torque-tables have recently been used to measure torque. In this type of transducer, hollow cylindrical springs are interposed between the stator of the machine and the solid base, together with magnetic reluctance gauges to detect the motion of the foot support with respect to the base mounting. Due to its elaborate construction, this type of transducer suffers from low accuracy, and it has been mainly used as a 5% torque meter for demonstration purposes.

An alternative to the torsion-gauges, previously mentioned, is the strain-gauge^{5,6} used to measure the strain of the shaft in a specified direction. In general, a set of four strain-gauges, placed around the shaft in the direction of the principal stresses and connected in a Wheatstone bridge arrangement, can be used to measure the strain in the shaft and as a result the torque transmitted through it.

Strain-gauges are preferred to any other type of transducer, due to the good linearity with low hysteresis of the output signal (better than 0.1% of full scale) and due to their ability to detect transient torques. However, they have certain serious limitations, namely, in overload capacity and output signal level. A 25% overload will affect the behaviour of the gauge, while a 50% overload will damage it beyond repair. It is, therefore, necessary to use gauges of higher load

capacity than is required, with consequent loss in accuracy and linearity. Furthermore, due to their low-level signal, (of the order of few millivolts), low-noise slip rings and amplification of the signal are necessary, thus increasing the cost of the device.

An entirely new method of measuring the stress in a shaft and hence the torque transmitted, is based upon the magnetostrictive properties of ferromagnetic materials, such as steel or nickel.

The Swedish company "ASEA", a decade ago, designed and manufactured the "Cross Torductor", the first magnetostrictive transducer of its kind . This simply consisted of two stationary windings mounted on two U-shaped, laminated iron cores, at right angles to each other in a measuring head, which is placed adjacent to the shaft with one core parallel to the axis of the shaft and with an air-gap of a few millimeters, between the shaft and the poles of the two iron cores. One core is magnetized with a.c., normally at 50 or 60 c/s, and induces a magnetic field in the shaft surface. Because of the symmetry, no flux passes through the other core, at zero stress. However, the magnetic potential pattern is distorted by torque, resulting in a proportionate flux in the secondary core. rate of change of this flux with the secondary coil produces an output signal, which, within certain limits, is proportional to the torque transmitted by the shaft.

The "Cross Torductor" was soon replaced by an improved version, the "Ring Torductor", both of which torductors, however, were speed dependent, (output signal varying by 25% over a range zero to 800 r.p.m.), a very undesirable feature, especially when this type of transducer is to be used for regulation purposes.

The American "WESTINGHOUSE" and the English "A.E.I" companies have also designed magnetostrictive torque meters, which were fitted on their "Generalised Machines".

The "WESTINGHOUSE" torque meter consists of a mild-steel hollow cylindrical tube, bearing two windings, a toroidal and a solenoidal winding, wound around the axis of the tube. When the hollow cylinder is twisted, the permeability of the specimen will increase in the direction of tension and decrease in the direction of compression by magnetostriction. Therefore, the flux which is parallel to the axis of the cylinder, as produced by the solenoidal winding, will find an easy direction along a 45° spiral path on the cylinder. If the solenoid is energized from an a.c. source, windings parallel to the axis of the cylinder will pick-up a voltage, which, for a small range of torques, can be assumed linear with applied torque. This type of torque meter requires slip rings for both windings, thus decreasing the sensitivity. It will read linearly over a range of +8 lb.ft. with an accuracy of 5%.

The "A.E.I" torque meter, operating on the same principle, disposes of a pair of slip rings by having a stationary pick-up coil; the accuracy of the device is 5%.

Although the "A.E.I" design appears to be quite satisfactory, it was hoped that by better scientific work on magnetostrictive torque meters and by the development of a theory explaining their operation, a precision torque meter could be developed.

This was achieved in this project by the development of a magnetic-anisotropy torque meter, being able to measure torque with an accuracy of better than 0.15%. Its output is in the form of an electrical signal (of the order of few volts), being able to operate directly an ordinary moving coil instrument

or a recorder. The linearity of the transfer characteristic is better than 0.1% for shear stresses up to 1.3 kg/mm² and does not exceed 0.3% of full scale for stresses up to 2.6 kg/mm². The hysteresis appearing in the output signal is well below 0.1% and variations in temperature, frequency and level of excitation, normally encountered in practice, do not seriously affect its sensitivity. The output signal is independent of the speed of rotation of the torque meter, as can be seen from its method of construction, so that calibration can be performed statically.

All these features of the transducer, together with its robustness, simplicity of construction and low cost, make the magnetic-anisotropy torque meter a very attractive proposition for measuring torque transmitted by a shaft.

CHAPTER II

THE MAGNETIC-ANISOTROPY TORQUE METER

2.1 Introduction

The purpose of this project was to investigate the behaviour of the magnetic-anisotropy torque meter under various conditions of operation and to develop a concrete theory explaining its performance. Under optimum conditions of operation, it was desirable to determine its limits of operation and hence decide on whether the torque meter could be used as a 0.1% precision measuring instrument, or as an industrial 1% torque transducer.

2.2 Construction

In its simplest form, the torque meter developed, consists of a cylindrical tube made of a magnetostrictive 9,10 material, such as steel or nickel, and two windings; a toroidal winding of 200 turns AWG23 HF insulated wire, hand-wound around the tube and acting as the magnetizing coil and a stationary axial solenoid, consisting of 300 turns of AWG32 wire and acting as the pick-up coil (Fig. 2-1).

The active length of the torque tube was arbitrarily chosen at 4" (Fig. 2-2), with two end rings, 1½" in length, each carrying eight slots for accommodating the magnetizing winding.

The interconnections of the coils in the slots were made inside the tube, and a one-turn axial coil, wound in a reverse direction, was inserted in the tube, thus nullifying the effect of the axial coil formed by the interconnecting wires. Any mutual coupling between magnetizing and pick-up coils was further minimized by the screening effect of eddy currents.

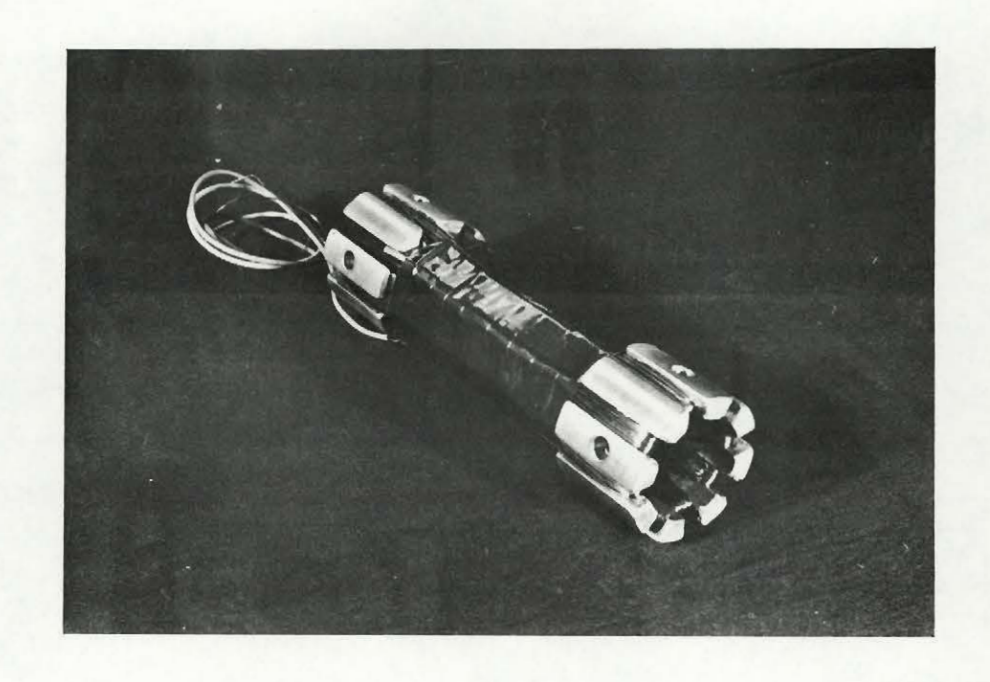


FIG. 2-1a. The torque tube and magnetizing coil.

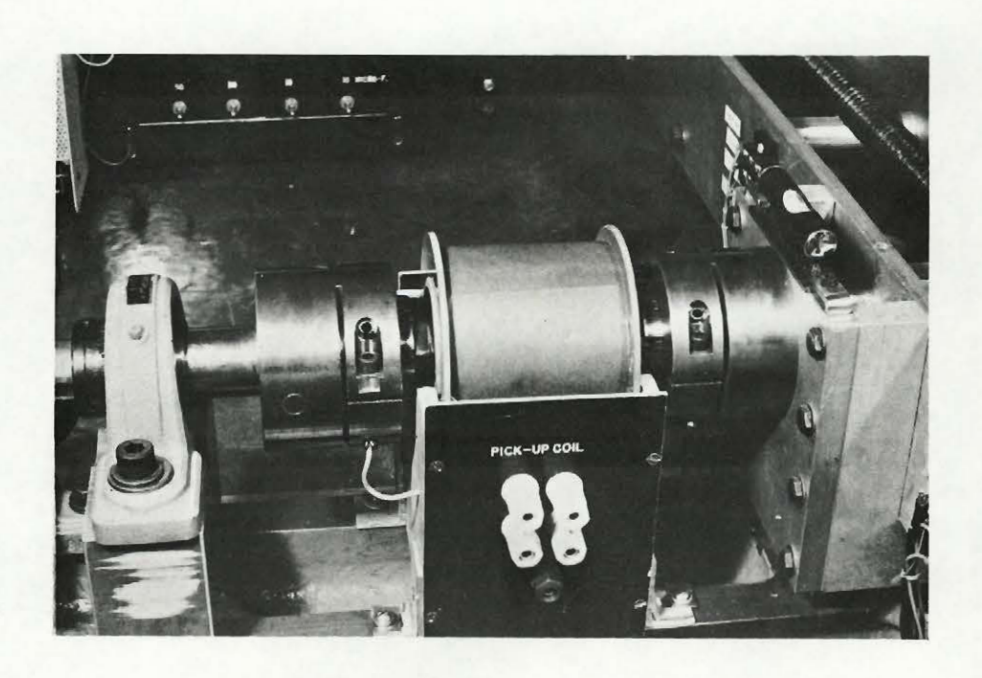


FIG. 2-1b. The torque tube coupled to the weighbeam.

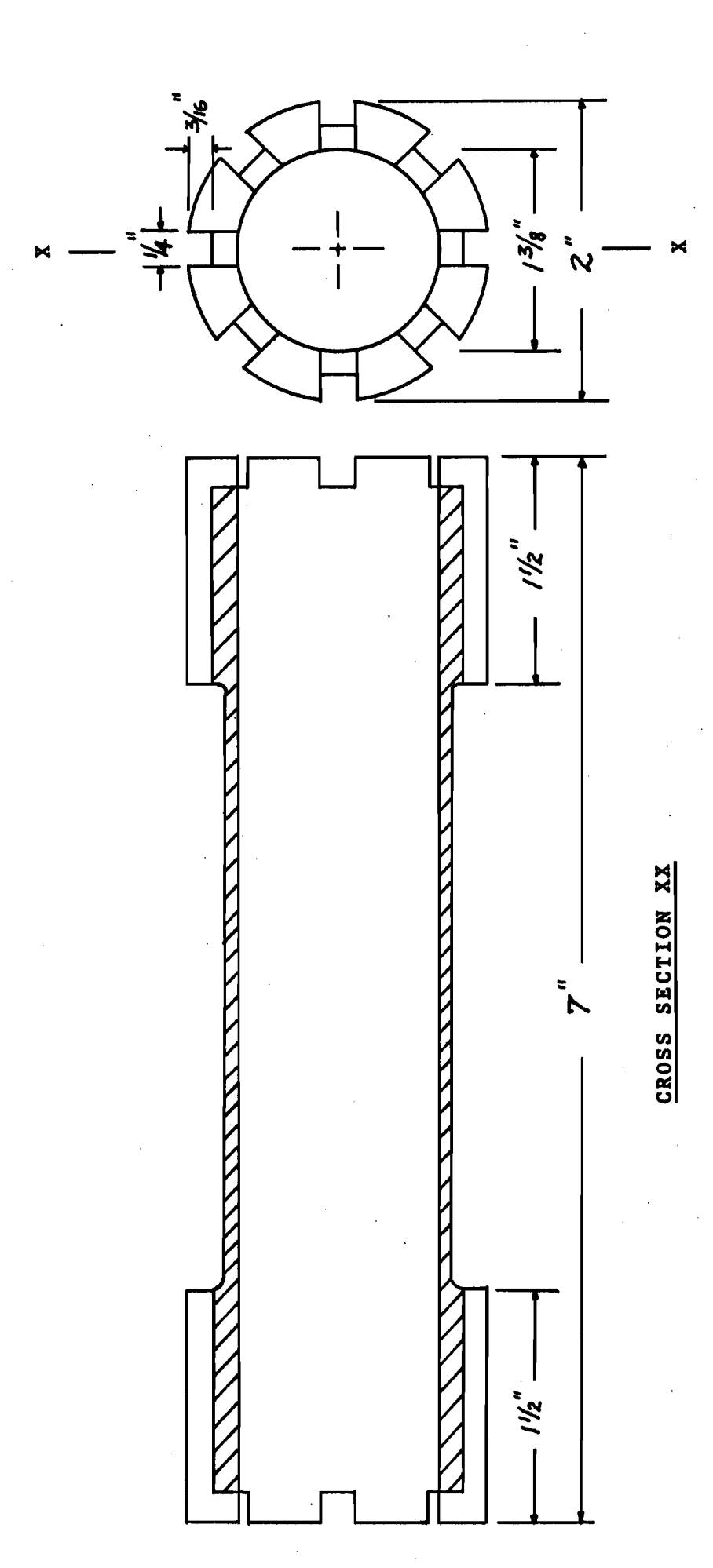


FIG. 2-2. The torque tube.

Since only a static calibration of the torque meter was necessary, no slip rings were fitted.

2.3 Method of Excitation

Two ways of exciting the torque meter were available; exciting tangentially and picking-up axially or exciting axially and picking-up tangentially.

After some preliminary investigation into the two possible methods, it was decided to adopt the first one, namely tangential excitation and axial pick-up. The main reasons that led the author to this decision were, first, simplicity in winding, there being no need for special low-noise slip rings, and, second, a high-permeability magnetic path in the excitation circuit.

There is no necessity for special low-noise slip rings for the magnetizing coil, which, at the same time, bears fewer turns than the pick-up coil, and, hence, can be more easily wound in a toroidal fashion around the torque tube.

The high-permeability path, provided by the torque tube circumference, makes it possible to achieve saturation of the material (a very desirable feature, as is seen in Chapter III), at a fairly low magnetizing field strength.

A slight drawback of the above method of excitation is the fact that the magnetic path for the resultant axial flux will vary with each particular set-up, thus necessitating on the spot calibration of the device. This can be avoided, however, by making the connections of torque meter to shaft by means of non-magnetic couplings, which results in fixing the magnetic path, provided that the induced eddy currents are kept low.

2.4 Principle of Operation

Although a more detailed analysis of its operation will be given at a later Chapter, a brief outline of its principle of operation is desirable at this stage.

Energizing the magnetizing winding from an a.c. source, say the 60 c/s mains, produces a magnetic field in the wall of the tube, its direction being tangential to the circumference at each point. As the two windings are magnetically at right angles, (this applies to the ideal case), there will be no mutual coupling and hence no e.m.f. will be induced in the pick-up coil.

Torque is now applied to the tube. This gives rise to the principal stresses at the 45° directions to the tube axis, a tensile stress, +6, in one 45° direction and a compressive stress, -6, in the other 45° direction, as shown in Fig. 2-3.

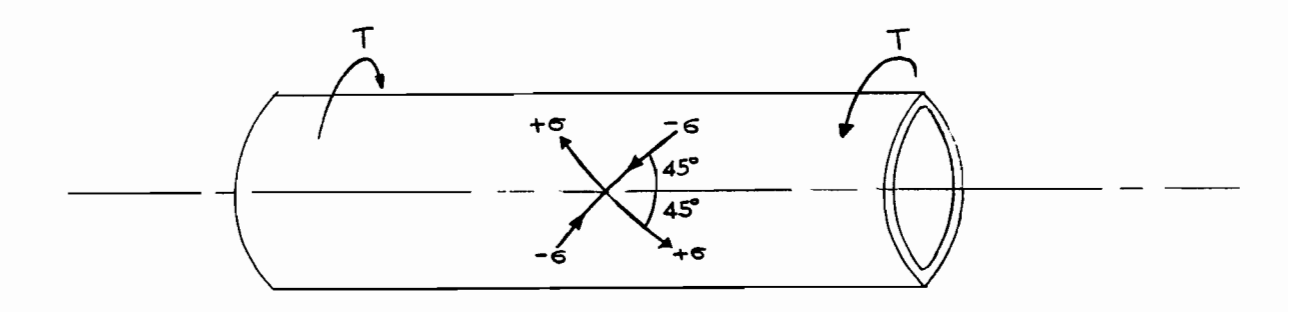


FIG. 2-3. Principal stresses, + 6, due to torque T.

Along the direction of tension the permeability 11 of the material will increase or decrease, depending on whether the material exhibits positive or negative magnetostriction

respectively. The opposite is true along the direction of compression. Thus, due to the magnetic-anisotropy caused by the stresses, a resultant flux, Φ_{α} , will appear along the axis of the torque tube, which, in turn, will induce an e.m.f. in the pick-up coil, given by

$$e = - N_p \frac{d \Phi_{\infty}}{dt} ,$$

 N_{p} being the number of turns of the pick-up coil.

The above relation indicates the dependence of the output signal on the following:

Level and frequency of excitation, Number of turns of pick-up coil, Applied torque T,

Construction and configuration of the torque meter.

Each of the above will be discussed in more detail in the next Chapter.

CHAPTER III

GENERAL SURVEY

A general survey was carried out in order to determine the factors affecting the behaviour of the torque meter and, hence, obtain the optimum conditions of operation. Choice of materials, frequency, level, method of excitation and temperature dependence were among the items investigated.

As it was desirable to obtain a great deal of information on the behaviour of the torque meters, without spending too much time and effort, the automatic plotting arrangement was adopted, thus limiting the accuracy of results to 0.5%, with a linearity of better than 0.1%.

Briefly, the signal from the pick-up coil was fed directly into the Y-amplifier of Moseley X-Y recorder, while the torque applied to the tube was determined by a position detector, whose output was fed into the X-amplifier of the recorder. A phase-sensitive detector was used in conjunction with the recorder, for plotting the locus of the output signal vector with reference to the magnetizing current. A detailed description of the equipment is given in Chapter VIII.

3.1 Choice of Materials

The availability of magnetostrictive materials in tubular form has limited the choice to:

- (i) Cold-drawn seamless steel
- (ii) Nickel "200" both in the annealed and stressrelieved state.

A number of torque tubes were carefully constructed. Their dimensions are given in Table 3-1.

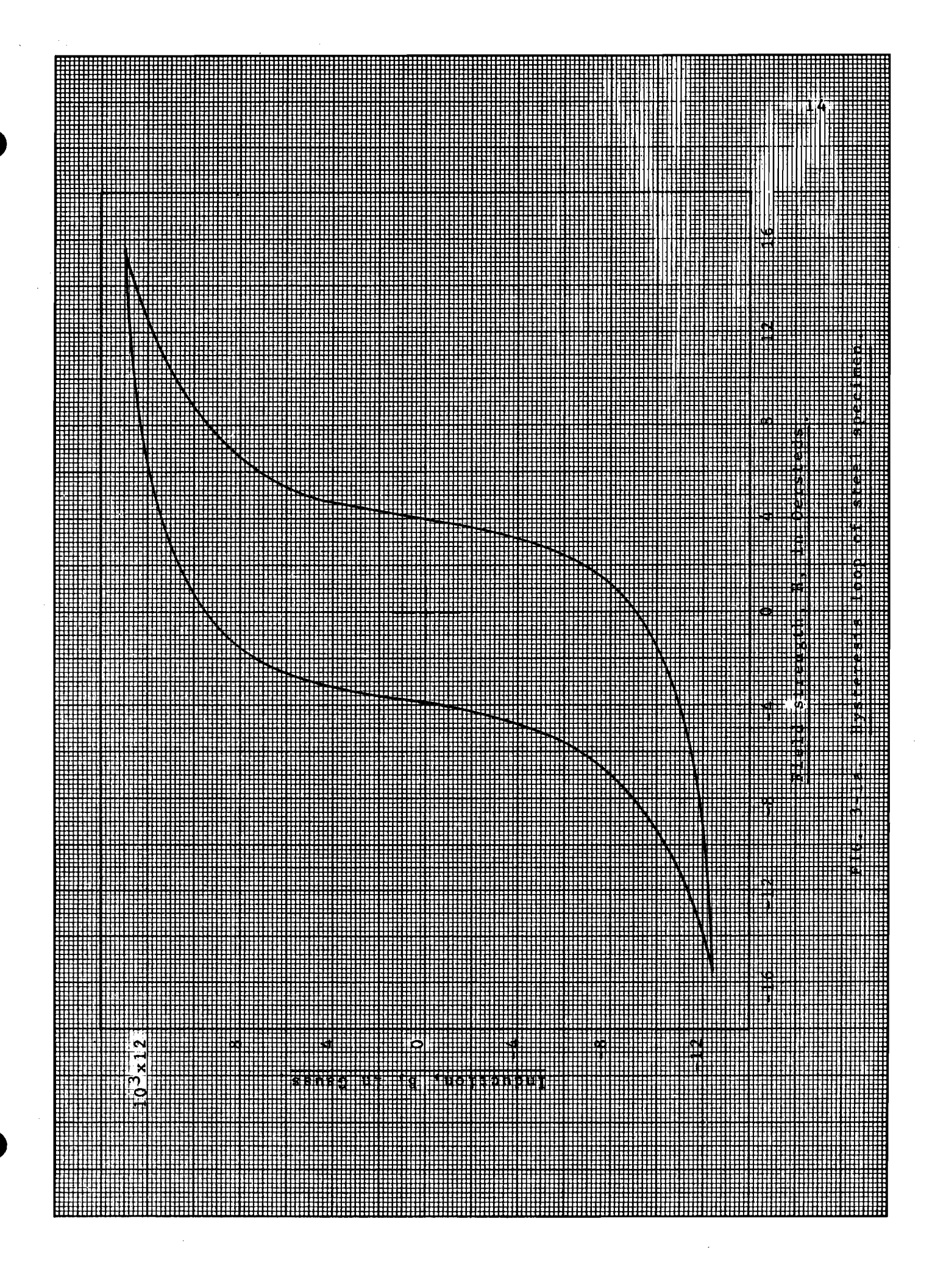
Material	Bore (Inches)	Wall thickness (Inches)
Stee1	1:3770 1.3770 1.3770	0:173 0.100 0.050
Nickel "200" Annealed	1.0535 1.0535	0.100 0.050
Nickel "200" Stress-relieved	1.1015	0.100 0.050

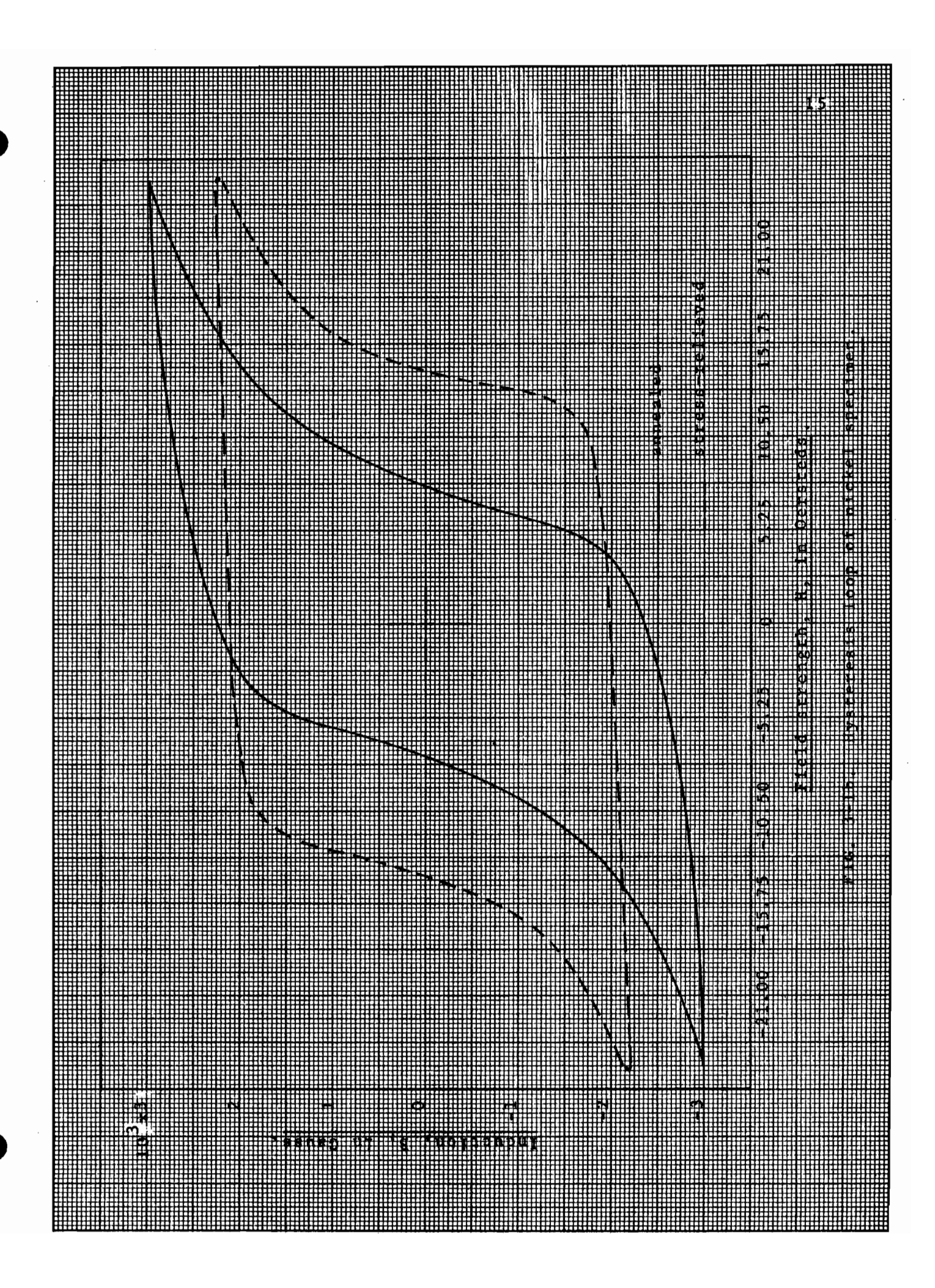
TABLE 3-1. Dimensions of torque tubes.

3.2 Hysteresis Loop Characteristics

As the magnetic characteristics of a material can vary with composition and heat treatment, it was found desirable to determine the B-H loop of the materials used in the construction of the torque tubes.

For this, specimen rings were fabricated and the usual toroidal windings were inserted. An amplidyne, driven by a Hewlett-Packard L.F. oscillator at 0.01 c/s (to minimize eddy currents), was used to excite the magnetizing coil, while the induced signal of the search coil was fed into a Philbrick operational amplifier, used as an integrator. Appropriate signals from the primary and secondary circuits were fed to the X- and Y-amplifiers of the recorder for automatic plotting of the hysteresis loops. These are shown in Fig. 3-1.





3.3 Transfer Characteristic

With the circuit set-up of Fig. 3-2, a typical transfer characteristic, i.e. output signal as a function of applied torque, was obtained (Fig. 3-3).

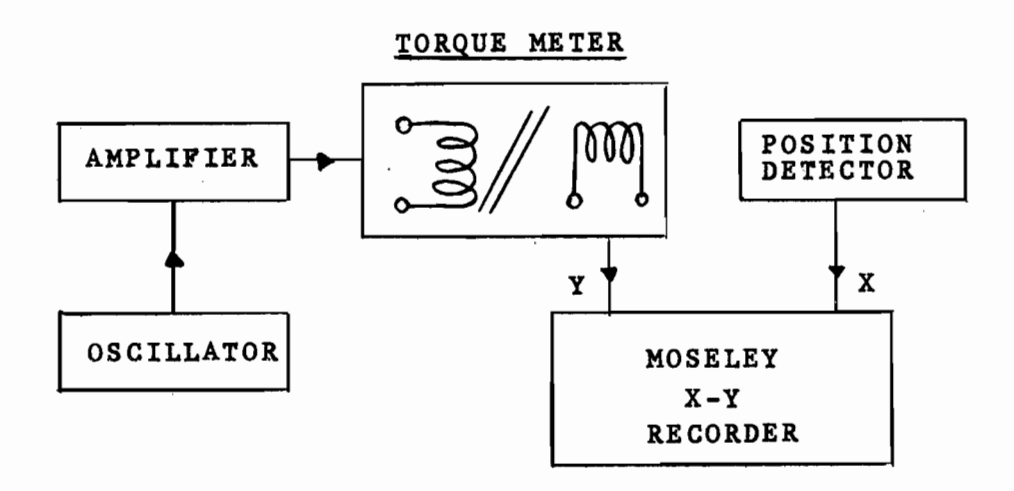


FIG. 3-2. Block diagram of equipment used for plotting transfer characteristic of torque meter.

The V-shape of the transfer characteristic is solely due to the phase-insensitivity of the external circuitry; it is not due to a deficiency of the torque meter. This can be remedied by inserting a phase-sensitive detector at the output of the pick-up coil.

A signal is present at zero torque, due to imperfect alignment of the magnetizing and pick-up coils, resulting in mutual coupling. In all cases, however, the zero-torque signal

was extremely small; a simple method of completely eliminating it, is discussed at the end of the Chapter.

The hysteresis and non-linearity of the transfer characteristic are very undesirable features and can be eliminated by raising the excitation as will be discussed later.

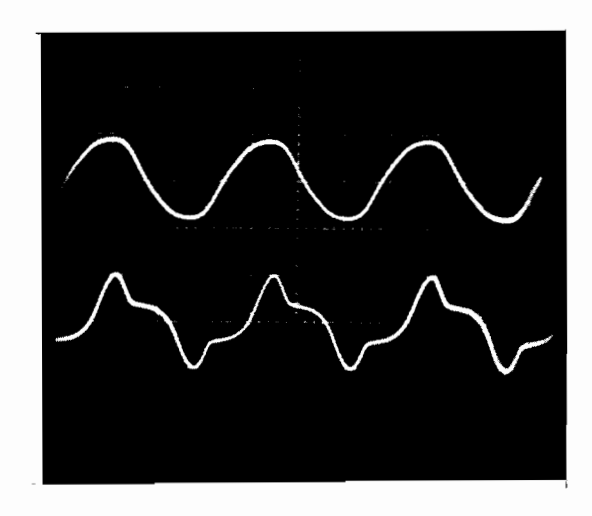
3.4 Output Signal Harmonics

The output signal waveform was distorted by the presence of eddy currents in the wall of the torque tube. An analysis of the harmonic content was made by means of a Bruel and Kjaer frequency analyzer, Type 2105, the results indicating the presence mainly of third and fifth harmonics of the order of 15% of the fundamental. However, filtering of the signal is not necessary even in cases of precision measurements. Typical signal oscillograms are shown in Fig. 3-4.

3.5 Linearity and Hysteresis

Increasing the magnetizing current increases the output signal, improves the linearity and reduces the hysteresis. A magnetizing level is reached where hysteresis disappears and linearity is extremely good. Any further increase above this optimum magnetizing level slightly decreases the sensitivity (defined as the output signal per unit torque applied, for small stresses in the tube), of the device, and has no effect on linearity and hysteresis. The sensitivity, as a function of magnetizing current at 60 c/s, is shown in Fig. 3-5, while typical recordings of the transfer characteristic at various excitations are displayed in Fig. 3-6.

At low field strengths, magnetization of the torque tube proceeds by domain wall movement. Because of magnetostriction there must be a dimensional change of the material



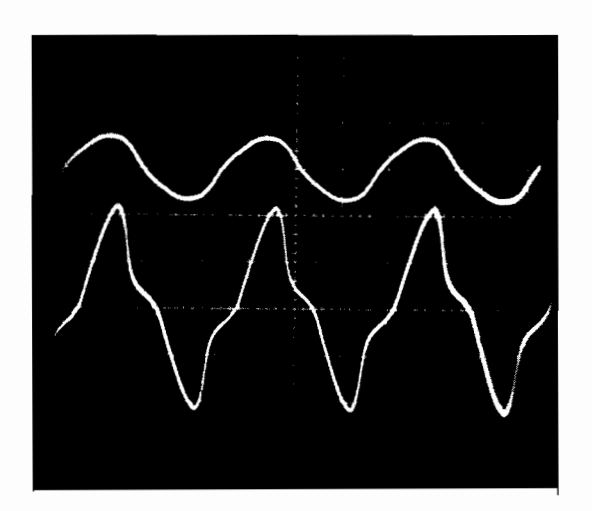
(a) Top trace: Magnetizing Current,
0.5 amp. at 60 c/s.

Bottom trace: Pick-up Coil Signal.

Scales vertical: 0.835 amp./div.

0.2 volt/div.

horizontal: 5 msec/div.



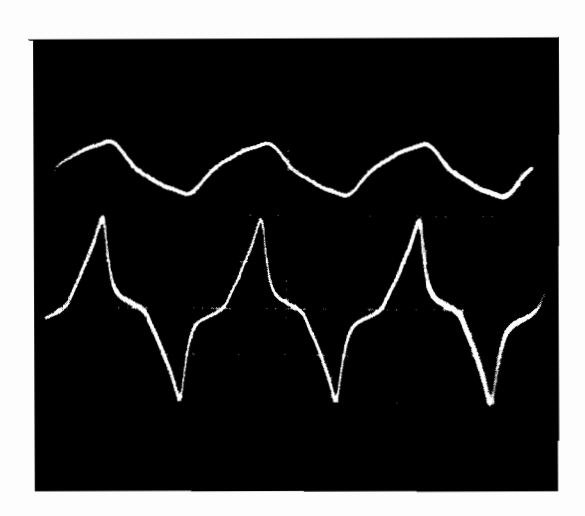
(b) <u>Top trace</u>: Magnetizing Current, 1.0 amp. at 60 c/s.

Bottom trace: Pick-up Coil Signal.

Scales vertical: 2.08 amp./div.

0.5 volt/div.

horizontal: 5 msec/div.



(c) Top trace: Magnetizing Current, 1.5 amp. at 60 c/s.

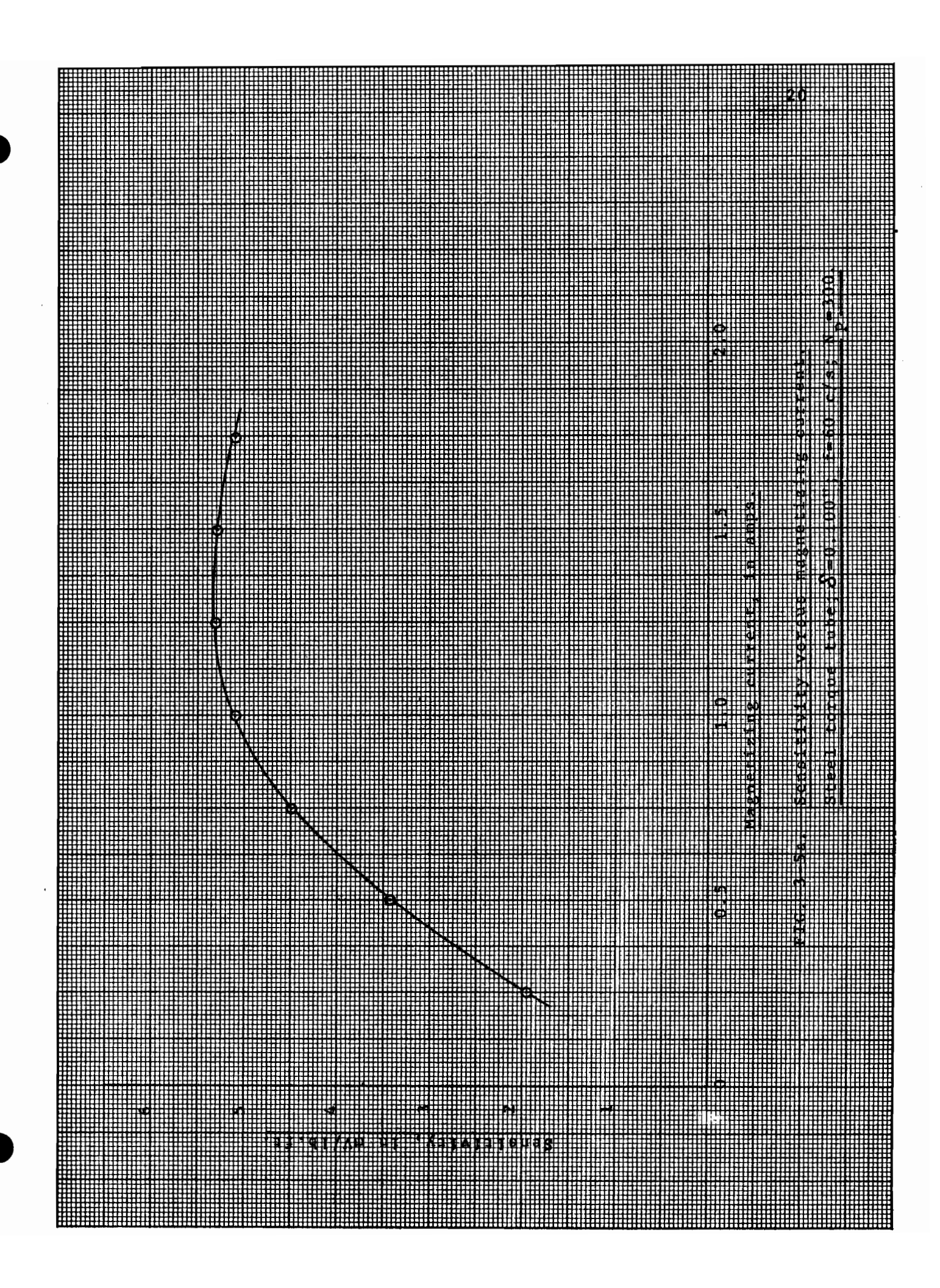
Bottom trace: Pick-up Coil Signal.

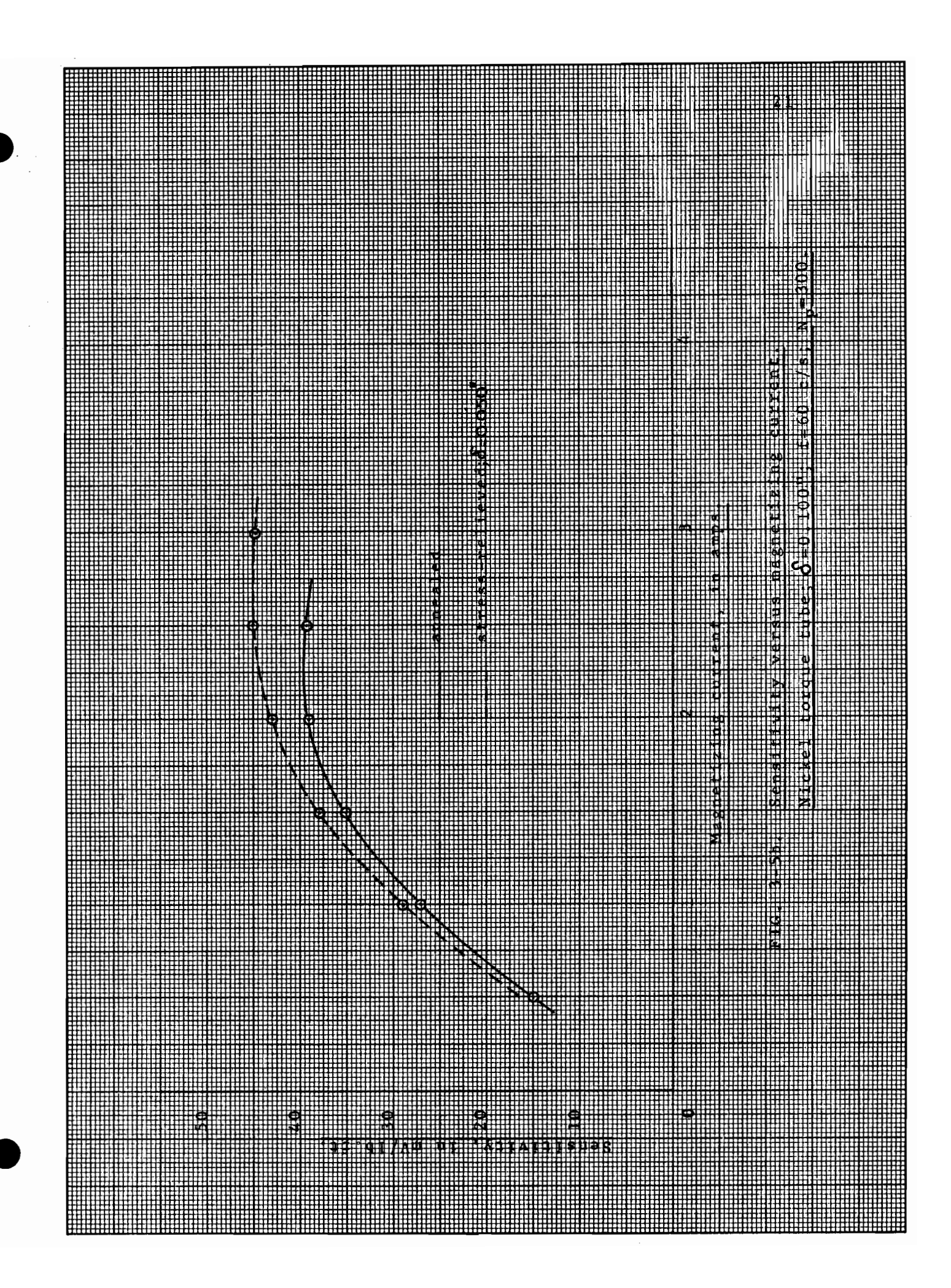
Scales vertical: 4.16 amp./div.

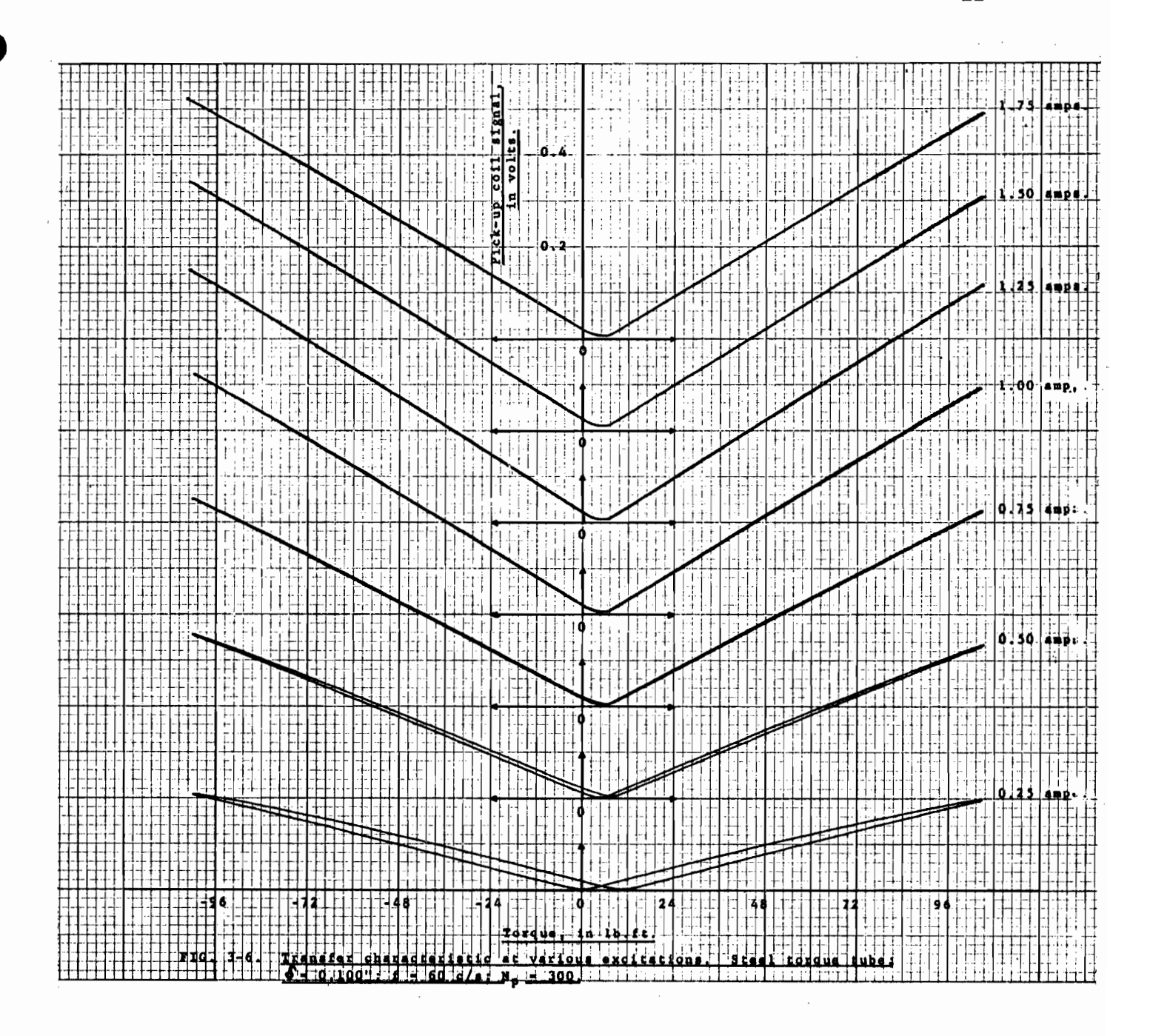
1 volt/div.

horizontal: 5 msec/div.

FIG. 3-4. Magnetizing current and pick-up coil signal waveforms; Nickel stress-relieved torque meter, $S = 0.100"; N_p = 300; T = 500 \text{ lb.in.}$







associated with the change of direction of the spontaneous magnetization. Thus a magnetostrictive strain is added to the applied strain. The domain walls tend to be pinned by impurities and local strains, and hence they are distorted if an external field or stress is applied. When the applied stress is reduced to zero, the domain walls will not necessarily return to their original position, so that a residual internal strain will be present, causing the appearance of the magnetomechanical hysteresis in the transfer characteristic. At medium and strong magnetic fields, the magnetization proceeds by rotation of the domains. As large fields or stresses are necessary to slightly rotate the magnetization vector, the hysteresis effect is extremely small at high field strengths.

Thus, to obtain good linearity and low hysteresis, it is desirable to operate the torque tube at the optimum magnetizing level. At this level of excitation, the sensitivity of the torque tube is almost unaffected by small variations in magnetizing current; hence, there is no need for a constant current source in the magnetizing circuit.

The optimum magnetizing level is greatly affected by the eddy currents induced in the wall of the torque tube, and, hence, depends on tube dimensions, materials and frequency of excitation. An approximate figure, at 60 c/s, is 15 Oersteds for steel, 50 Oersteds for annealed-nickel and 70 Oersteds for stress-relieved nickel torque tubes.

3.6 Optimum Stress Level

So far the sensitivity has been defined as the initial slope of the transfer characteristic. For optimum excitation, the slope remains unchanged, until a certain stress level is reached, above which the slope will either increase or decrease depending on the material and operating temperature. This

optimum stress level corresponds to approximately, 4 kg/mm² for steel; 2.5 kg/mm² for annealed-nickel; 3 kg/mm² for stress-relieved nickel. Within the stress limits, the change in slope and, hence, the deviation from linearity, will not exceed 0.5%. Closer stress limits, giving a 0.1% deviation from linearity, are given in Chapter VI.

Exceeding the optimum stress level, which is well below the elastic limit of the material, does not result in any mechanical deformation of the torque tube; however, a certain degree of curving of the transfer characteristic is evident, which disappears again with the stress being reduced below the optimum level. The torque meter is thus a robust device and this should be borne in mind when comparing it with other types of torque-gauges in particular strain-gauges.

3.7 Torque Tube Wall Thickness

For a specified torque to be applied to the tube, reducing the wall thickness, raises the stress level and, hence, increases the output signal, while at the same time, the screening effect of eddy currents is greatly reduced. Hence, in choosing wall thickness, a compromise should be made between good saturation at desirable operating temperature and low input power, with a shear stress not exceeding the optimum stress level. Torque tubes of thickness 0.100" were quite satisfactory at frequencies up to 1 kc/s.

3.8 Effect of Eddy Currents

Eddy currents induced in the walls of the torque tube by the magnetizing current, are very undesirable; they result in unnecessary heating of the tube, and their screening effect prevents one from driving all of the material into saturation at a fairly low input power. This is more apparent at higher frequencies. Although the theory of eddy currents assumes constant permeability, i.e. low field strengths, which is not the case for torque meters driven to saturation, the results of the analysis can be used as a guide in choosing wall thickness and input power required at a particular frequency of excitation.

Since the wall thickness is very small compared with the radius of the torque tube, the cylindrical surface was approximated by a flat sheet. The field amplitude H inside such a sheet diminishes with distance below the surface, according to the expression 12;

$$\frac{H}{H_0} = \left[\frac{\cosh(2\theta x/\delta) + \cos(2\theta x/\delta)}{\cosh\theta + \cos\theta} \right]^{\frac{1}{2}}$$

where x is measured from the middle of the sheet, H_{o} is the amplitude of a sinusoidally varying field, applied to the sheet, parallel to its surface, and

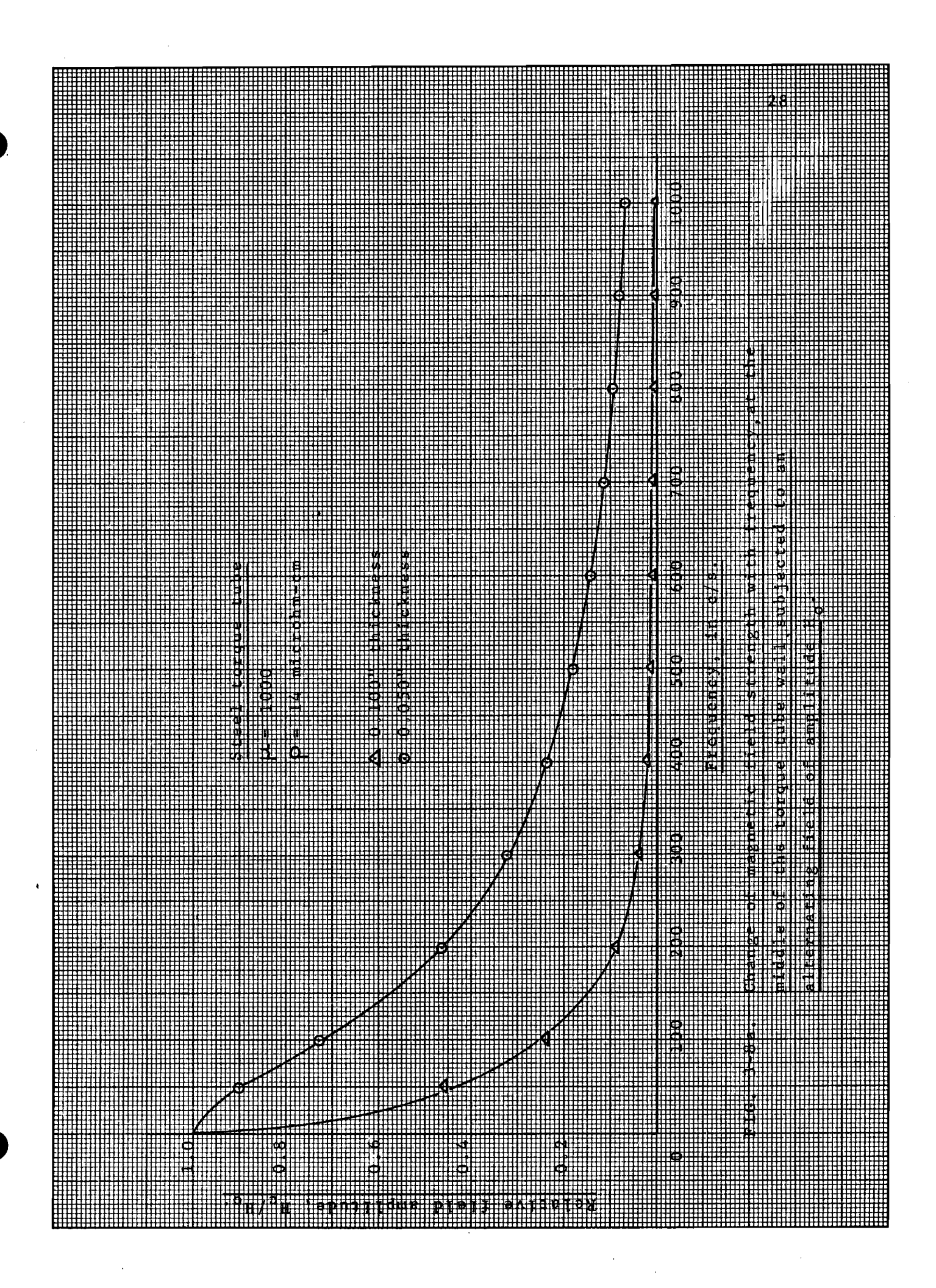
$$\theta = 2\pi \delta \sqrt{\frac{\mu f}{\rho}}$$

 δ being the thickness of the sheet; μ and ρ the permeability and resistivity respectively and f the frequency of applied field.

The change in $\mathrm{H/H_0}$ with wall thickness as well as the change in $\mathrm{H_c/H_0}$ with frequency, $\mathrm{H_c}$ being the amplitude of the field in the middle of the tube wall, are shown in Fig. 3-7 and 3-8, respectively. The screening effect of eddy currents plays an important role in the choice of frequency of excitation.

3.9 Frequency of Excitation

The possibility of exciting the torque meters at frequencies higher than 60 c/s, in order to increase the sensitivity and avoid interference from neighboring 60 c/s apparatus, was investigated. Frequencies higher than 1 kc/s



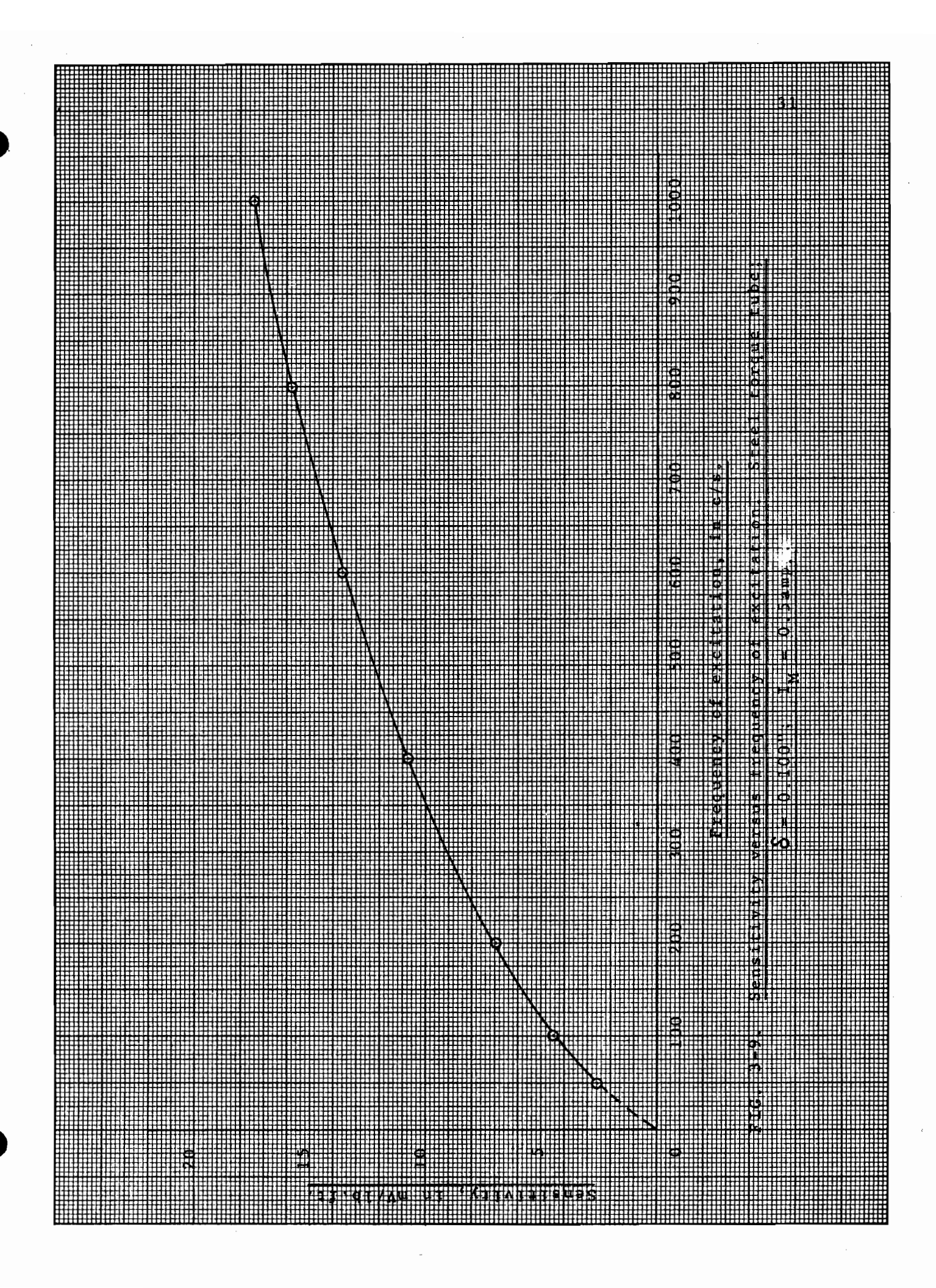
were considered unsuitable, due to the high input power requirements to drive the tube into saturation.

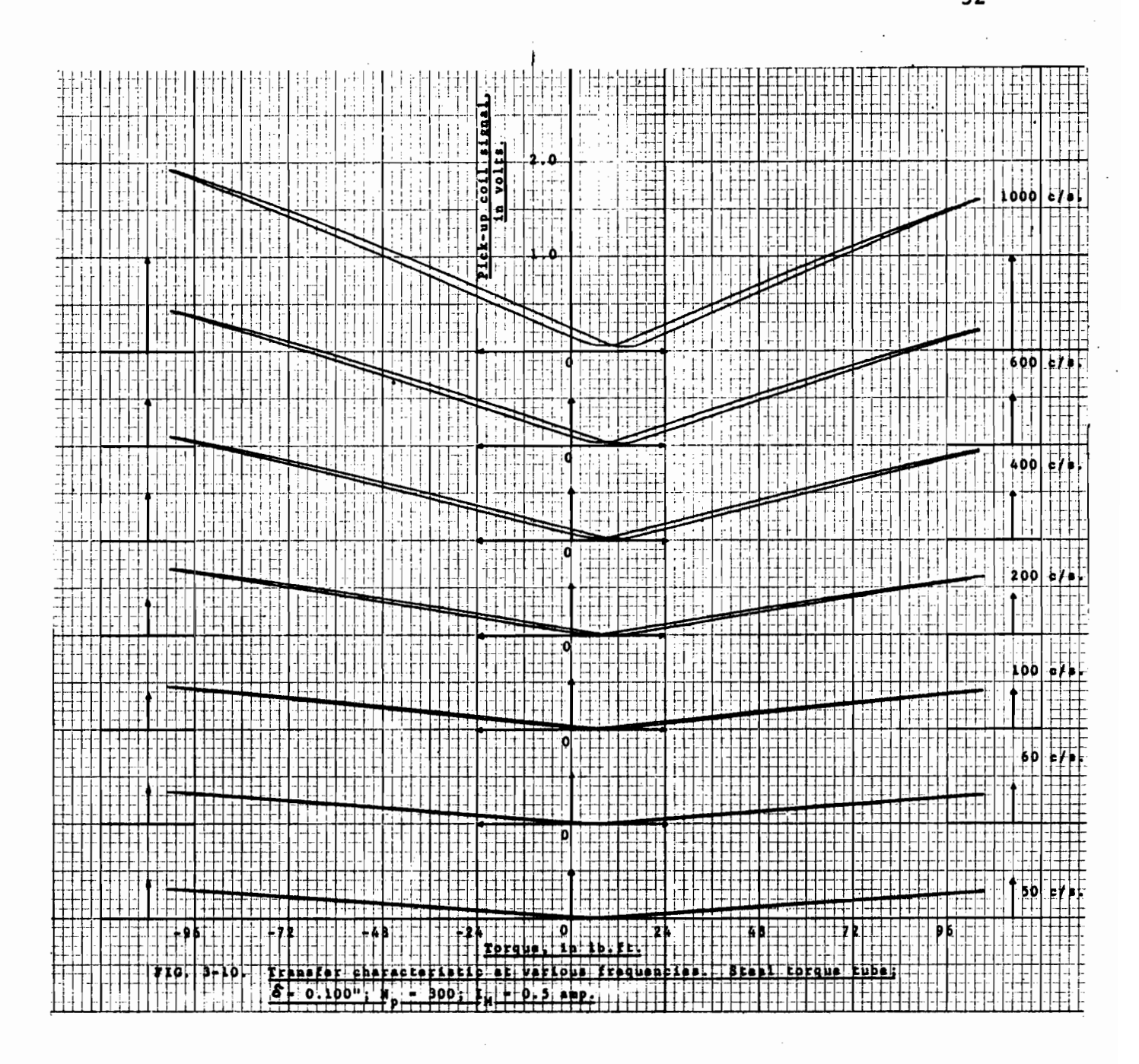
Increasing the frequency, while keeping the magnetizing level constant, increases the sensitivity, as shown in Fig. 3-9, with a corresponding increase in hysteresis; typical X-Y recordings of the transfer characteristic are shown in Fig. 3-10. As in the 60 c/s case, the hysteresis can be reduced by increasing the magnetizing current until an optimum level is reached that will give good linearity and low hysteresis. This optimum magnetizing level varies with frequency, a typical value at 400 c/s being given in Fig. 3-11.

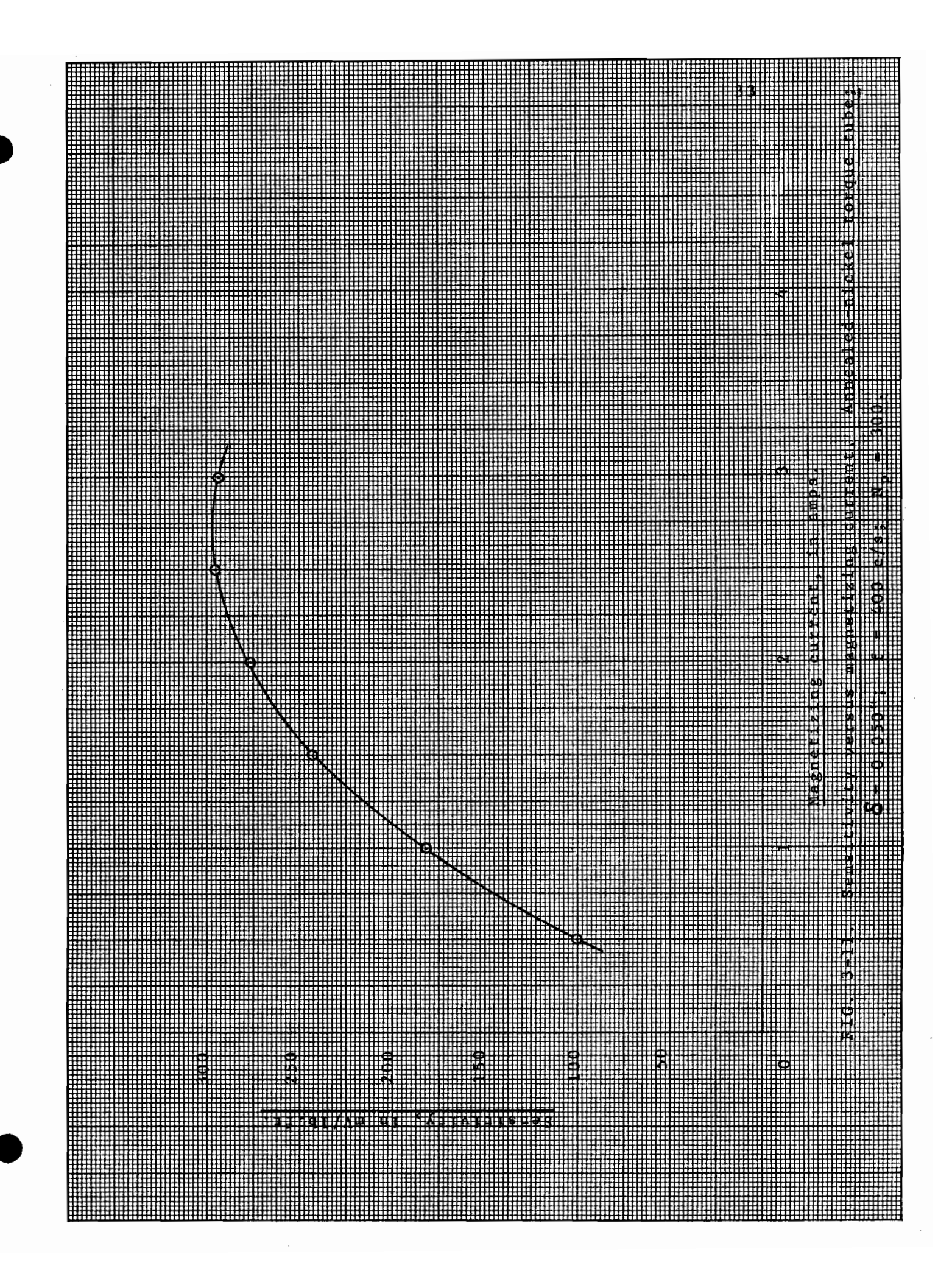
Figure 3-7 shows clearly the variation of the field strength inside the wall of the torque tube. The minimum field strength, appearing in the middle of the sheet, must, at all times, be higher than the corresponding saturation value. As the frequency of excitation is increased, the screening effect of eddy currents becomes more serious, with the result that the field strength at the middle of the tube wall drops below the desirable value. This can be overcome by a corresponding increase of the magnetic field at the surface of the tube. Thus at higher frequencies, the optimum magnetizing level, previously discussed, still exists, but it is of a higher value than in the 60 c/s case.

3.10 Output Signal

The output signal is independent of the position of the pick-up coil along the axis of the tube and is not affected by the proximity to the set-up of foreign magnetic materials, indicating that the axial magnetic lines run very close to the torque tube. It is, however, directly proportional to the number of turns of the pick-up coil, provided that the diameter of the coil does not exceed 4 inches, for the particular set-up used,







as shown in Fig. 3-12.

For 300 turns, 60 c/s and optimum magnetization, the torque meter has a maximum sensitivity of:

- (i) 0.18 volts per kg/mm², for steel
- (ii) 0.54 volts per kg/mm², for stress-relieved nickel
- (iii) 0.90 volts per kg/mm², for annealed nickel

Pick-up coils with higher number of turns, namely up to 20,000 turns, were tested, with an output signal directly proportional to the number of turns.

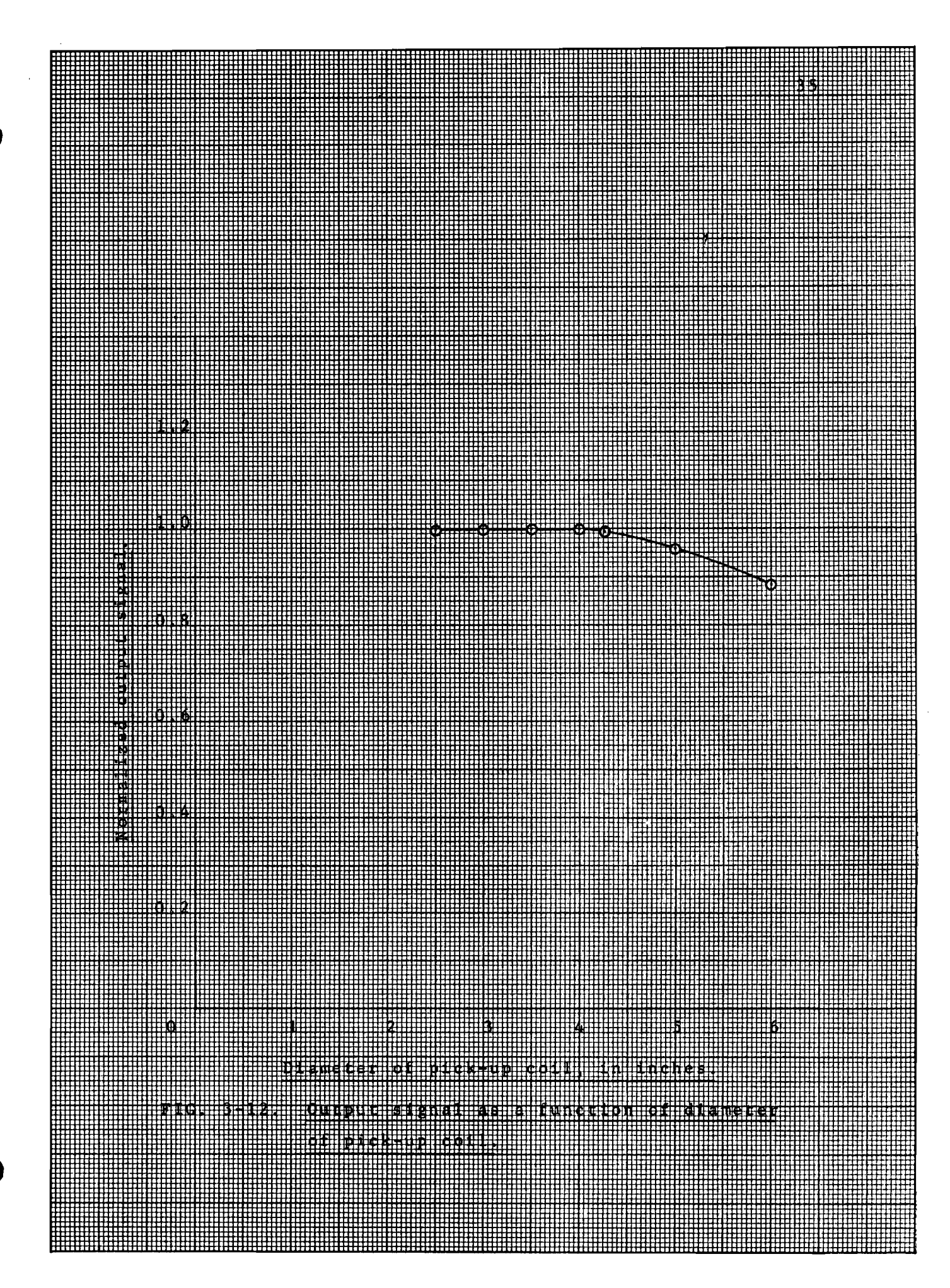
3.11 Nickel-plated Brass Torque Tube

Reducing the wall thickness of the torque tube presents a mechanical problem, so far as machining to thicknesses below, say 0.025", is concerned. This can be overcome by nickel-plating a tube, made of non-magnetic material, such as brass.

A brass tube, having the same dimensions as the 0.100" steel one, with a 0.008" nickel-plating on the active part, was constructed and tested. Saturation of the tube could be attained at very low field strengths, even at frequencies of 1 kc/s. However, in designing such a torque tube, care must be taken to ensure that the stress level in the plating is below the optimum one, if the linearity of the transfer characteristic is to be preserved.

3.12 Re-annealing the Nickel Torque Tubes

The nickel torque tubes were re-annealed; this resulted in higher sensitivity, but as the material became soft, the tube was unsuitable for high torques.



3.13 Effect of Temperature

The eddy currents tend to heat up the tube. Under optimum magnetizing conditions, the temperature was of the order of 80° C, with the exception of the 0.050" steel torque tube, whose operating temperature was 40° C.

Temperature variations affect the sensitivity. For steel torque meters, a 0.5% change in sensitivity occurs for a \pm 30°C temperature variation, while for nickel a similar temperature change has a 5% effect.

3.14 Locus of Output Signal Vector

Using the set-up of Fig. 3-13, the locus of the output signal vector with reference to the magnetizing current, was traced on the recorder, a typical one being shown in Fig. 3-14. The linearity of the locus improves and the hysteresis diminishes with increasing magnetizing current. The zero-torque signal, represented by vector \overrightarrow{OA} , can be eliminated by injecting in the pick-up coil circuit a voltage equal in amplitude and in anti-phase to \overrightarrow{OA} . As \overrightarrow{OA} may vary in amplitude and phase with the particular set-up, it is preferable to null the signal by appropriate adjustment of the amplitude of two voltages, injected in the circuit and differing in phase by 90° (Fig. 3-15).

3.15 Final Transfer Characteristic

With the set-up of Fig. 3-16, a typical transfer characteristic under optimum conditions of operation is shown in Fig. 3-17.

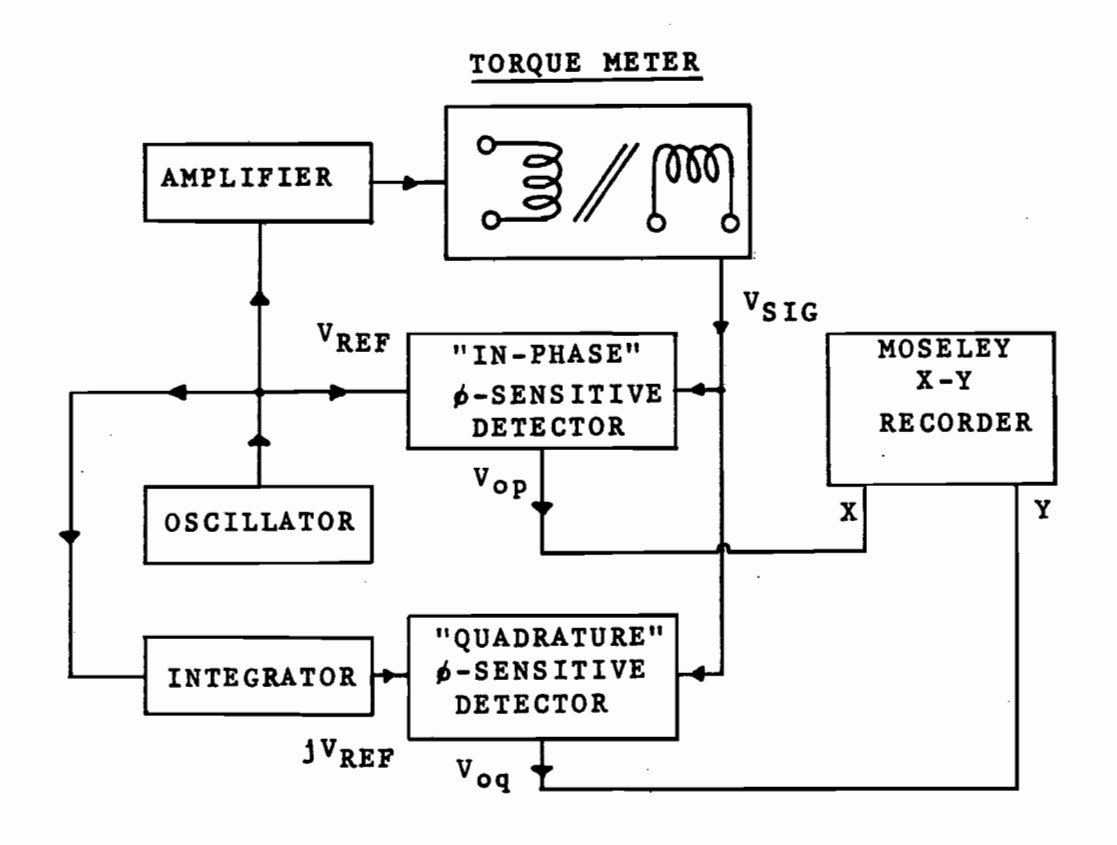


FIG. 3-13. Block diagram of equipment used to trace locus of pick-up coil signal.

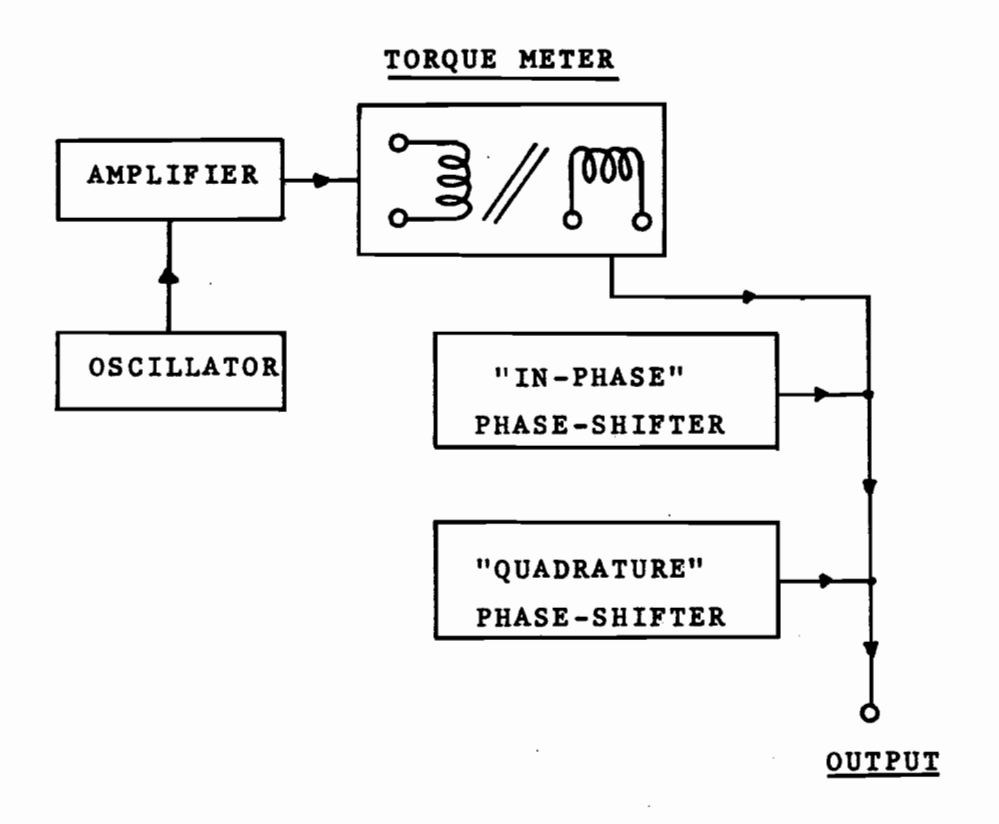


FIG. 3-15. Block diagram of zero-torque signal suppressor circuit.

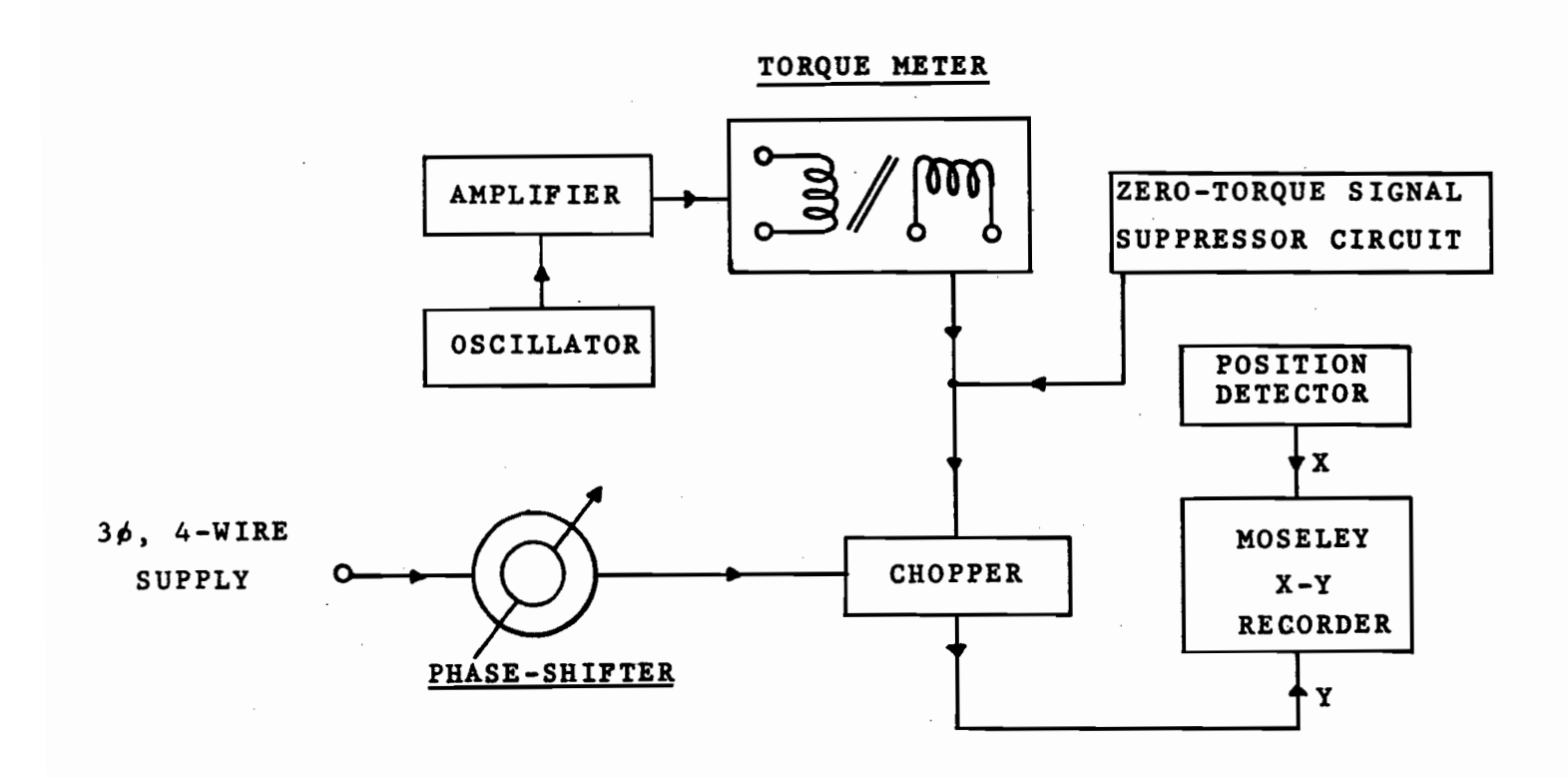


FIG. 3-16. Block diagram of final set-up.

		***************************************	09
		#	-0.050
			40
			THE BE CE
		*	torque meter;
			Z 0 2
			c of
			Torian II
			Final transfer charac
			ranefer
			t t
		1111112	
G.	6	y	
18270	v nt dishata iton q	->1056	

3.16 Conclusions

Nickel torque meters exhibit a higher stresssensitivity at the expense of higher input power; they are very temperature dependent and must be operated at fairly low stress levels, if a linear transfer characteristic is desirable.

Steel torque meters, on the other hand, maintain a linear transfer characteristic, up to fairly high stresses, of the order of 4 kg/mm²; maximum sensitivity is of the order of 600 μV per kg/mm² per turn, at 60 c/s and temperature or magnetizing current variations, normally encountered in practice, do not seriously affect it; thus, they are to be preferred to nickel torque meters.

CHAPTER IV

THEORETICAL SURVEY

A theory was developed explaining the behaviour of the torque meter under various conditions of operation. Quantitative as well as qualitative agreement has been obtained between theory and experiment, as is demonstrated in Chapter V.

4.1 Domains

It has been mathematically established and verified from experience that the elementary magnets, on which the elementary theory of magnetism was based, do exist in the form of groups of atoms called 11,13 "domains".

Each domain is spontaneously magnetized to saturation; however, when the material is unmagnetized, these domains are oriented at random, so that the resultant magnetization of the whole body is zero in any direction. When an external field H is applied to the material, a resultant magnetization appears in the direction of the applied field. To a first approximation, two distinct magnetization mechanisms exist: wall displacement and the rotation of magnetic moments. Usually in weak fields, magnetization proceeds by wall displacement; however in medium and strong fields, magnetization is achieved by rotation of the domains.

4.2 Stability of Domain Orientation

The direction of magnetization in a domain is determined by the crystal structure, by stress and by magnetic field. The relative importance of the three factors may be derived by considering the corresponding energies involved, namely:

- (i) Crystal anisotropy energy,
- (ii) Magneto-elastic energy,
- (iii) Magnetostatic energy.

4.2.1 Crystal Anisotropy Energy

In a ferromagnetic single crystal, there are directions of easy magnetization and directions of difficult magnetization; thus, it is easier to rotate the spins in some direction than in others; the forces opposing this rotation are those due to crystal anisotropy.

For cubic symmetry, as is the case for iron and nickel, the anisotropy energy density is given by:

$$W_{K} = K_{1}(\alpha_{1}^{2} \alpha_{2}^{2} + \alpha_{2}^{2} \alpha_{3}^{2} + \alpha_{3}^{2} \alpha_{1}^{2}) + K_{2}\alpha_{1}^{2}\alpha_{2}^{2}\alpha_{3}^{2} + \dots$$
 (4.1)

where α_i are the direction cosines of the saturation magnetization M_s , with respect to the crystallographic axes, K_i are the anisotropy constants.

In the absence of magneto-elastic and magnetostatic energies, the directions of minimum anisotropy energy are those of easy magnetization; they may be the cube edges, [100], the body diagonals of the cube, [111], or the face diagonals of the cube, [110]. An example of the first type is the iron crystal, while the nickel crystal can have any one of the directions, depending on the temperature of the specimen.

4.2.2 Magneto-elastic Energy

The crystal anisotropy energy discussed is that of a crystal which has not been permitted to deform under the influence of either magnetostriction or externally applied stresses.

Actual polycrystalline materials are both stressed and deformed. Thus two closely related effects must be taken into account; the first is that of spontaneous, magnetostrictive deformation on effective anisotropy constants, the second that of external stresses on magnetic properties.

(i) Effective Anisotropy and Magnetostriction

The effective anisotropy constants K depend on the intrinsic anisotropy constants k of the undeformed crystal, on the magnetostriction constants λ , and on the elastic moduli C.

For an unstressed cubic crystal, the effective anisotropy energy may be expressed (up to the fourth order of the direction cosines α_i of spontaneous magnetization) as:

$$W_{K} = K_{1}(\alpha_{1}^{2} \alpha_{2}^{2} + \alpha_{2}^{2} \alpha_{3}^{2} + \alpha_{3}^{2} \alpha_{1}^{2})$$

where
$$K_1 = k_1 + \Delta K_1$$

and
$$\Delta K_1 = \frac{9}{4}(C_{11}-C_{12}) \lambda_{100}^2 - 2C_{44} \lambda_{111}^2$$

Here λ_{100} and λ_{111} are the saturation values of the longitudinal magnetostriction in the [100] and [111] directions respectively; c_{11} , c_{12} and c_{44} are the three elastic moduli of the cubic crystal.

(ii) Stress Energy

When external stresses are applied to the crystal, a further term W_S must be added to the anisotropy energy, W_K . In the case of cubic symmetry and uniform compression σ , in a direction specified by the direction cosines ψ_i , the stress energy is found to be:

$$W_{s} = \frac{3}{2} \epsilon \left[\lambda_{100} \sum_{i} \alpha_{i}^{2} \chi_{i}^{2} + 2 \lambda_{111} \sum_{i>j} \alpha_{i} \alpha_{j} \chi_{i} \chi_{j} \right]$$
 (4.2)

Thus, the total magnetic energy of a cubic crystal under an applied uniform compression can be expressed by: $W = V \left(\frac{2}{3} \times \frac{2}{3} + \frac{2}{3} \times \frac{2}{3} + \frac{2}{3} \times \frac{2}{3} + \frac{2}{3} \times \frac{2}{3} \right) + V \left(\frac{2}{3} \times \frac{2}{3} + \frac{2}{3} \times \frac{2}{3} + \frac{2}{3} \times \frac{2}{3} + \frac{2}{3} \times \frac{2}{3} \right) + V \left(\frac{2}{3} \times \frac{2}{3} + \frac{2}{3} \times \frac{2}{3} + \frac{2}{3} \times \frac{2}{3} + \frac{2}{3} \times \frac{2}{3} \right) + V \left(\frac{2}{3} \times \frac{2}{3} + \frac{2}{3} \times \frac{2}{3} + \frac{2}{3} \times \frac{2}{3} + \frac{2}{3} \times \frac{2}{3} \right) + V \left(\frac{2}{3} \times \frac{2}{3} + \frac{2}{3} \times \frac{2}$

$$W = K_1(\alpha_1^2 \alpha_2^2 + \alpha_2^2 \alpha_3^2 + \alpha_3^2 \alpha_1^2) + K_2 \alpha_1^2 \alpha_2^2 \alpha_3^2$$

(4.3)

$$+ \ \frac{3}{2} \, \sigma \left[\lambda_{100} (\alpha_1^2 \chi_1^2 + \alpha_2^2 \chi_2^2 + \alpha_3^2 \chi_3^2) + 2 \, \lambda_{111} (\alpha_1^2 \alpha_2^2 \chi_1^2 \chi_2^2 + \alpha_2^2 \alpha_3^2 \chi_2^2 \chi_3^2 + \alpha_3^2 \alpha_1^2 \chi_3^2 \chi_1^2) \right]$$

For isotropic magnetostriction, i.e. $\lambda_{100} = \lambda_{111} = \lambda_{\rm S}$, equation (4.2) reduces to:

$$W_{S} = \frac{3}{2} \delta \lambda_{S} \cos^{2} \Psi \tag{4.4}$$

where Ψ is the angle between the direction of spontaneous magnetization and that of the applied compression.

Thus, from equations (4.3) and (4.4) the following statements can be made:

In the case of predominant crystal anisotropy energy (i.e. $W_K > W_S$), the directions of easy magnetization are essentially determined by crystal anisotropy; the stress merely favours one of these directions at the expense of the others.

When the anisotropy constant K_1 is small compared to λ_{100} 6 and λ_{111} 6, the preferential directions are essentially determined by the relative values of the magnetostriction constants.

When, the anisotropy constant still being negligible, the magnetostriction is isotropic, the directions of easy magnetization are determined by the direction of the applied stress. If $\epsilon \lambda_{\rm S}$ is positive, the directions of easy magnetization are situated in a plane perpendicular to the stress axis. If, on the contrary, $\epsilon \lambda_{\rm S}$ is negative, the domain magnetization vectors orient themselves parallel to the stress axis.

4.2.3 Magnetostatic Energy

The last two types of energy, which are of importance, are the self-energy of a permanent magnet in its own field (demagnetizing energy), and the energy of interaction of such a magnet with an external field (field energy).

(i) Demagnetizing Energy

The demagnetizing field of a permanent magnet arises from inhomogeneities of magnetization. It is very difficult to calculate accurately the demagnetizing energy, except for some very simple models. In the case of an isolated, homogeneous ellipsoid, the demagnetization energy is:

$$W_{d} = \frac{\mu_{o}}{2} M_{S}^{2} (N_{1}\alpha_{1}^{2} + N_{2}\alpha_{2}^{2} + N_{3}\alpha_{3}^{2})$$
 (4.5)

where N_1 are the demagnetization factors along the three axes of the ellipsoid, and μ_0 is the permeability in vacuo. Equation (4.5) implies that the demagnetizing energy depends on crystal properties (through the saturation magnetization M_S) and on structure properties (through the demagnetization factors N_1).

(ii) Field Energy

The field energy density of interaction of a permanent magnet of saturation magnetization M_S , with an external field H is:

$$W_{H} = - \stackrel{\rightarrow}{M}_{S} \cdot \stackrel{\rightarrow}{H} = - M_{S} H \cos \phi \qquad (4.6)$$

 ϕ being the angle between \overrightarrow{M}_S and \overrightarrow{H} .

4.3 Anisotropy and Magnetostriction Constants

The anisotropy 11,14,15,16 and magnetostriction 17,18,19 constants are experimentally obtained data, tabulated in any book on Ferromagnetism. Since no data for steel could be found in the literature, the corresponding constants for iron were used.

These constants for iron and nickel are temperature dependent and the typical values used, are given in Table 4-1.

Material	Temp.	K ₁ ×10 ⁻⁴ (ergs/cm ³)	K ₂ ×10 ⁻⁴ (ergs/cm ³)	λ ₁₀₀ ×10 ⁶	λ ₁₁₁ ×10 ⁶	M _s (Gauss/cm ³)	B _s
	20	45.2	20.5	10.0	-19.5	1714	21580
Iron	40	43.5	21.3	9.7	-18.2	1712	21530
	60	42.0	21.8	9.4	-16.9	1710	21490
	80	40.5	22.0	9.2	-16.0	1708	21440
	100	39.0	22.5	9 • 0	-15.2	1705	21400
Nickel	20	-5.0	5.0	-46.0	-25.0	488	6140
	40	-4.0	4.8	-42.8	-24.5	480	6020
	60	-2.0	4.5	-40.5	-23.7	473	5950
	80	-1.0	4.2	-38.2	-23.3	468	5880
	100	+0.8	3.9	-36.8	-22.7	462	5800

TABLE 4-1. Anisotropy and magnetostriction constants for iron and nickel at various temperatures.

Temperature variations have a more pronounced effect on nickel than iron. Hence, for nickel, K_1 and $\lambda 100$ are reduced by 80% and 16% over a temperature range of 20 to 80°C, while the corresponding changes for iron are 10% and 8% respectively. These variations of the values of anisotropy and magnetostriction constants with temperature will have an effect on the induced axial magnetization, as is discussed in Chapter V.

4.4 Polycrystalline Materials

The magnetic materials used commercially are always polycrystalline; that is, each specimen is composed of a large number of small crystallites.

In many materials the crystallites are oriented more or less at random, so that for some purposes certain properties of the polycrystalline specimen may be obtained by averaging the corresponding single crystal property over all directions. In other materials, in particular those subjected to cold working, the crystallite axes are not necessarily distributed at random, but a considerable degree of orientation may exist.

Confining the argument to the case of cold-drawn tubing, as used in the construction of the torque tubes, the following can be said regarding crystal orientation.

In cold-drawn low-carbon steel tubing, certain degree of crystal orientation is to be expected. J.T. Norton quotes "If the reduction in wall thickness and circumference are essentially of the same magnitude, the crystals are aligned so that each has a [110]-axis parallel to the axis of the tube; but the arrangement is random about this axis. This is equivalent to the structure in wires. In case the tube has been reduced largely in wall thickness, the structure is similar to that found in sheet, and the crystallites are arranged so that a cube

face is parallel to a plane tangent to the tube wall, and a [110]-axis is parallel to the tube axis".

Thus, the results of Norton's investigation indicate that the crystal structure depends upon the dimensional changes which have taken place during the reducing process.

For cold-drawn nickel tubing, no information regarding crystal structure, could be found in the literature; hence, the crystal orientation present in cold-drawn nickel wires 21, namely, with either [111] - or [100]-directions, appearing along the wire axis, was therefore taken as a guide in the investigation of nickel torque tubes.

CHAPTER V

THEORETICAL ANALYSIS OF THE TORQUE METER

5.1 Introduction

In the absence of external magnetic field, applied stress and neglecting the internal stresses that might be present in the torque tube, strong internal forces, due to crystal anisotropy, will tend to align the domains along the directions of easy magnetization. As there is more than one possible direction, the net magnetization in any specified direction will be zero.

If an external stress is applied to the domains, the magnetization vector, \overrightarrow{M}_S , will rotate in a certain direction, depending on the values of magnetostriction constants and applied stress, until the total energy of the domains becomes a minimum. As, however, both positive and negative directions are equally favoured by stress, no net magnetization will appear in any direction.

An external field \overrightarrow{H} , of sufficient magnitude to be able to cause rotation of \overrightarrow{M}_S , is now applied to the torque tube; the directions closer to \overrightarrow{H} will be favoured resulting in a net magnetization of the specimen along and perpendicular to the direction of \overrightarrow{H} .

In the following analysis a uniform distribution of stress along the torque tube wall is assumed, (this is a reasonable assumption since the wall thickness is very small compared with the radius of the torque tube), and the effects of magnetostriction and demagnetization are neglected, as they are extremely small. The cases of steel and nickel torque tubes are separately examined and the predicted results are correlated

with the experimental ones at the end of the Chapter.

5.2 Steel Torque Meter

Consider a single domain, subjected to a field \hat{H} at an angle θ_0 to the direction of easy magnetization, [100], as shown in Fig. 5-1.

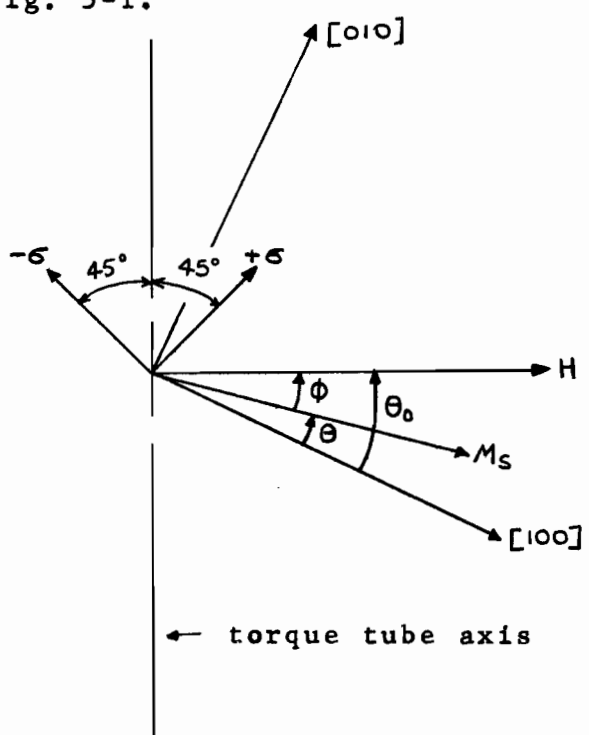


FIG. 5-1. Vectors and angles used in calculating the axial component of magnetization.

When torque is applied to the tube, the principal stresses $\pm \sigma$ appear in the 45° directions to the tube axis, as shown in Fig. 5-1.

It is assumed here that M_S lies in the same plane as \widetilde{H} and [100], namely the (001) - plane; this simplifies calculations without any appreciable change in the accuracy of the method.

The total energy of the domain is given by (see Appendix B):

$$W_{T} = \frac{K_{1}}{8} (1 - \cos 4\theta) - HM_{S} \cos \phi$$

$$+ \frac{3}{2} \delta \left[\lambda_{100} \sin 2\theta_{o} \cos 2\theta - \lambda_{111} \cos 2\theta_{o} \sin 2\theta \right]$$

The angle of deviation θ may be calculated by minimizing the total energy; this energy is a minimum when $\partial^W T/\partial_\theta = 0$ and $\partial^2 W T/\partial_\theta^2$ has a positive value; therefore,

$$\frac{K_1}{2} \sin 4(\theta_0 - \phi) - 36 \left[\lambda_{100} \sin 2\theta_0 \sin 2(\theta_0 - \phi) + \lambda_{111} \cos 2\theta_0 \cos 2(\theta_0 - \phi) \right]$$

$$= HM_S \sin \phi \qquad (5.1)$$

At this time, the axial magnetization is M_S sin ϕ and, hence, the axial induction B_S sin ϕ , where B_S = $4\pi M_S$ in Gauss. The rate of change of this flux with the pick-up coil results in the output signal of the torque meter.

Equation (5.1) will give angle ϕ as a function of H, σ and θ_0 , where θ_0 is an angle depending on the original crystal orientation. The effect of random crystal orientation in a polycrystalline material can be simulated by varying θ_0 from -45° to +45° and averaging θ_0 sin ϕ over the interval; the two extreme limits are imposed by the specified direction of \hat{H} , as if θ_0 exceeds either limit, an instantaneous change in the direction of easy magnetization to the nearby cube edge, occurs, resulting in a similar situation, as described above. Thus, it is sufficient to average sin ϕ over the 90° interval, resulting in:

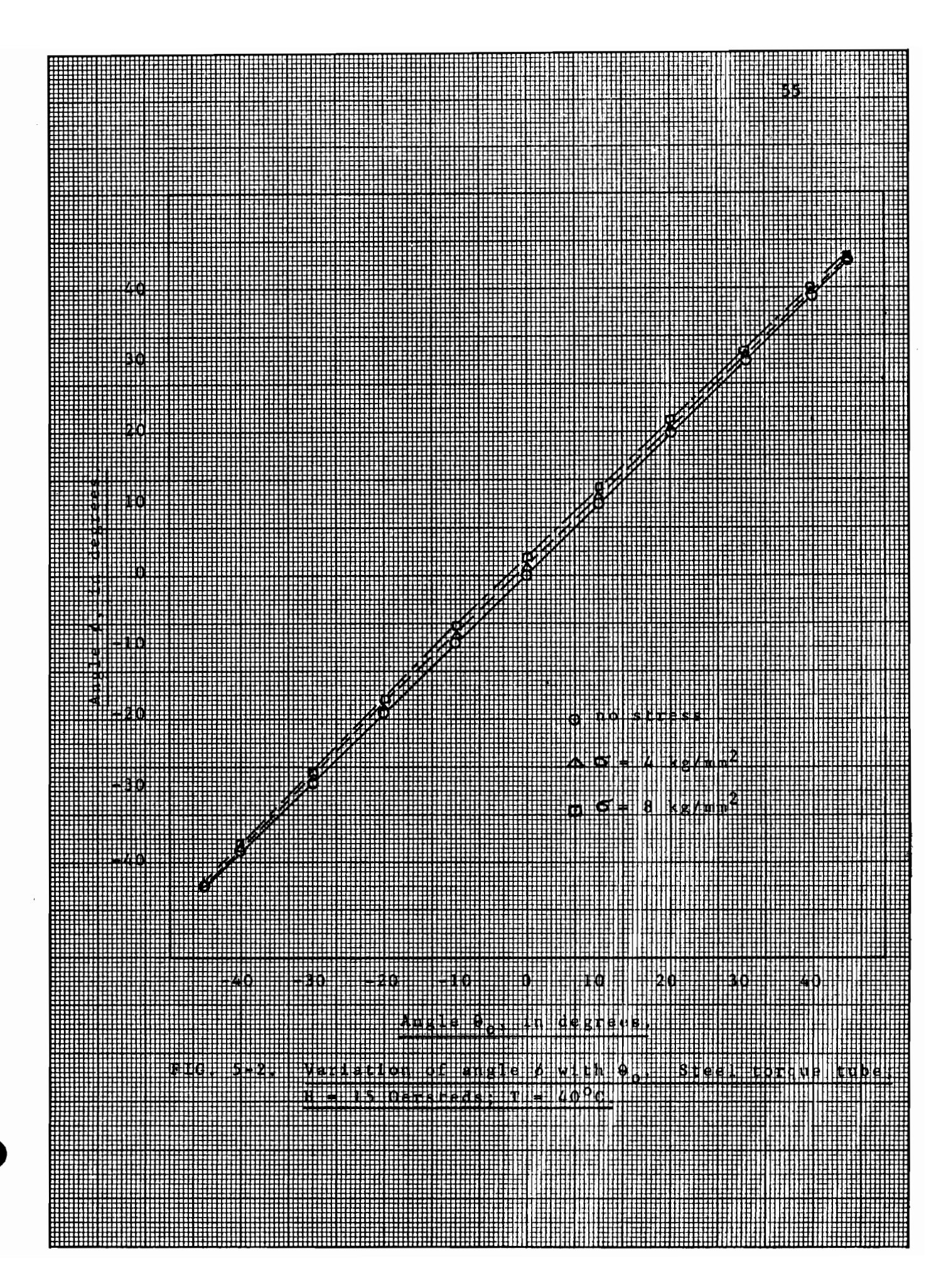
$$\overline{B}_{a} = B_{S} \overline{\sin \phi} \tag{5.2}$$

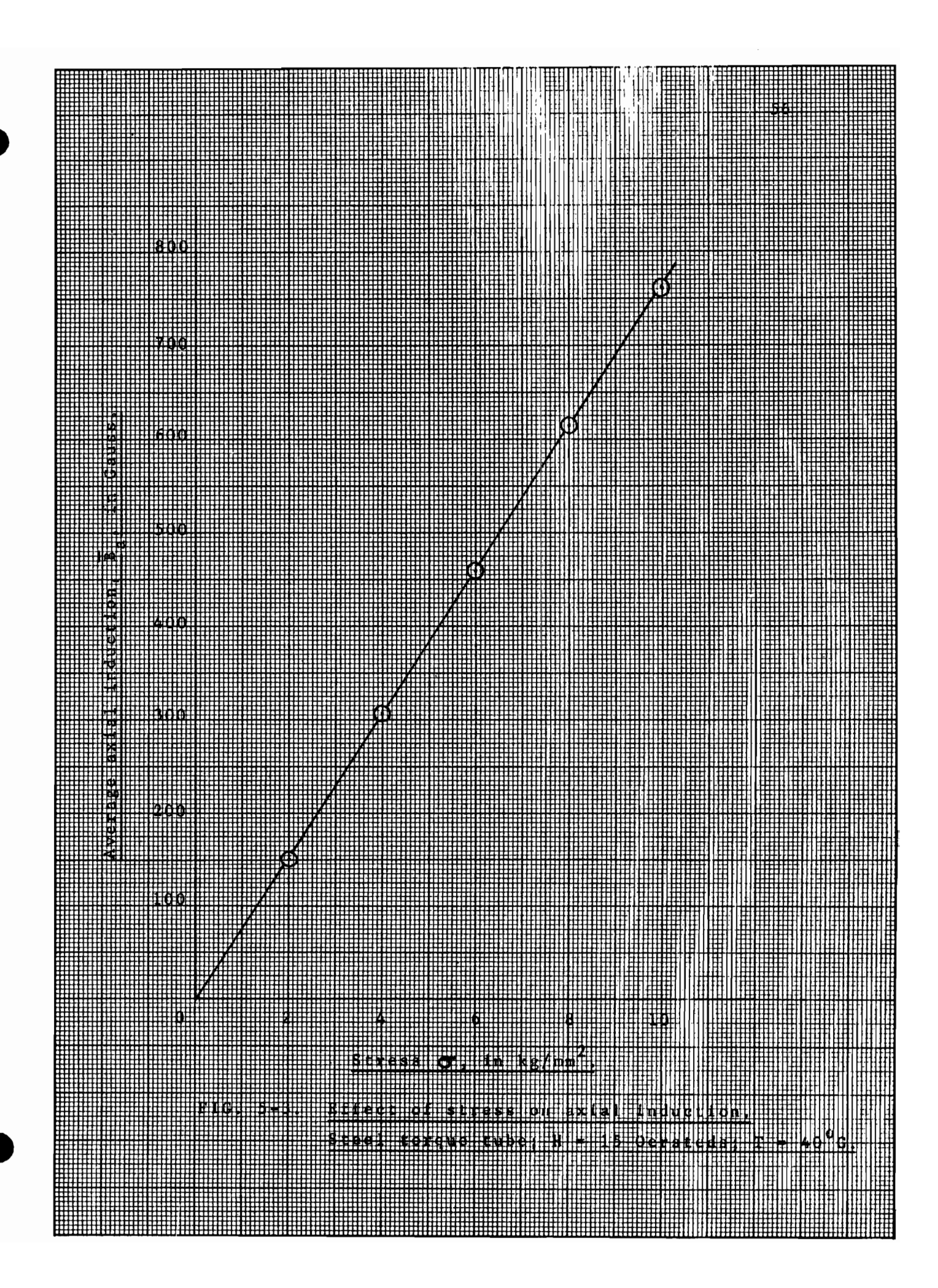
where sing denotes the corresponding average value of sing.

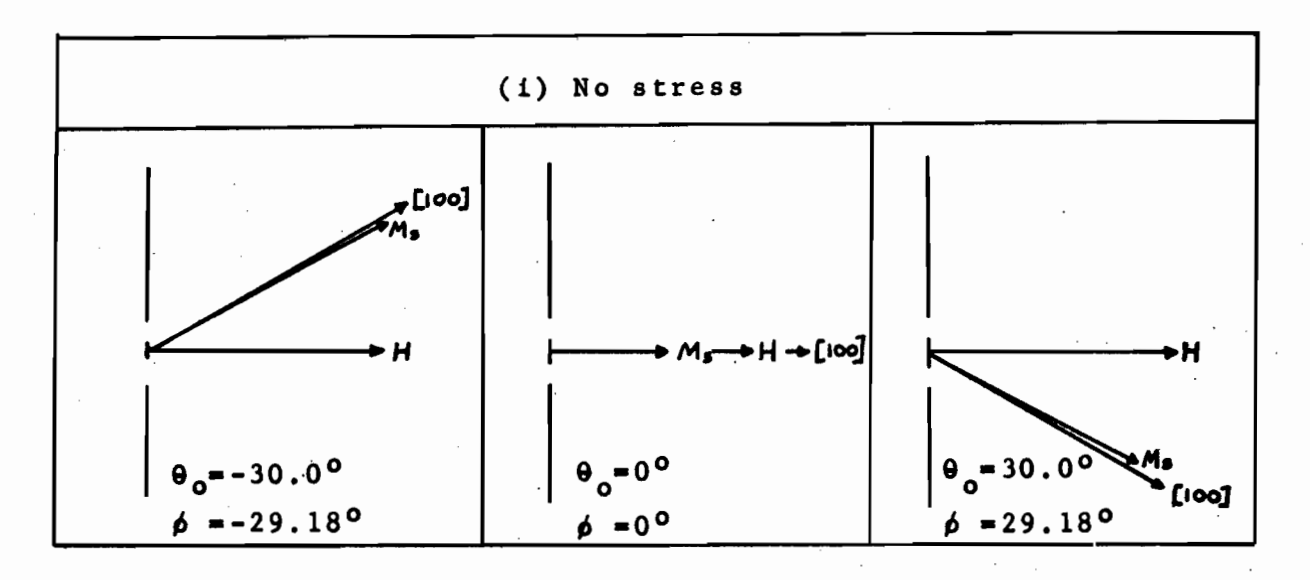
Clearly, more than one solution of equation (5.1) exists; however, the solution of interest is the one giving minimum energy, i.e. angle θ being very small. As no exact analytical solution (an approximate solution is given in Appendix B) could be readily obtained, equation (5.1) was solved numerically on the IBM 7040 digital computer. The procedure simply consists of assigning values to θ varying from -45° to +45° in convenient steps of 5°, solving equation (5.1) for ϕ with chosen values of H and Θ and finally averaging $\sin \phi$ over the 90° interval to obtain \overline{B} from equation (5.2).

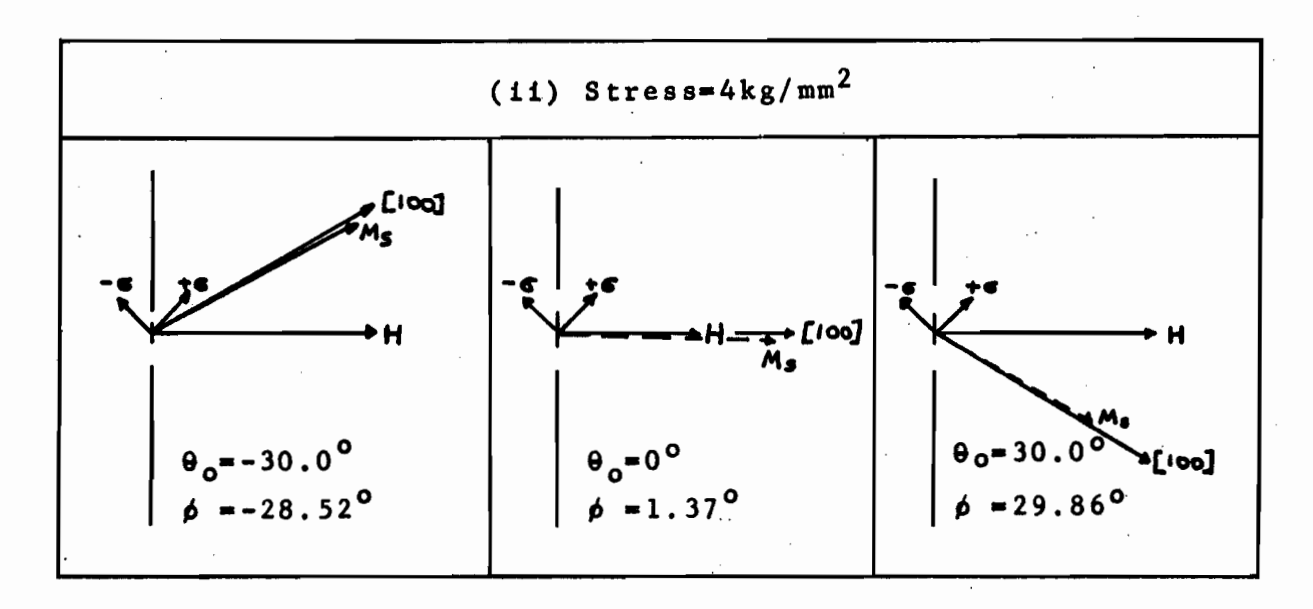
To facilitate the understanding of the mechanism of operation of the torque meter, the three types of energy involved were separately calculated. Although the concept of energy is a useful one, yet a clearer picture can be obtained, if one thinks of the rotational torques, (defined by the negative rate of change of the corresponding energy with respect to angle θ), acting on \overrightarrow{M}_S . These are shown in Fig. 5-5.

Although the anisotropy energy is small compared with either the magneto-elastic or magnetostatic energies, its rate









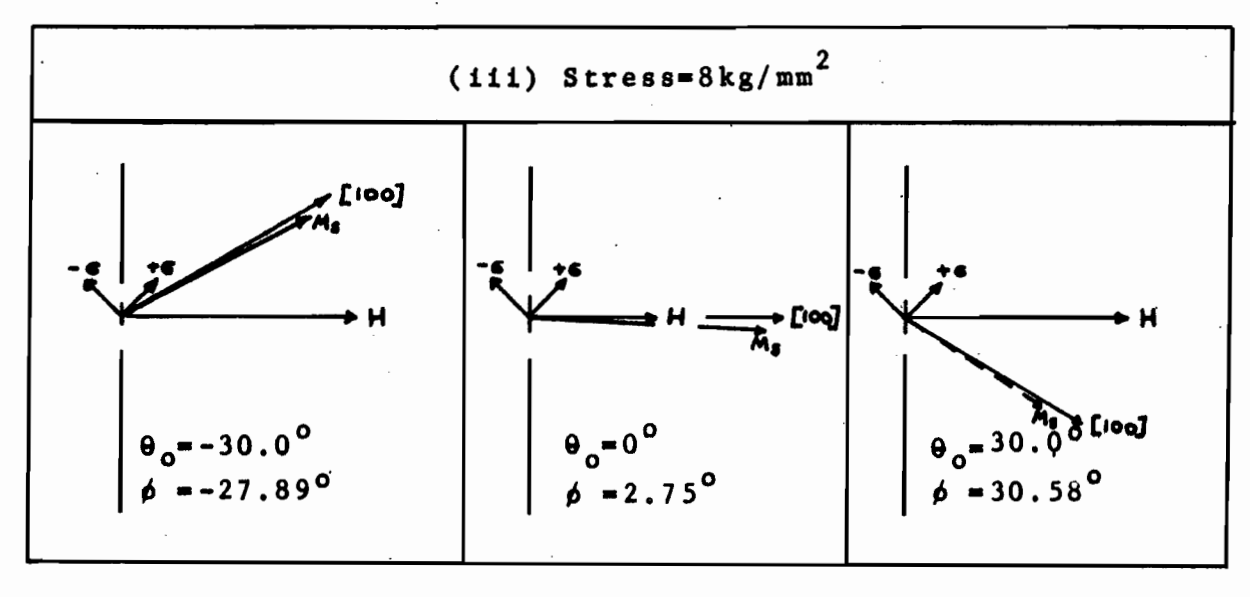
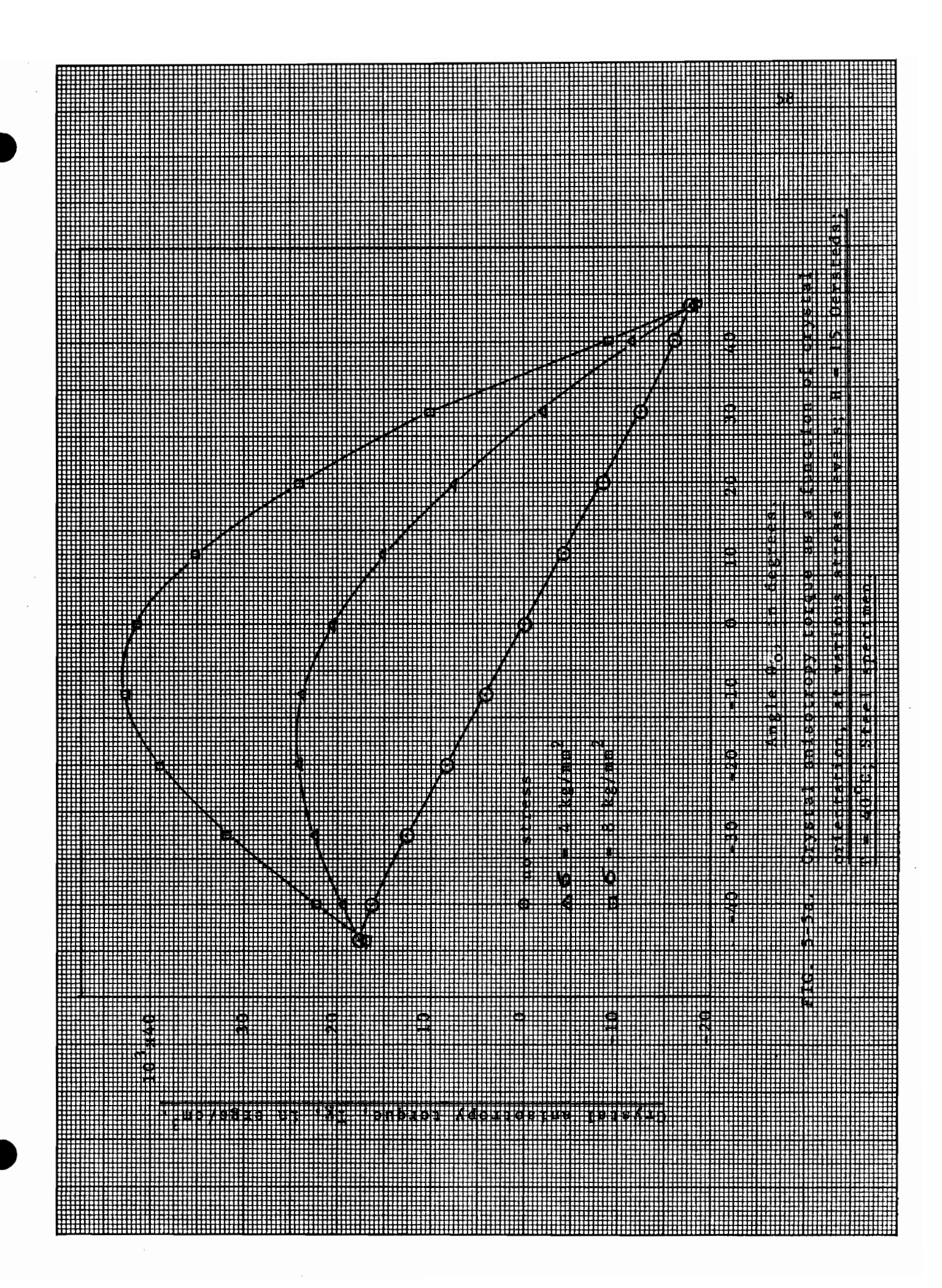
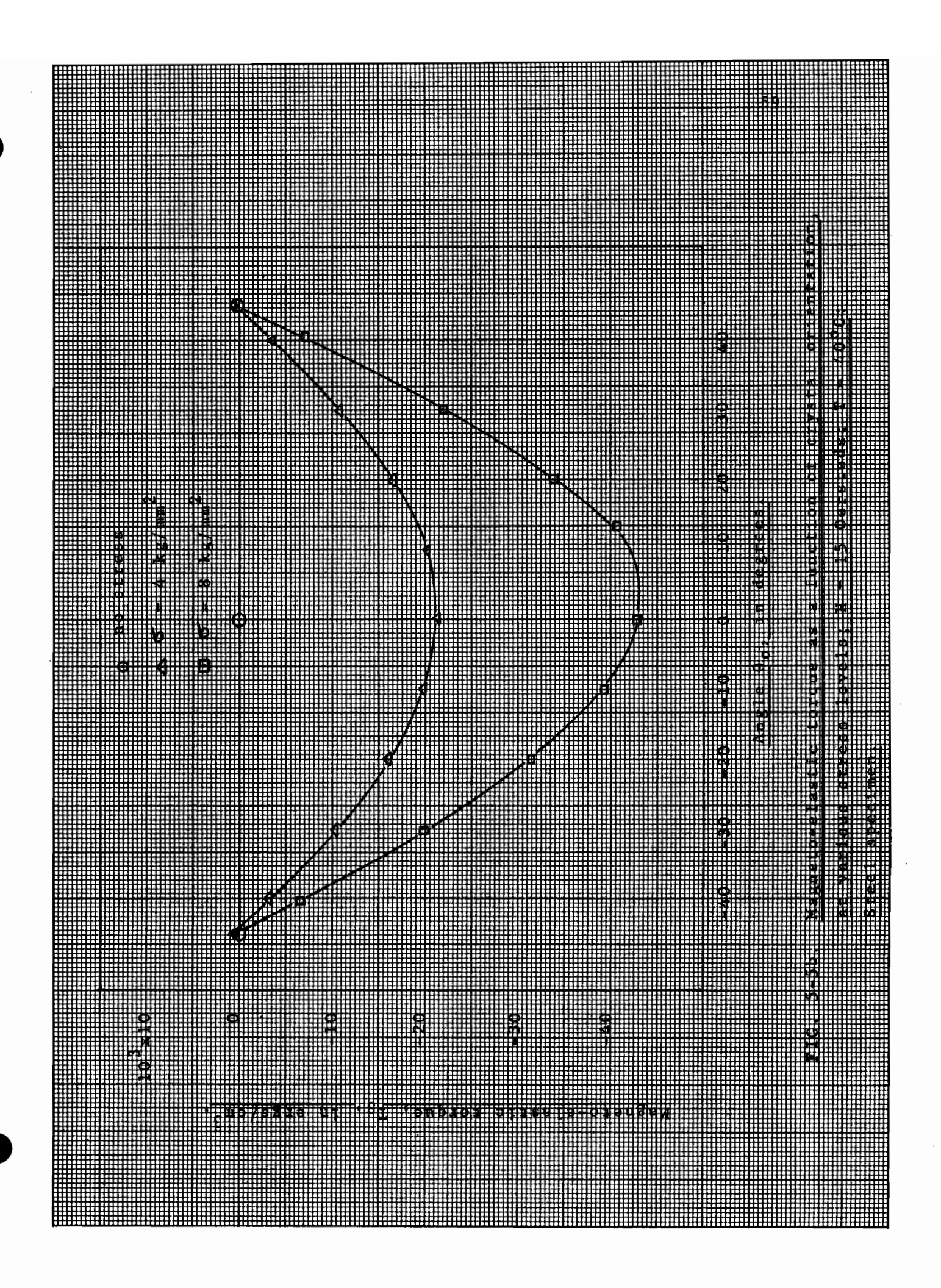
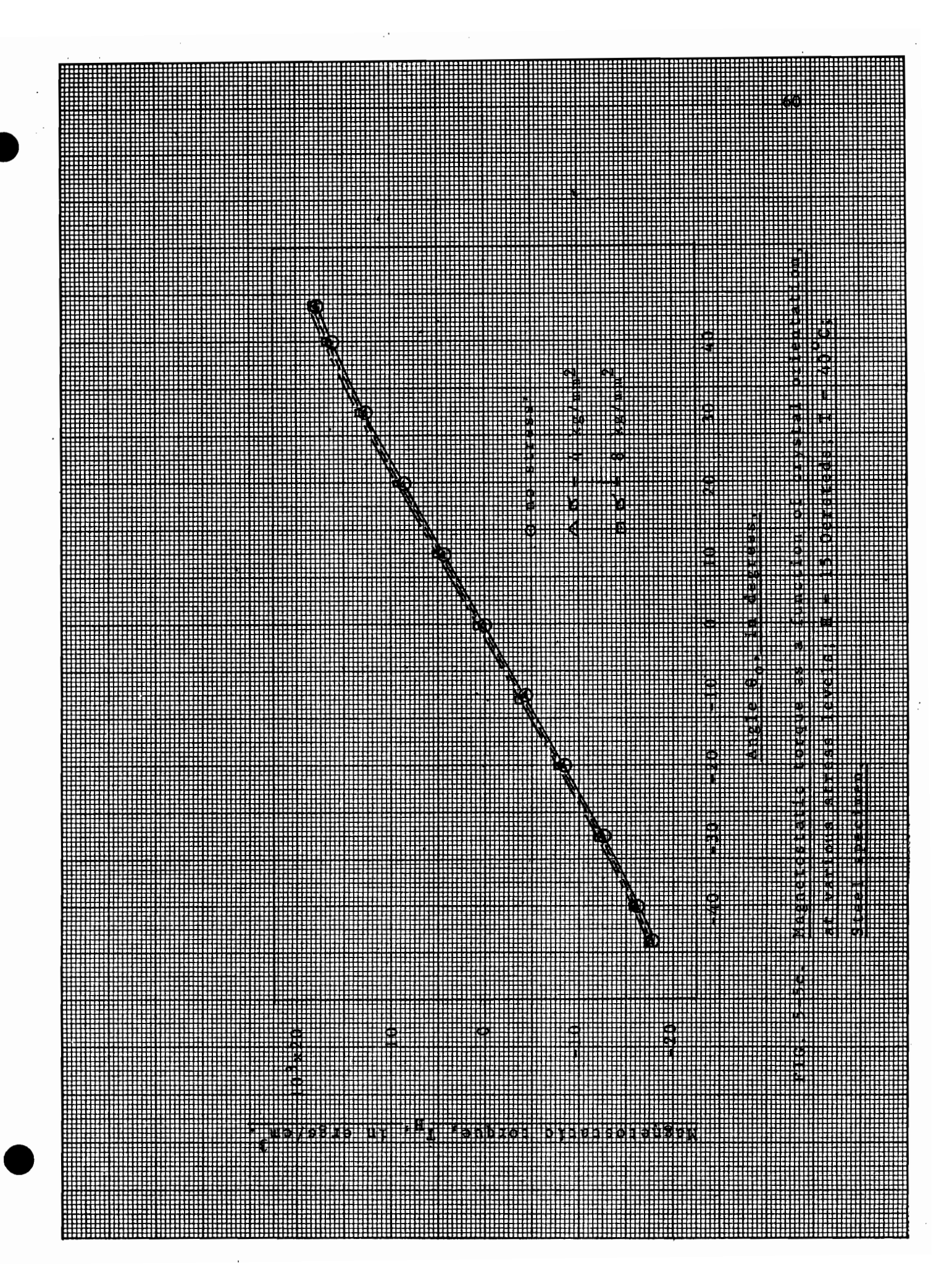


FIG. 5-4. Vector diagrams showing effect of applied stress on the orientation of $\frac{1}{M_S}$. Steel torque tube; H = 15 Oersteds; T = 40° C.







of change is quite large making the anisotropy torque the dominant factor in determining the equilibrium position of M_S . As the stress level goes up, the magneto-elastic energy and torque increase. The anisotropy torque increases too, while the magnetostatic torque remains almost unchanged. At high stress levels, i.e. above 10 kg/mm², the magneto-elastic torque becomes the dominant factor, thus resulting in the curvature of the axial induction versus stress characteristic.

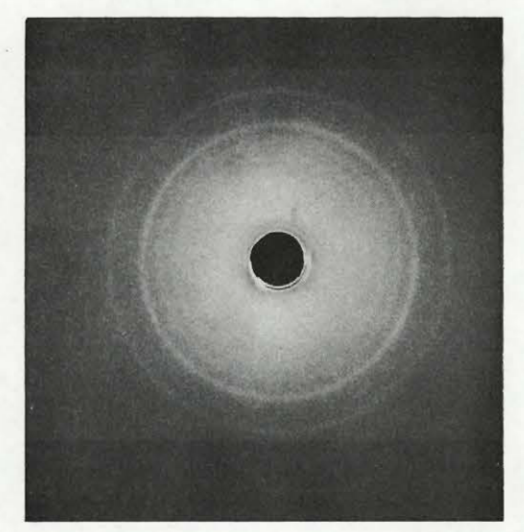
A point of interest is that the greatest variations in magneto-elastic torque occur at θ_0 =0 and the smallest ones at θ_0 = $\pm 45^\circ$; this implies that to achieve the highest stress-sensitivity from steel torque meters, one must use materials with a preferred crystal orientation, namely, with a cube edge along the axis of the tube. Random crystal orientation results in a fairly good stress-sensitivity (of the order of 70% of the preferred orientation), while crystal orientation with a face diagonal along the tube axis, gives a very low sensitivity.

5.3 Crystal Orientation

As has been previously discussed, a certain degree of crystal orientation may exist in cold-drawn steel tubing. In accordance with the results of Norton's investigation, the two cases of possible crystal orientation were analysed. It was found that, in both cases, the stress-sensitivity was extremely low (approximately one hundredth of the random crystal orientation sensitivity). As this did not accord with the experimental results, it was suspected that a random crystal orientation might exist in the specimens. This was confirmed by an X-ray investigation of the possible crystal orientation in a specimen cube cut from the material used in the construction of the steel torque meters. X-ray pictures of the three sections of the cube were taken (Fig. 5-6); the



(a) Longitudinal



(b) Transverse



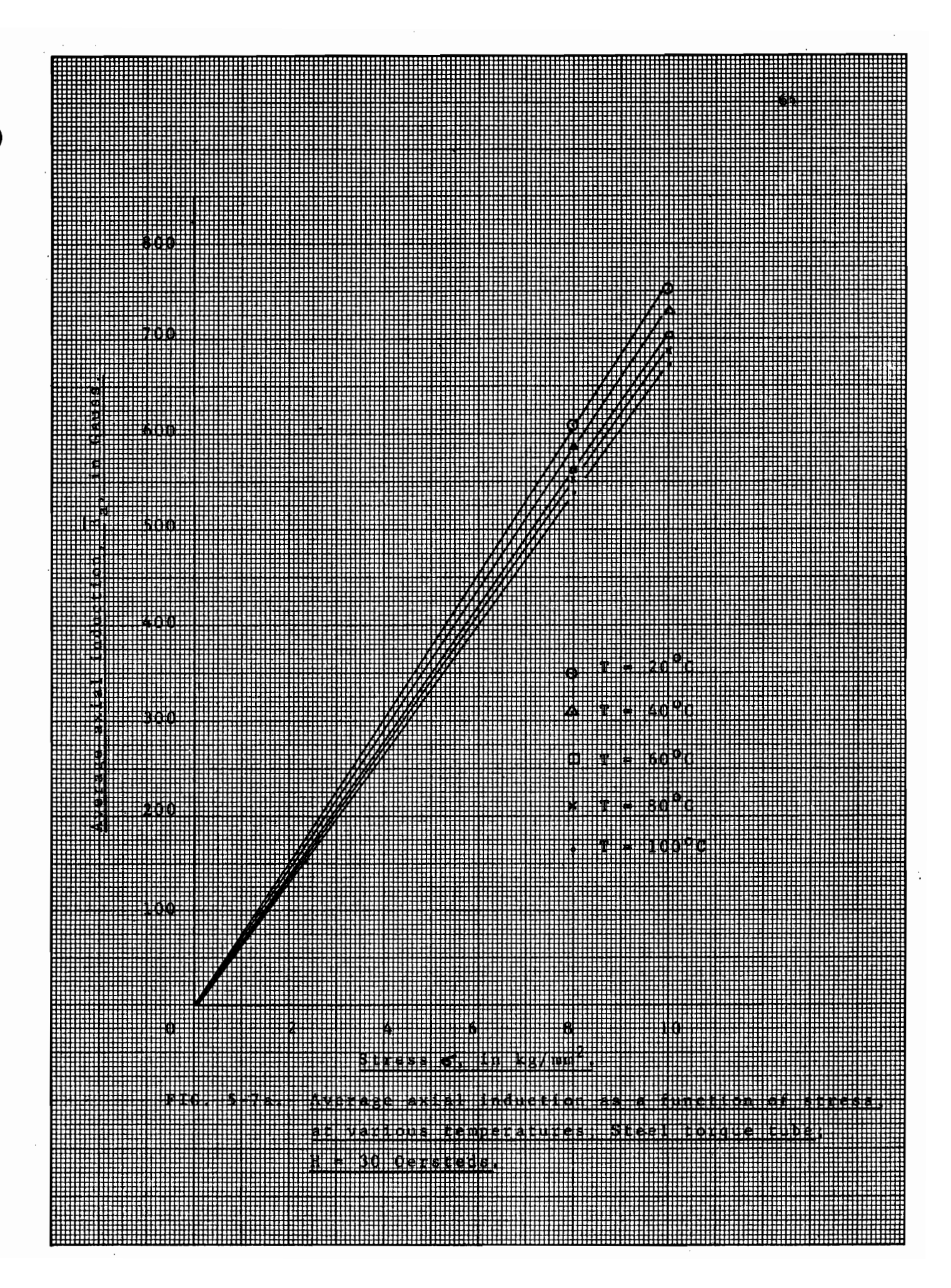
(c) Tangential

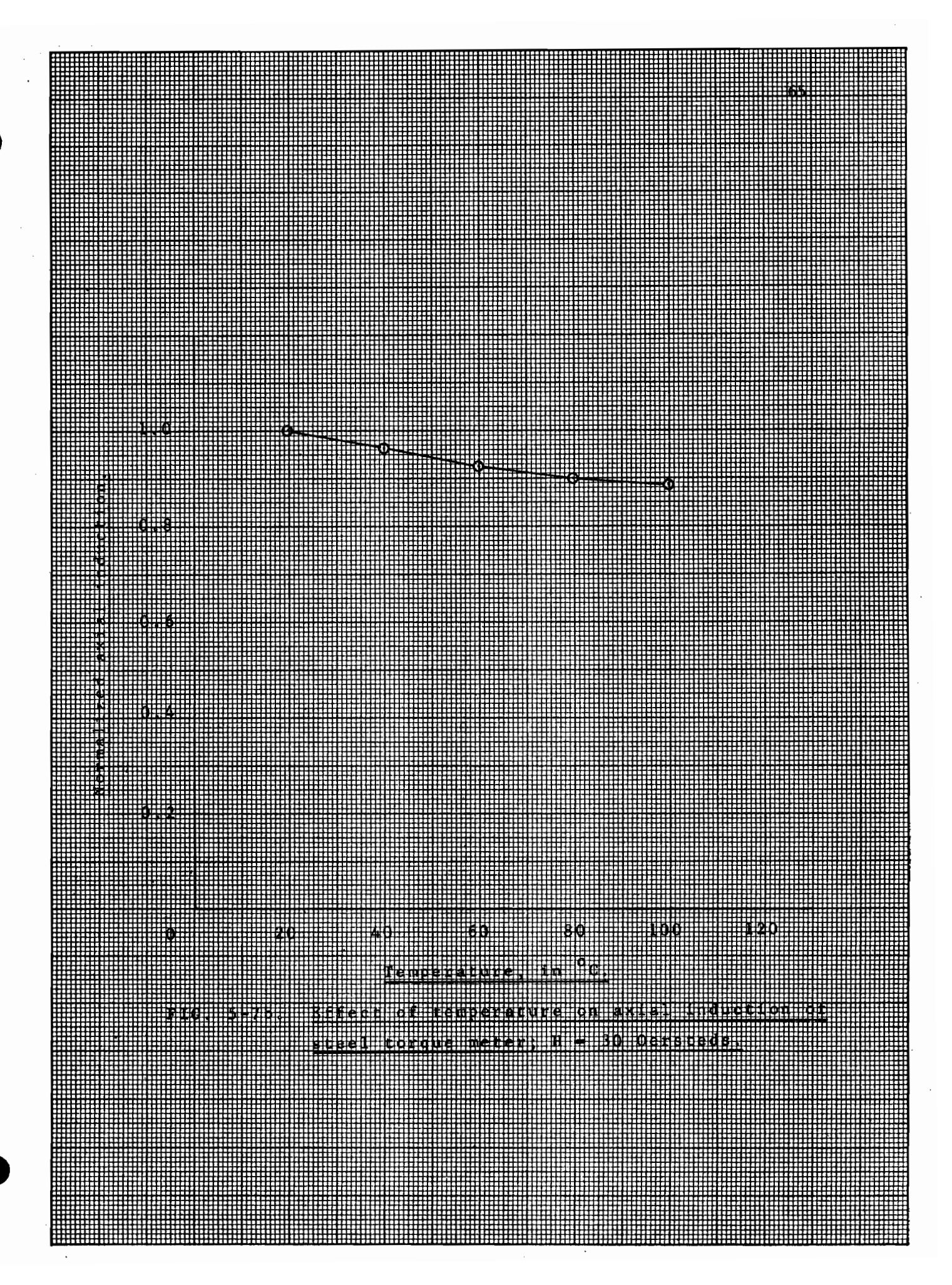
FIG. 5-6. Actual patterns of cold-drawn seamless steel tubing.

uniform intensity circles 20,21 clearly indicate a random crystal orientation in all directions.

5.4 Effect of Temperature

Using the proper values of constants, given in Table 4-1, the axial induction was calculated for temperatures up to 100°C, as shown in Fig. 5-7. The axial induction decreases with increasing temperature, rapidly at first and very slightly at higher temperatures. It is, thus, desirable to operate the torque meter at temperatures around 80°C in order to minimize the effect of temperature on the axial induction. This temperature dependence does not accord with the experimental results, as is expected, since the anisotropy and magnetostriction constants used are those of iron.





5.5 Nickel Torque Meter

A similar analysis was adopted for the nickel torque meter, with the exception that at temperatures below 80° C, the body diagonal of the nickel crystal is the direction of easy magnetization (Fig. 5-8 and 5-9).

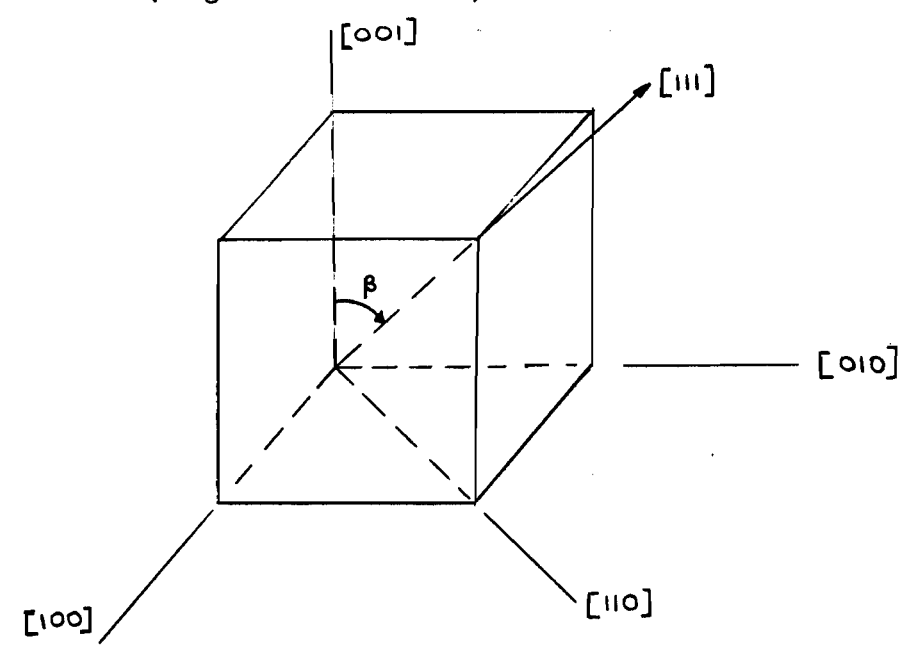


FIG. 5-8. Nickel crystal with Miller indices indicating various directions.

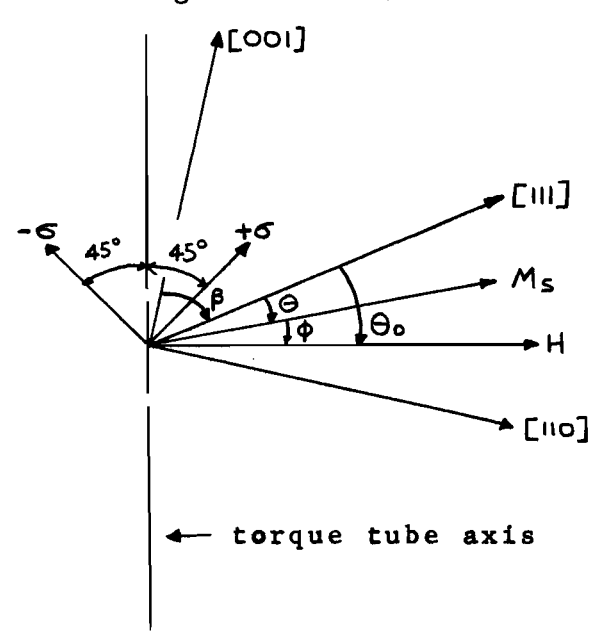


FIG. 5-9. Vectors and angles used in calculating the axial component of magnetization.

It is assumed that \overrightarrow{M}_S lies in the plane of [111] and \overrightarrow{H} , namely (1 $\overline{10}$), for reasons already outlined. The positions of stable equilibrium of \overrightarrow{M}_S are determined by minimizing the total magnetic energy (see Appendix C). This gives

$$\frac{K_{1}}{48} \left[-4\sin^{2}(\theta_{0}-\phi) + 8\sqrt{2}\cos^{2}(\theta_{0}-\phi) - 14\sin^{4}(\theta_{0}-\phi) - 8\sqrt{2}\cos^{4}(\theta_{0}-\phi) \right]$$

$$+\frac{K_{2}}{576} \left[-3\sin^{2}(\theta_{0}-\phi) + 6\sqrt{2}\cos^{2}(\theta_{0}-\phi) - 28\sin^{4}(\theta_{0}-\phi) - 16\sqrt{2}\cos^{4}(\theta_{0}-\phi) \right]$$

$$-23\sin^{6}(\theta_{0}-\phi) + 10\sqrt{2}\cos^{6}(\theta_{0}-\phi) \right] + \frac{1}{8} \in \left[(\lambda_{100} - \lambda_{111}) \left\{ 4\sqrt{2}\sin^{2}(2\theta_{0}-\phi) - 7\cos^{2}(2\theta_{0}-\phi) \right\} + 3(3\lambda_{100} + 5\lambda_{111})\cos^{2}\phi \right] = HM_{S}\sin^{4}\phi$$

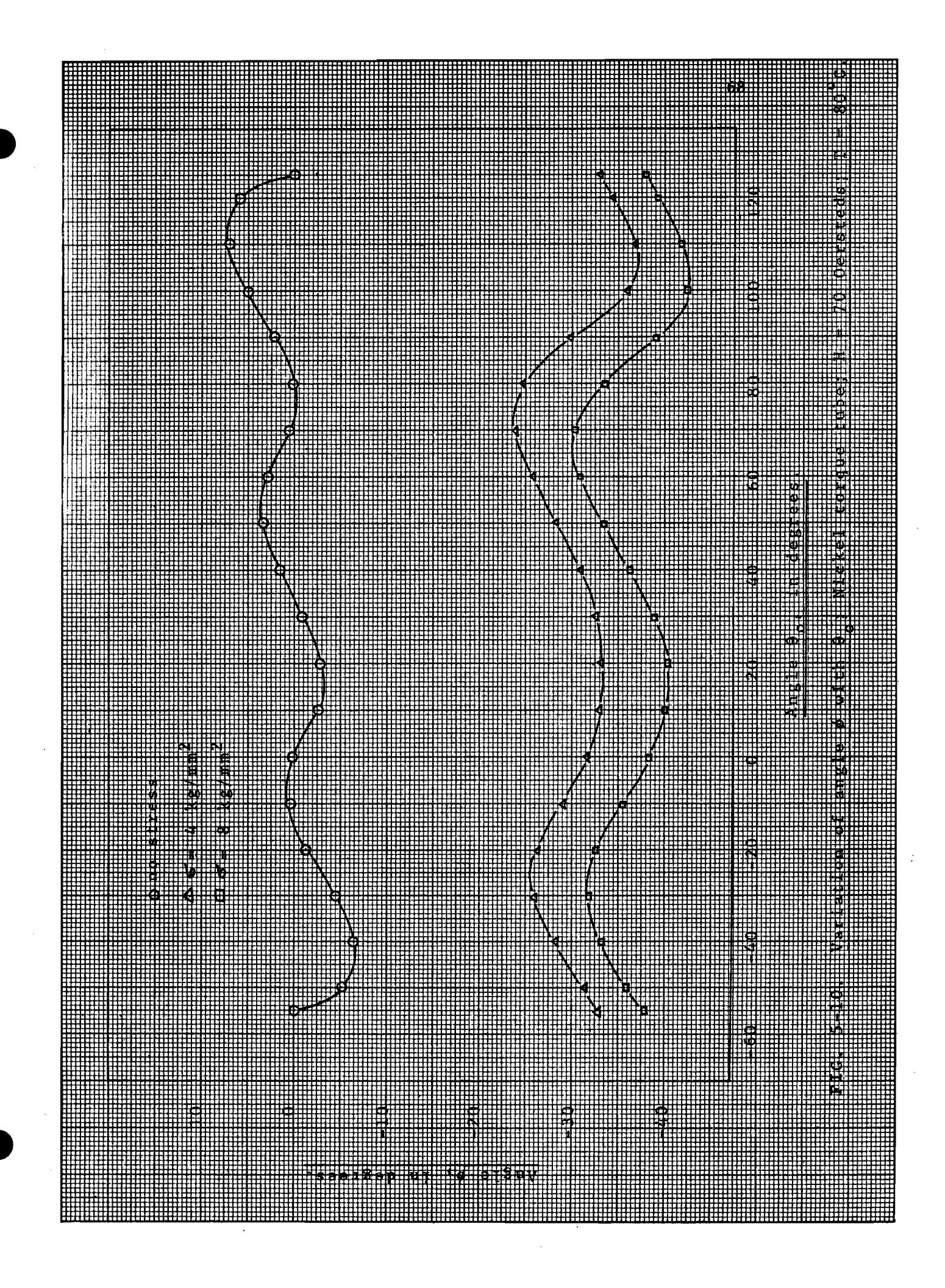
$$(5.3)$$

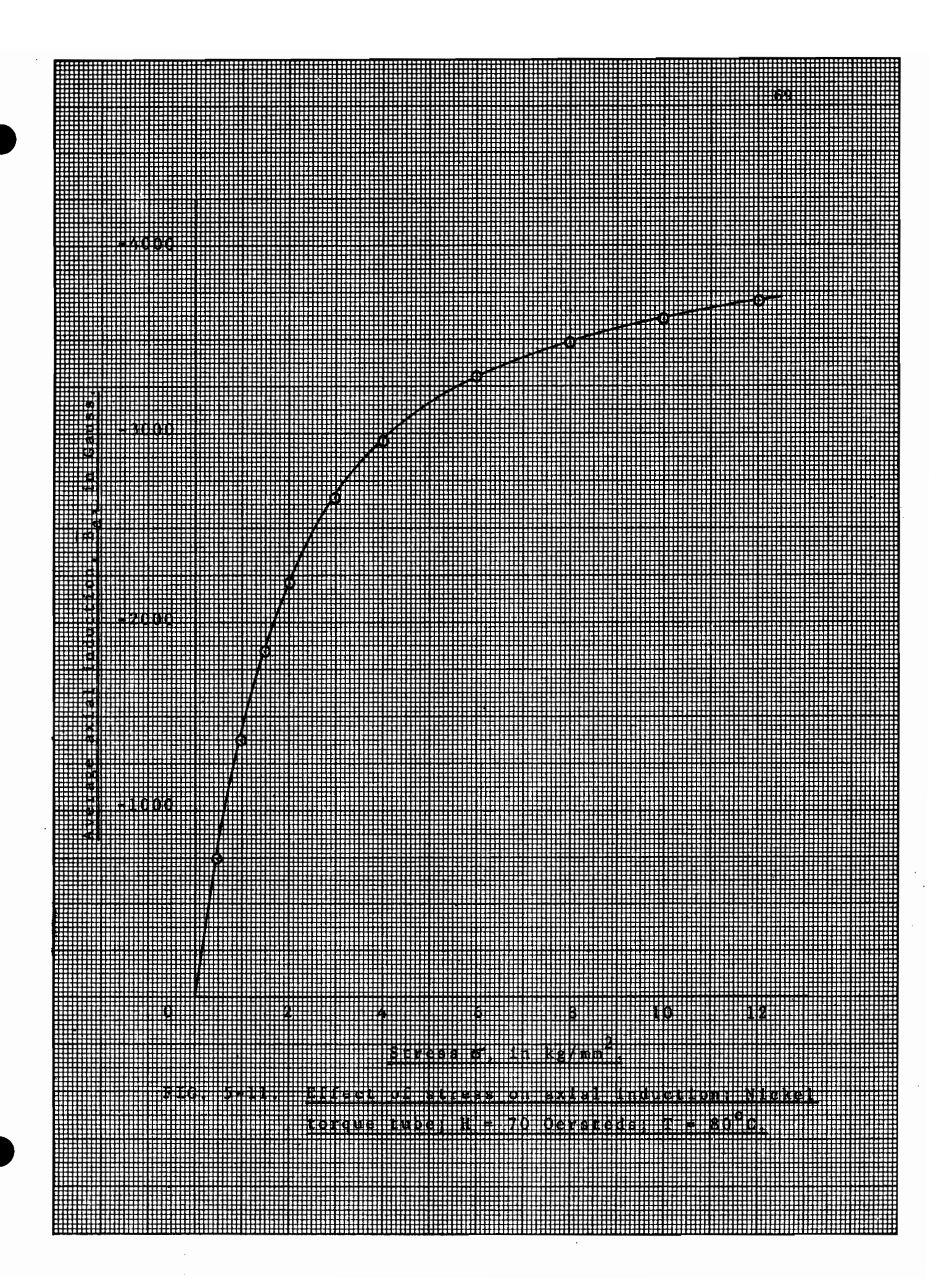
and an axial induction $B_a = B_S \sin \phi$.

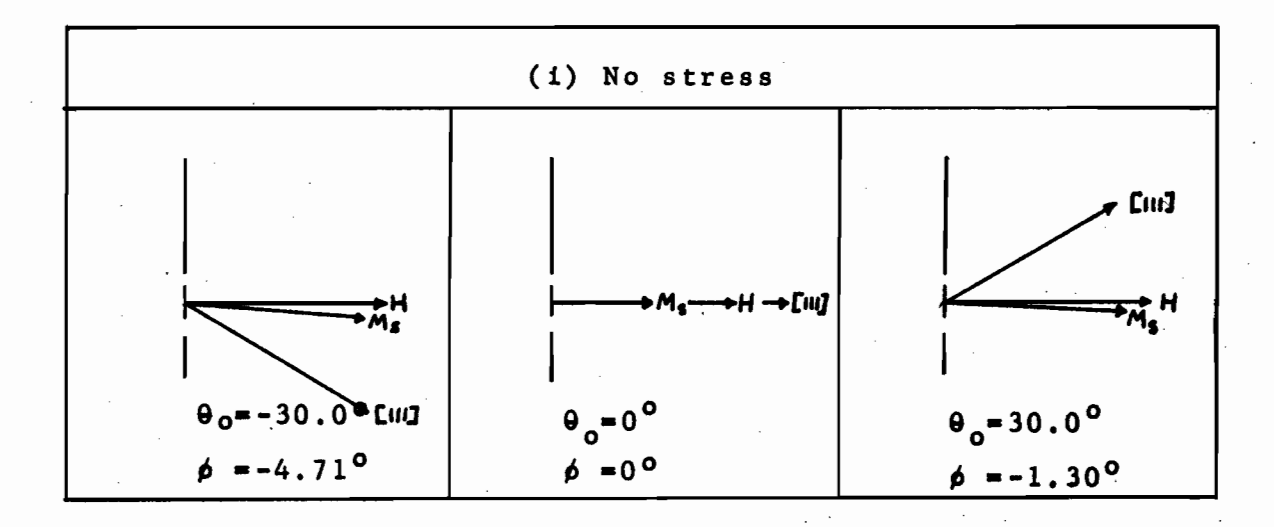
As before, for random crystal orientation, the average axial induction is given by equation (5.2), with θ_0 varying from -54°.44' to +125°.16'. Solving equation (5.3) for ϕ , by an iteration method on the IBM 7040 digital computer, and using equation (5.2) to calculate \overline{B}_a , the variation of angle ϕ with θ_0 and of \overline{B}_a with stress, are shown in Fig. 5-10 and Fig. 5-11, respectively, while Fig. 5-12 gives typical vector diagrams indicating the position of \overline{M}_S at various stress levels. The rotational torques, tending to align \overline{M}_S , are given in Fig. 5-13.

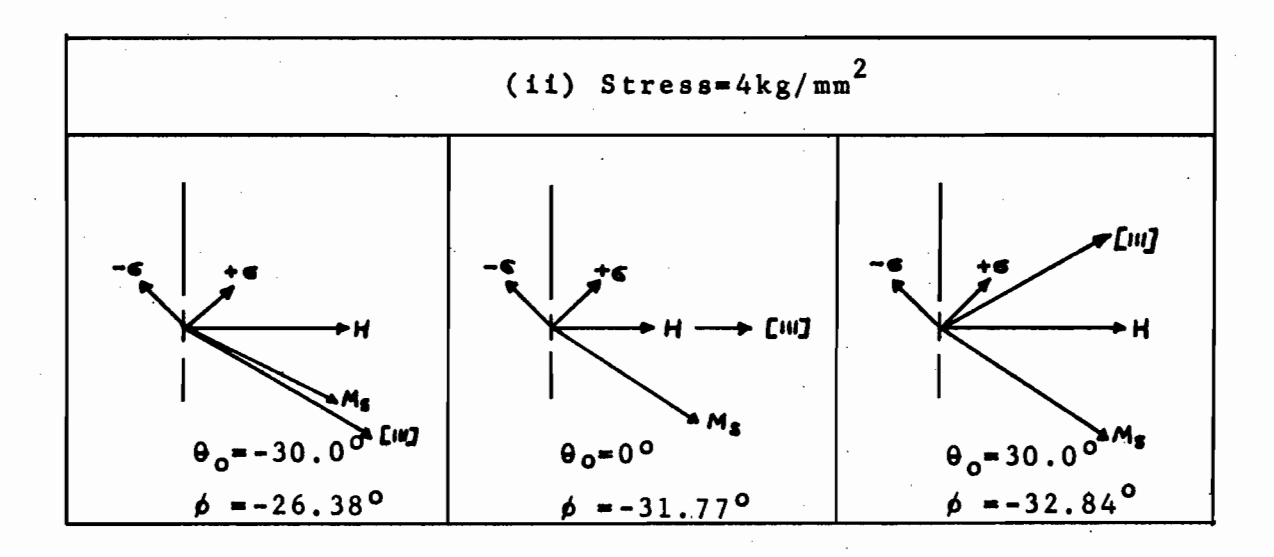
The negative sign of the axial induction merely indicates the appropriate direction of magnetization of nickel. This is opposite to the direction of the steel specimen, as is expected, since, although both materials exhibit negative magnetostriction at saturation, they have an opposite sign for the first anisotropy constant K_1 , as shown in Table 4-1.

When stress is applied to the specimen the magneto-elastic torque tends to rotate $\stackrel{\rightarrow}{M}_S$ in a direction closer to the compressive stress, against the action of the anisotropy and









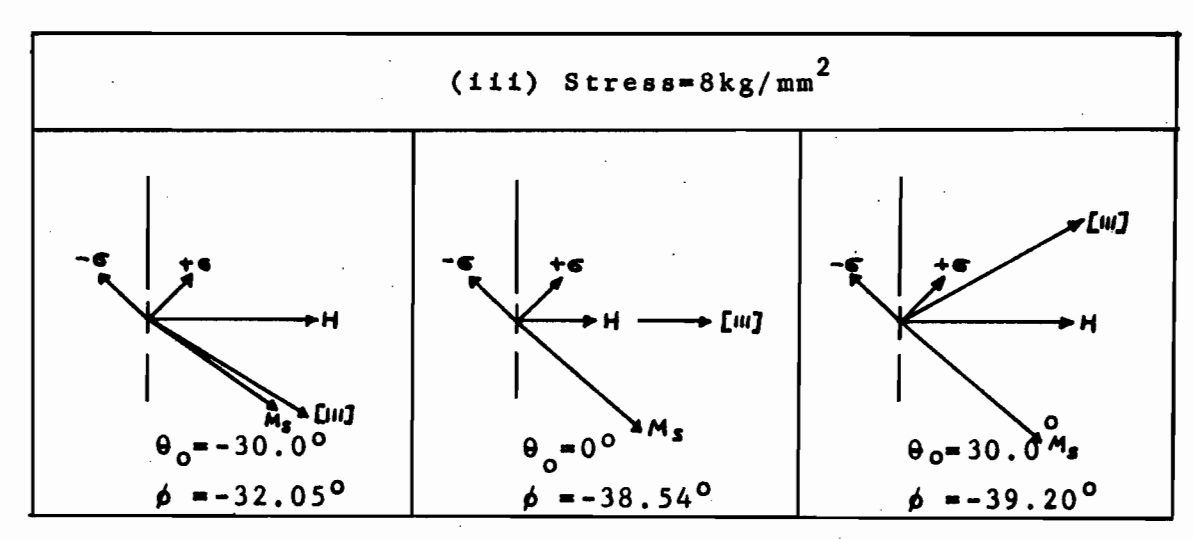
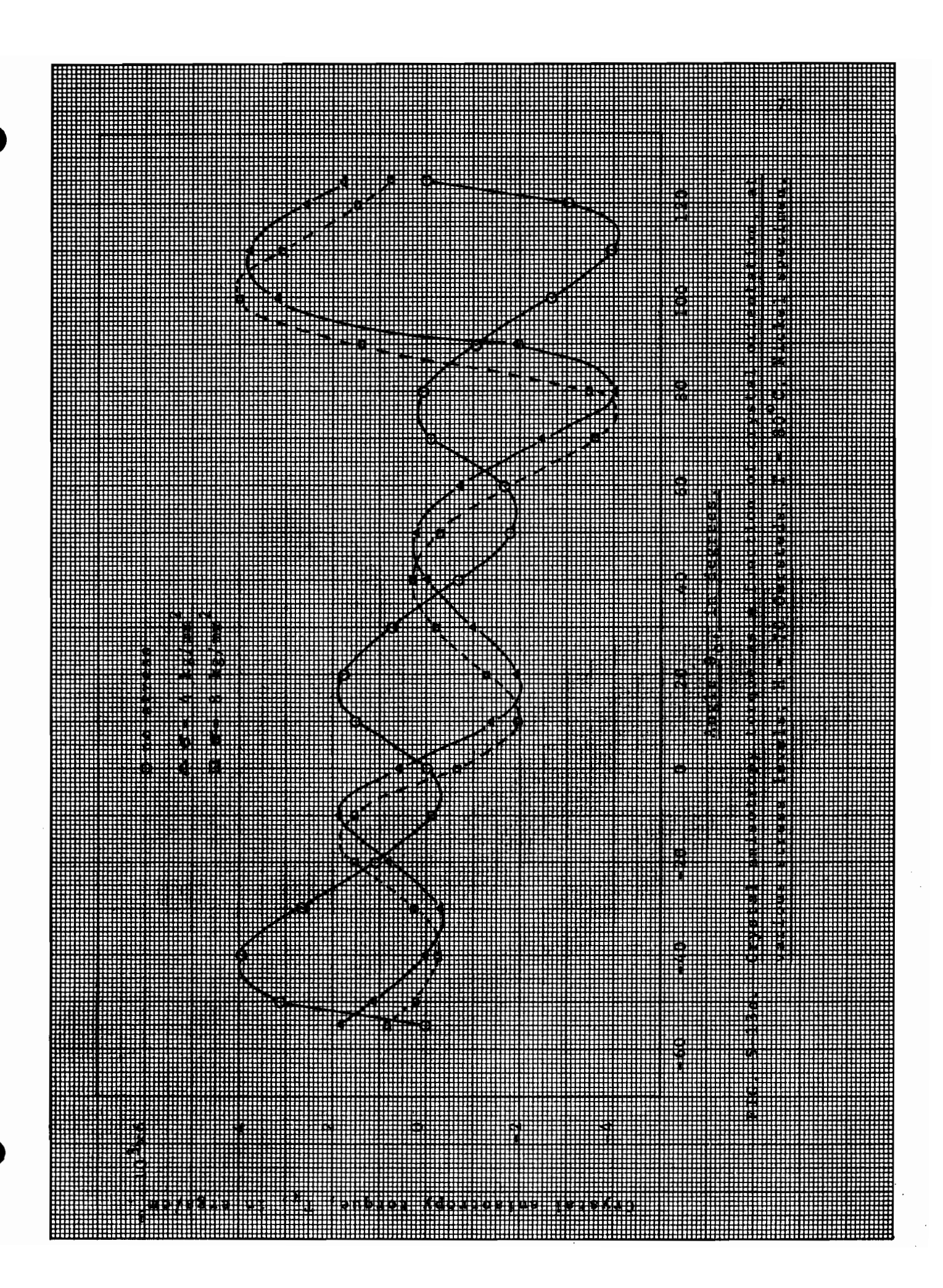
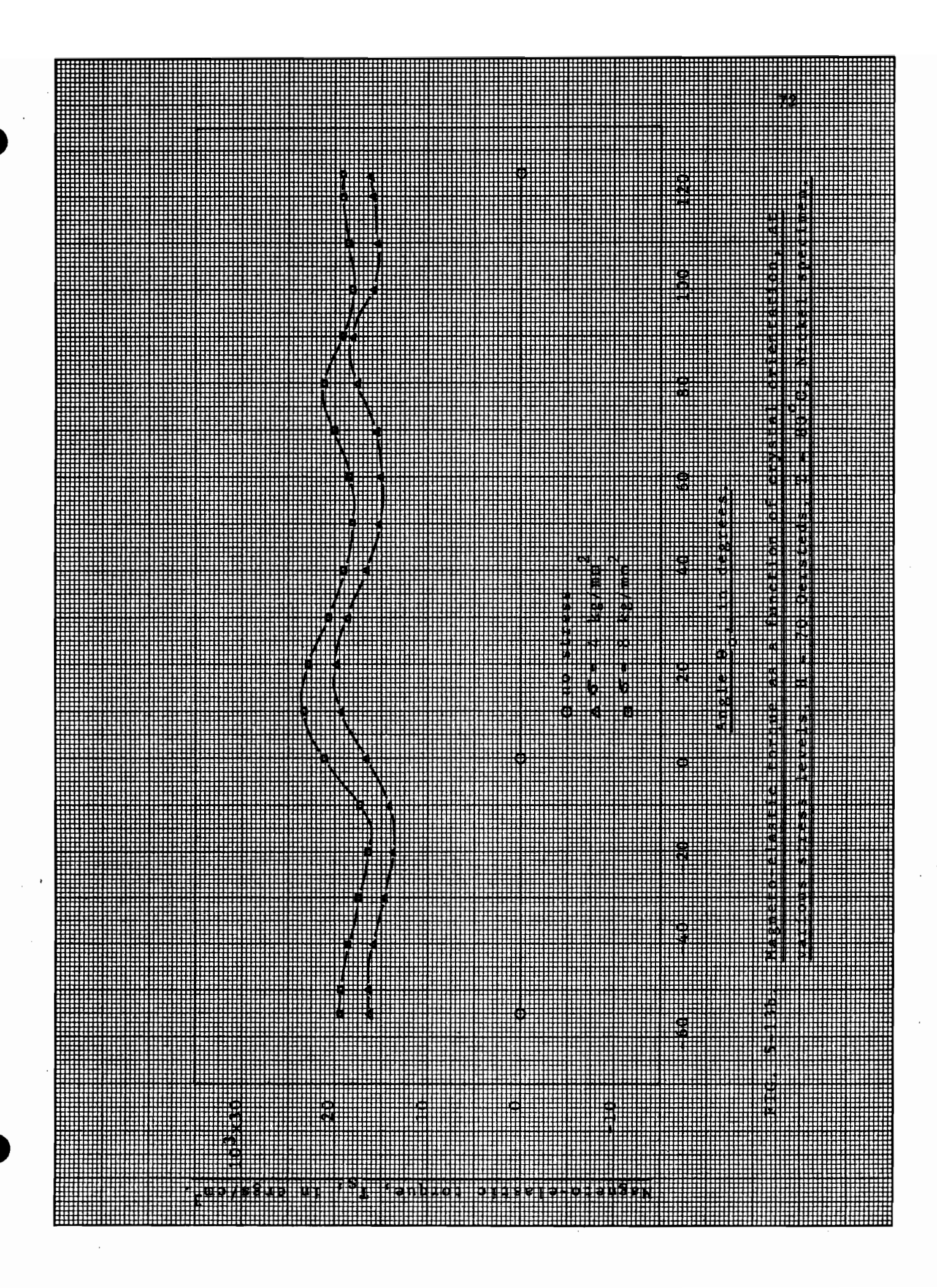


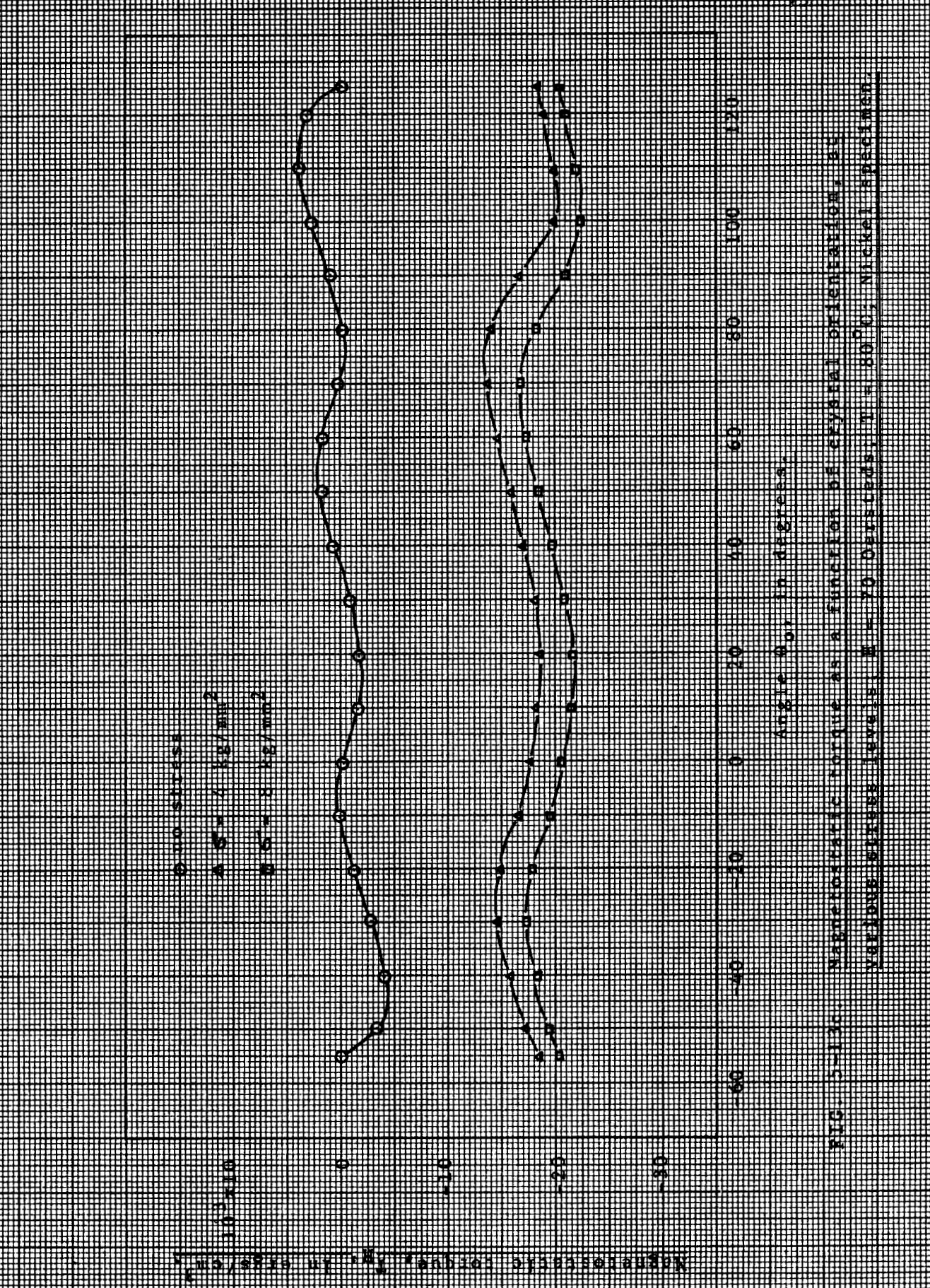
FIG. 5-12. Vector diagrams showing effect of applied stress on the orientation of M_S . Nickel torque tube;

H = 70 Oersteds; T = 80° C.









magnetostatic torques, that tend to align \overline{M}_S along the [111] and \overline{H} , respectively. Hence, up to a shear stress of approximately 2 kg/mm², the axial induction, \overline{B}_a , varies linearly with stress.

As the stress is further increased, the magneto-elastic torque increases quite rapidly, until a stress level is reached, when it becomes the dominant factor in aligning \vec{M}_S . Any further increase in stress, has a slight effect on the orientation of \vec{M}_S and, hence, on the value of \vec{B}_a . This saturation value of \vec{B}_a corresponds to approximately two-thirds of \vec{B}_S , namely 4,000 Gauss.

Thus, contrary to the case of steel, nickel, due to its high magnetostriction and low anisotropy, approaches saturation in the axial direction, at fairly low stress levels, and, hence, becomes unsuitable for the construction of torque meters operating at fairly large stress levels.

5.6 Crystal Orientation

Fig. 5-13b shows that the variations in magneto-elastic torque with stress are of approximately equal magnitude, irrespective of the crystal orientation; hence, there is practically no preferred crystal orientation in nickel, giving maximum stress sensitivity. The results of an assumed crystal orientation with a body diagonal along the tube axis, i.e. θ_0 =0, are compared in Table 5-1 with those of random orientation. It can be seen that no appreciable difference in B_a exists.

	Axial Induction, B _a , (Gauss)	
Stress (kg/mm ²)	Random Orientation	Preferred Orientation, 0 = 0
0	0	.0
0.5	-737.5	-824.0
1.0	-1358.5	-1530.0
1.5	-1834.2	-2000.0
2.0	-2191.1	-2350.2
2.5	-2461.0	-2590.0
3.0	-2669.0	-2830.5

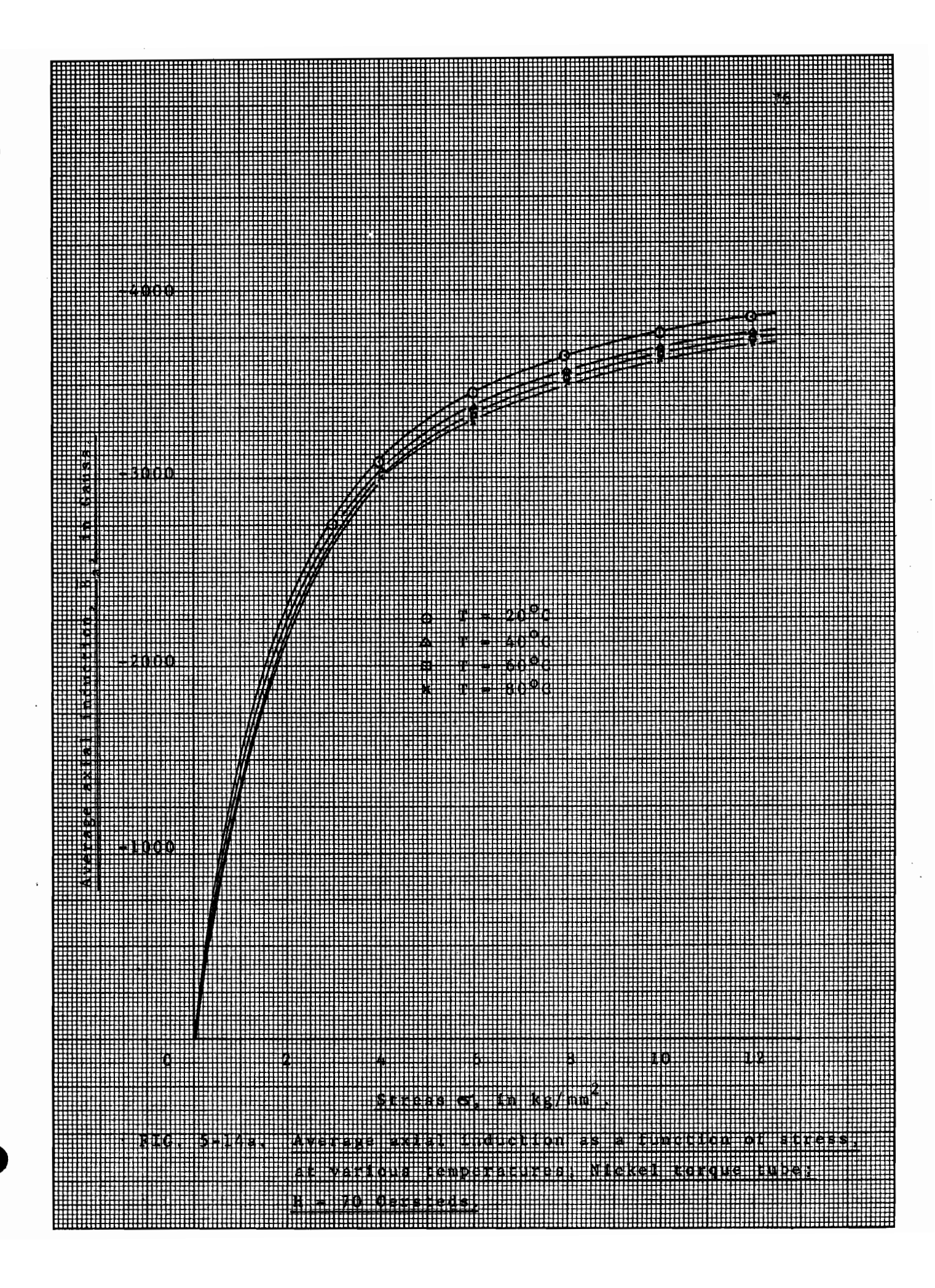
TABLE 5-1. Effect of crystal orientation on axial induction of nickel torque meter; H = 70 Oersteds, T = 80°C.

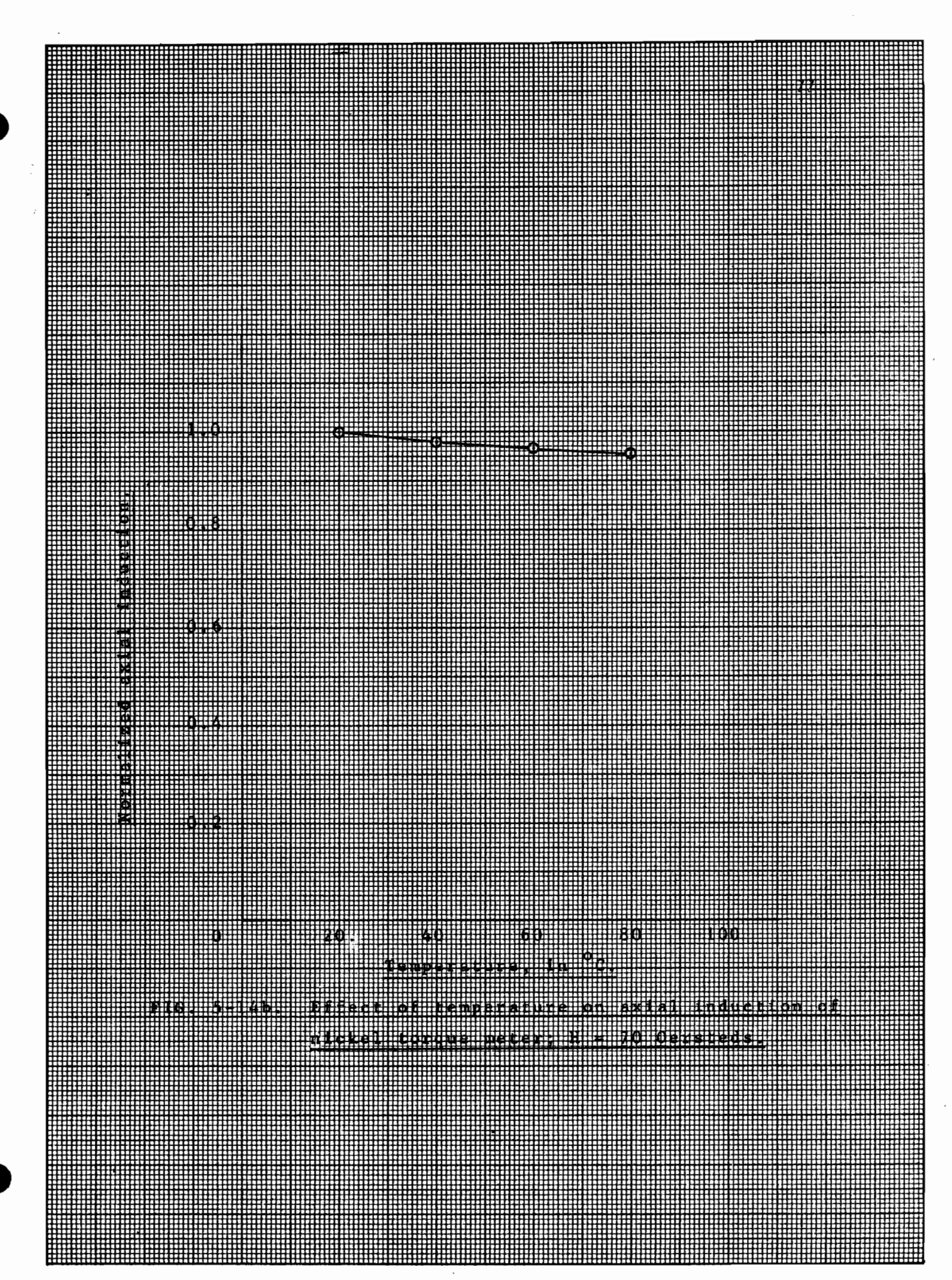
5.7 Effect of Temperature

Temperature changes affect the axial induction as previously discussed. The axial induction decreases with increasing temperature, as shown in Fig. 5-14. Thus for a 60 °C temperature change, the axial induction decreases by 5%.

5.8 Nickel at Temperatures 80-100°C

During the experiments with nickel torque tubes, the temperature of the specimens varied from 70 to 110°C, depending on the exciting level and frequency. As, in this temperature range, changes occur in the direction of easy magnetization, the above range of temperature was investigated.





In the range $80\text{-}100^{\circ}\text{C}$, nickel has the face diagonal as a direction of easy magnetization. The results of the analysis (see Appendix C) are shown in Fig. 5-15. It should be noted that for small stresses, up to $1.5\,\text{kg/mm}^2$, the axial induction increases as the temperature rises from 80 to 100°C . Contrary to the case of steel, the magnitude of the variation of \overline{B}_a depends largely on the operating stress level. This is to be expected, as at low stress levels the orientation of \overline{M}_S , and hence the amplitude of \overline{B}_a , depends largely on the anisotropy which changes appreciably with temperature, while at high stress levels, it depends largely on the magneto-elastic torque.

Hence, this point should be borne in mind, when choosing suitable stress level of operation of a nickel torque meter.

5.9 Nickel at Temperatures above 100°C

Above 100° C, the cube edge of the nickel crystal becomes the direction of easy magnetization. The analysis carried out (see Appendix C) yielded similar results to those of Fig. 5-15, for T= 100° C.

5.10 Correlation of Theory with Experiment

The axial induction B_a, predicted from theory, can be used to obtain the pick-up coil signal; the latter is given by:

$$E = C \omega N_p A B_a$$

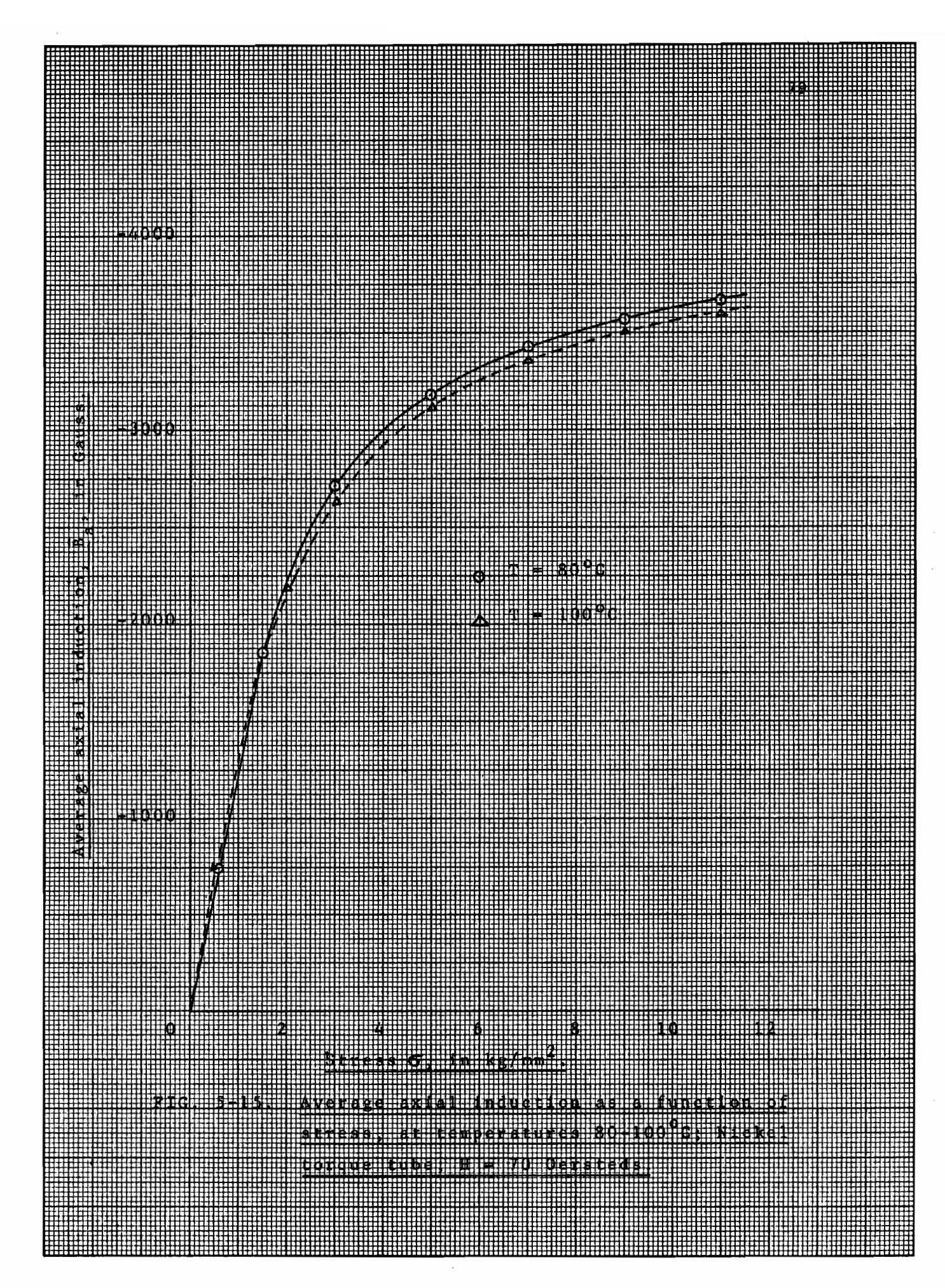
where ω is the circular frequency of the magnetizing current

A the effective cross-sectional area of the tube

N the number of turns of the pick-up coil

E the e.m.f. induced in the coil

C a factor depending on the choice of units.



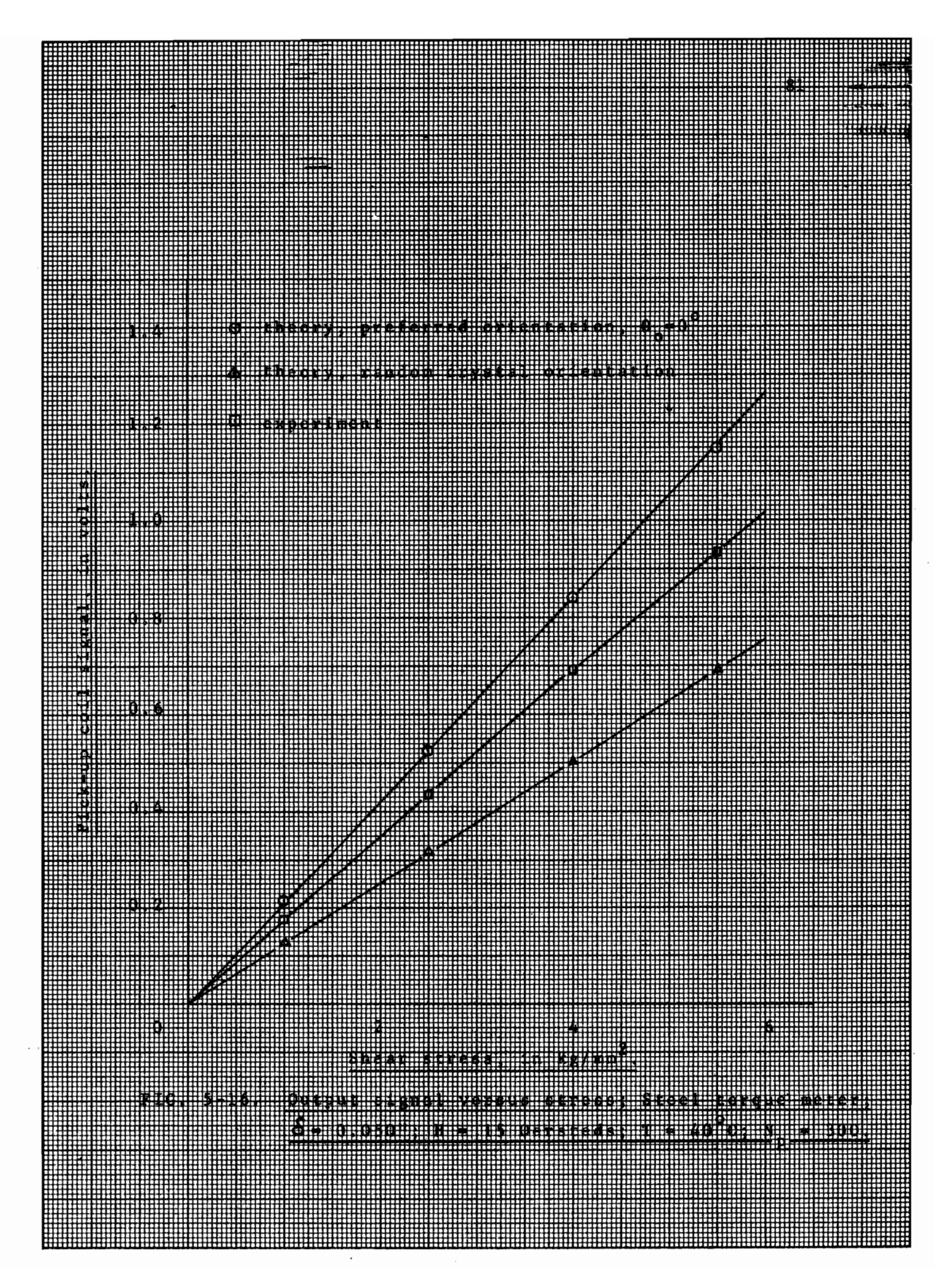
To avoid the introduction of the "skin thickness", a factor that accounts for the screening effect of eddy currents and depends largely on the permeability and resistivity of the material, the experimental results of thin tubes, such as 0.050" thick, are compared to the predicted ones.

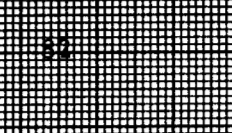
Thus, for steel torque meters, $\delta = 0.050$ ", operating at H=15 Oersteds, T=40°C and f=60 c/s, the results are shown in Fig. 5-16. Similar data are given in Fig. 5-17 and Fig. 5-18 for annealed and stress-relieved nickel torque meters, operating at H=50 and 70 Oersteds, respectively, at a temperature of 80°C.

The agreement between theoretical and experimental results is of the order of 15%. This slight deviation is due to various factors, the most important being the fact that demagnetization, magnetostriction and the effect of eddy currents have been neglected.

5.11 Conclusions

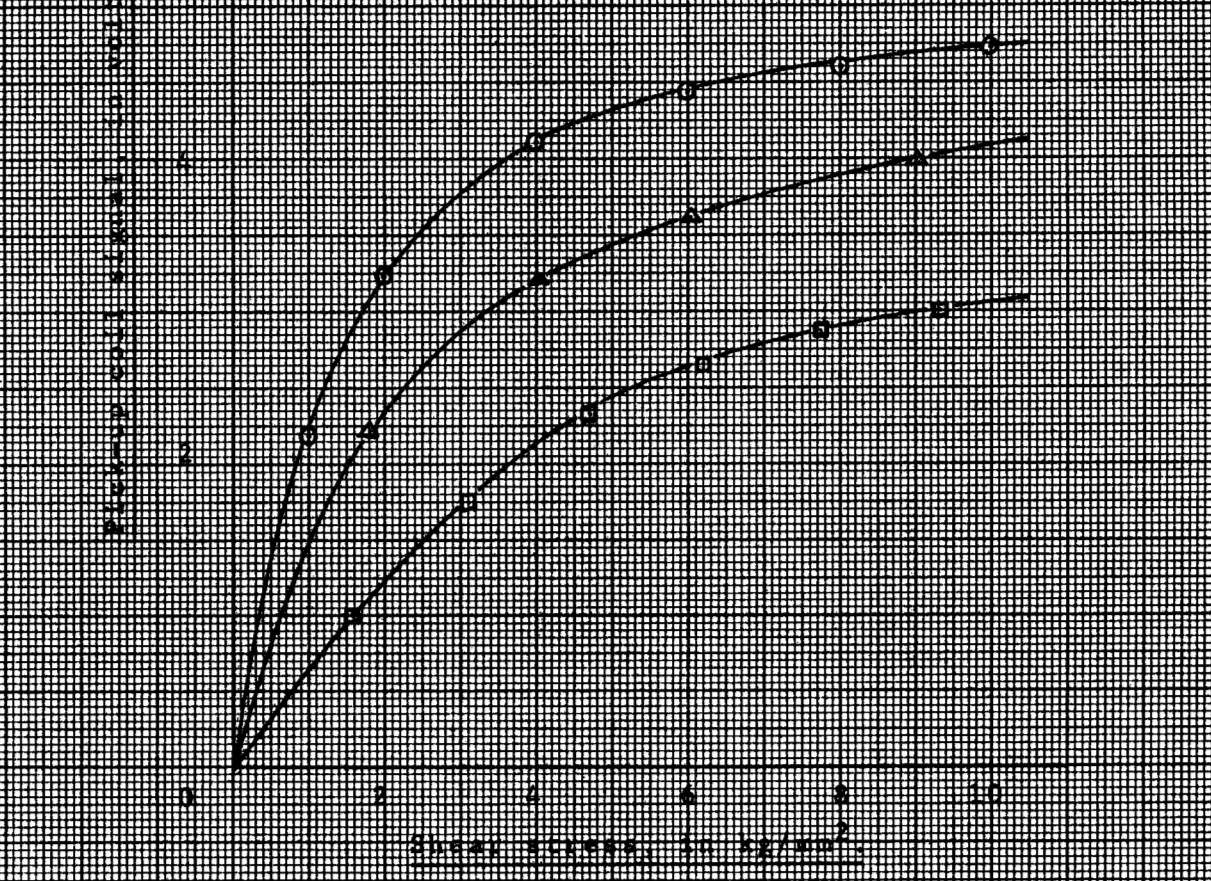
The theory outlined, explains clearly the mechanism of operation of the magnetic-anisotropy torque meter. Its behaviour under various conditions can now be predicted, so that better torque meters can be designed to meet any specific requirement. If linearity in the transfer characteristic is of prime importance, torque tubes made of materials with fairly high anisotropy and moderate magnetostriction constants, should be preferred. The relatively low stress-sensitivity of such a torque meter can be overcome by either increasing the frequency of the magnetizing current or by using more turns on the pick-up coil. For steel torque tubes, an operating temperature of 80°C is to be preferred, irrespective of the stress level, while for nickel torque tubes, temperatures higher than 80°C should be avoided.

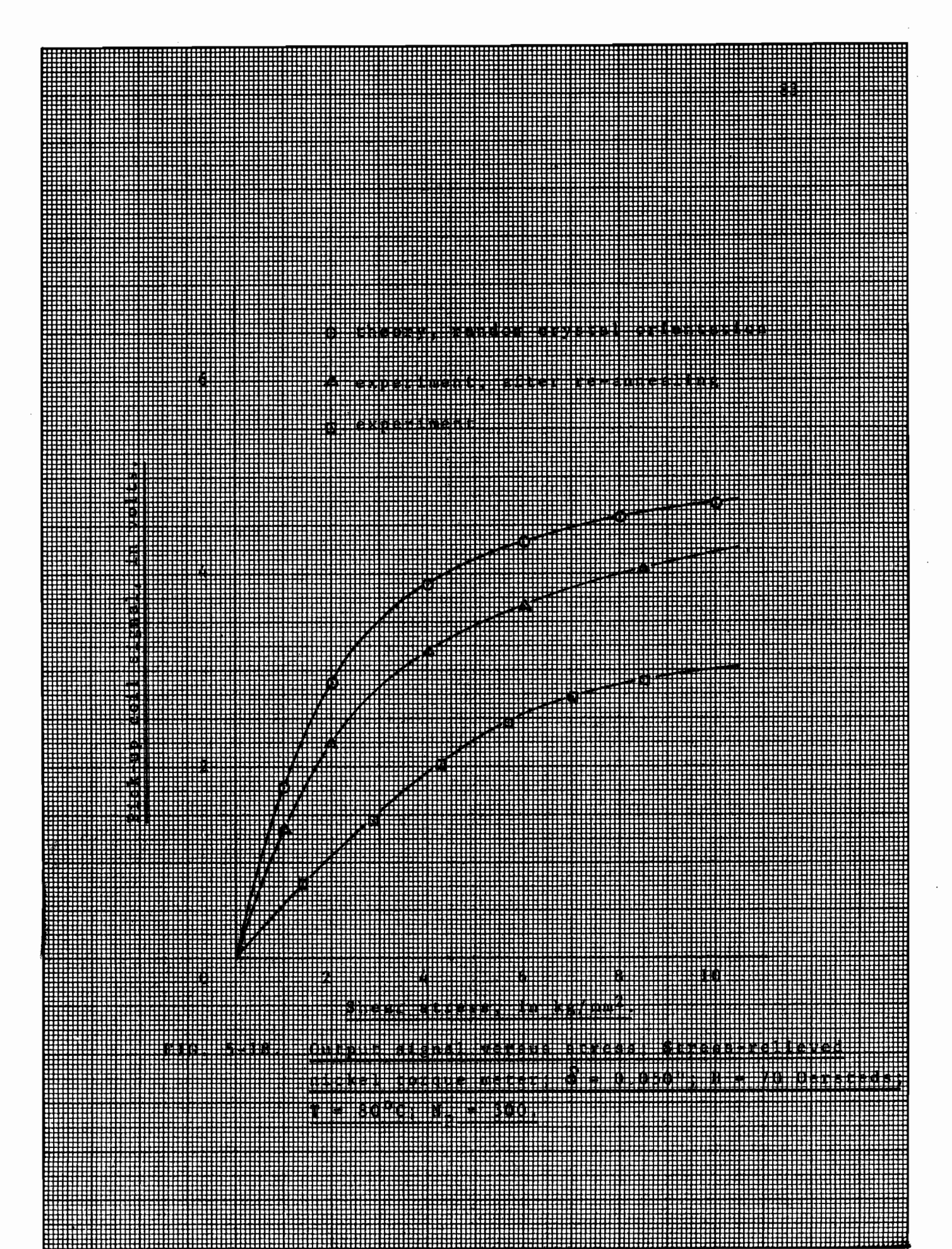






a experiment after 25 binealist





CHAPTER VI

PRECISION MEASUREMENTS

6.1 Introduction

The results of the general survey, as well as the predicted ones from theory, clearly indicate that steel torque tubes of wall thickness approximately 0.100", operating at shear stresses not greater than 2.5 kg/mm 2 approximately, offer greatest hope of successful application.

The factors affecting the performance of such a torque meter and the limits of its performance under optimum conditions were investigated. Affecting the behaviour are:

- (i) Excitation Level,
- (ii) Temperature,
- (iii) Load Impedance,
 - (iv) Frequency,
 - (v) Waveform.

The limits of performance under optimum conditions, i.e. with above factors held within appropriate limits, are defined principally by reproducibility. However, although not vital as reproducibility is, linearity, i.e. the expression of the transfer characteristic by a constant, is most important in a useful precision instrument.

Since the determination of performance limits is a tedious, time consuming business, it is appropriate to separate from it the factors affecting the performance.

6.2 Factors Affecting Performance

These were investigated by using the X-Y recorder preceded by a mechanical chopper to record the transfer characteristic under various conditions, the accuracy being better than 0.2% (d.c. scales of recorder used).

To eliminate items (iv) and (v), experiments were carried out with the magnetizing coil connected to the 60c/s mains at times when the load was small, i.e. during the evenings. The supply frequency was checked at regular intervals during the experiments, by means of a Beckman digital counter and the period was found to vary from 16.65 to 16.67 msec.

To control and vary the temperature of the torque tube, a heating element, bifilar wound, and d.c. operated to eliminate stray a.c. magnetic fields, was placed inside the tube.

A complete set-up of the circuit used, is shown in Fig. 6-1, the load resistor R_L intended to simulate a modern moving coil instrument. The purpose of the mechanical chopper, connected at the output of the pick-up coil and driven by a 60c/s phase-shifter, was twofold: the circuit was now phase-sensitive and harmonics present in the pick-up coil signal were attenuated, as described in Chapter VIII.

By properly adjusting the phase of the phase-shifter, the quadrature component in the signal was completely eliminated at the input to the recorder.

6.2.1 Excitation Level

The normal exciting current is that which seems most generally satisfactory as a compromise between good saturation and heating of the torque tube.

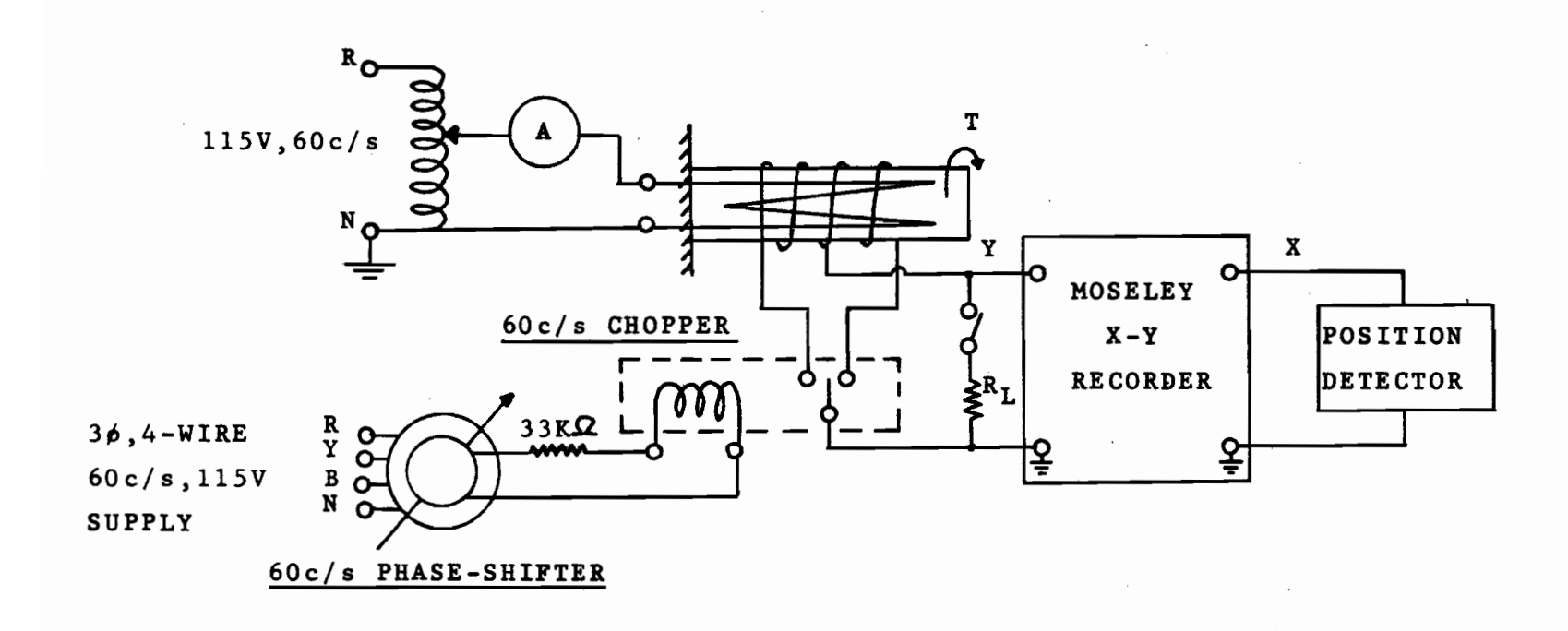


FIG. 6-1. Circuit diagram of set-up used for precision measurements.

For the particular tube tested, 1.30 amps. was the normal exciting current, the temperature stabilizing at 80° C. Thus, keeping the temperature constant at 80° C, the transfer characteristic of the device was recorded at exciting currents varying from 80 to 120% normal.

The sensitivity, as a function of exciting current, is shown in Fig. 6-2. A $\pm 10\%$ change in the exciting current has no appreciable effect on the sensitivity, while a $\pm 20\%$ change, lowers it by 1%.

6.2.2 Temperature

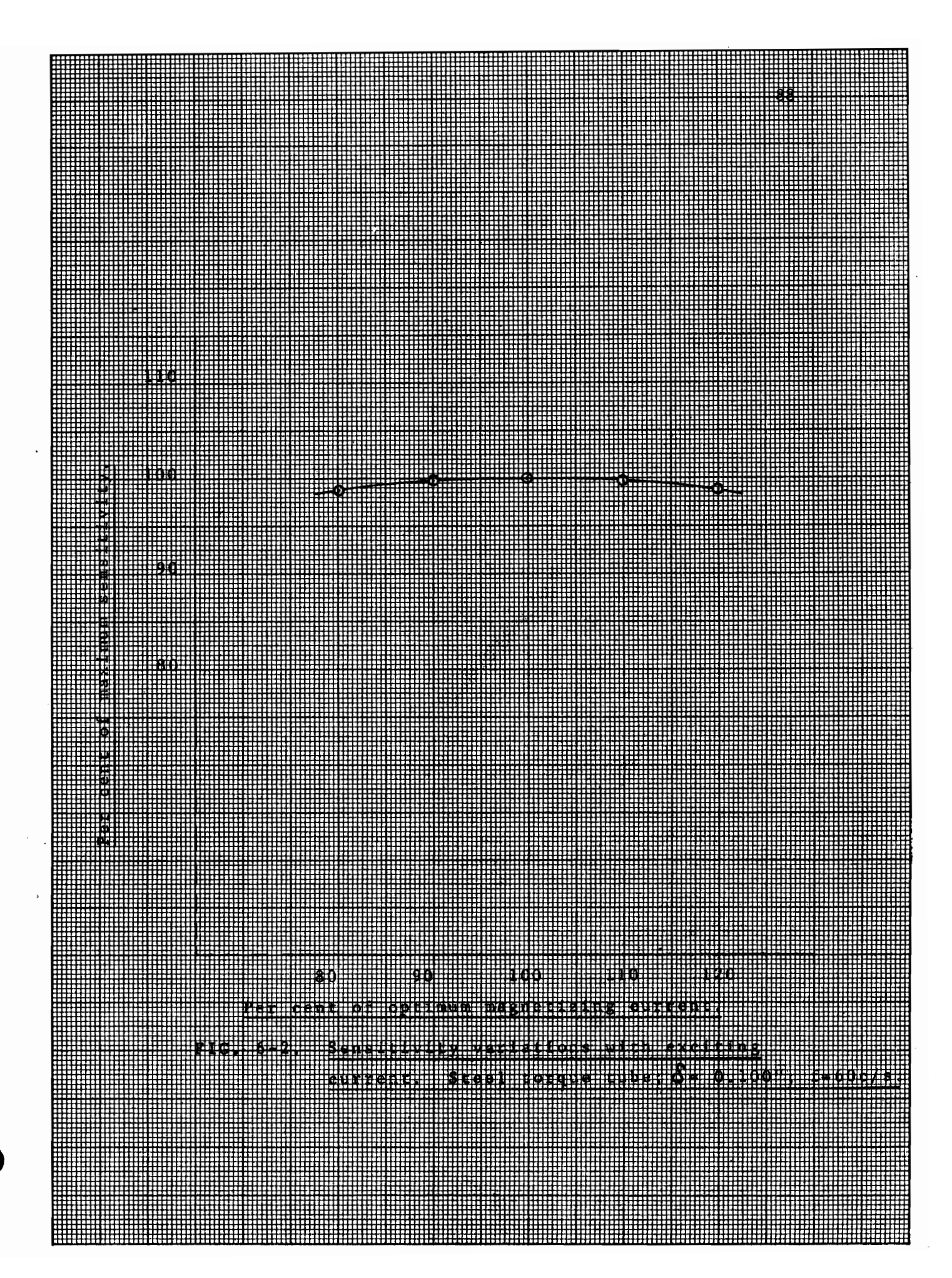
With normal excitation and temperature, the transfer characteristic was recorded. This was repeated at various temperature levels, using either the heater or a cooling fan to keep the temperature of the torque tube constant. It was observed that a $\pm 30^{\circ}$ C change in the normal operating temperature had no effect on the sensitivity of the torque meter greater than 0.5%.

6.2.3 Load Resistance

As before the transfer characteristic was recorded at various values of load resistance, with normal excitation and temperature. The Thevenin impedance of the device at 60c/s and 300 turns on the pick-up coil, was found to be of the order of 50 ohms.

6.3 Stability of Normal Characteristics

With all normal settings, the above experiments were repeated at regular intervals over a period of a month, without



any detectable change in the results obtained. It was, thus, concluded that changes of $\pm 10\%$ in normal excitation or $\pm 30\%$ C in temperature have a 0.1% and 0.5% effect, respectively, on the sensitivity of the torque meter.

6.4 Reproducibility and Linearity

Using optimum conditions of operation, as previously determined, an attempt was made to measure the transfer characteristic to one part in one thousand. For this, a null method was adopted with a circuit set-up, as shown in Fig. 6-3.

A galvanometer (G) and a standard cell (S.C.) of 1.0187 volts were used to calibrate a 10 K Ω Voltage Decade Divider (V.D.D.), connected to a mercury cell through a variable resistance R.

With G connected to S.C. and the setting of V.D.D. fixed at, say 9 K Ω , resistor R was adjusted until there was no deflection of the light beam of G, indicating that the voltage appearing across V.D.D. was equal to the e.m.f of S.C. Thus, a base for calibration of the V.D.D. was obtained. This was repeated before and after each experiment to ensure correct calibration.

With G now connected to the chopper and torque applied to the tube, the pick-up coil signal was nulled by a corresponding voltage from the V.D.D. The setting of the V.D.D., as well as the position of the weight on the weighbeam were recorded; this was repeated for random values of torque.

The best linear fit to the experimental points was determined, using the method of Least Squares and the IBM 7040 digital computer. The percentage deviation of these points from the regression line was also calculated, typical values being given in Fig. 6-4. The maximum deviation from linearity

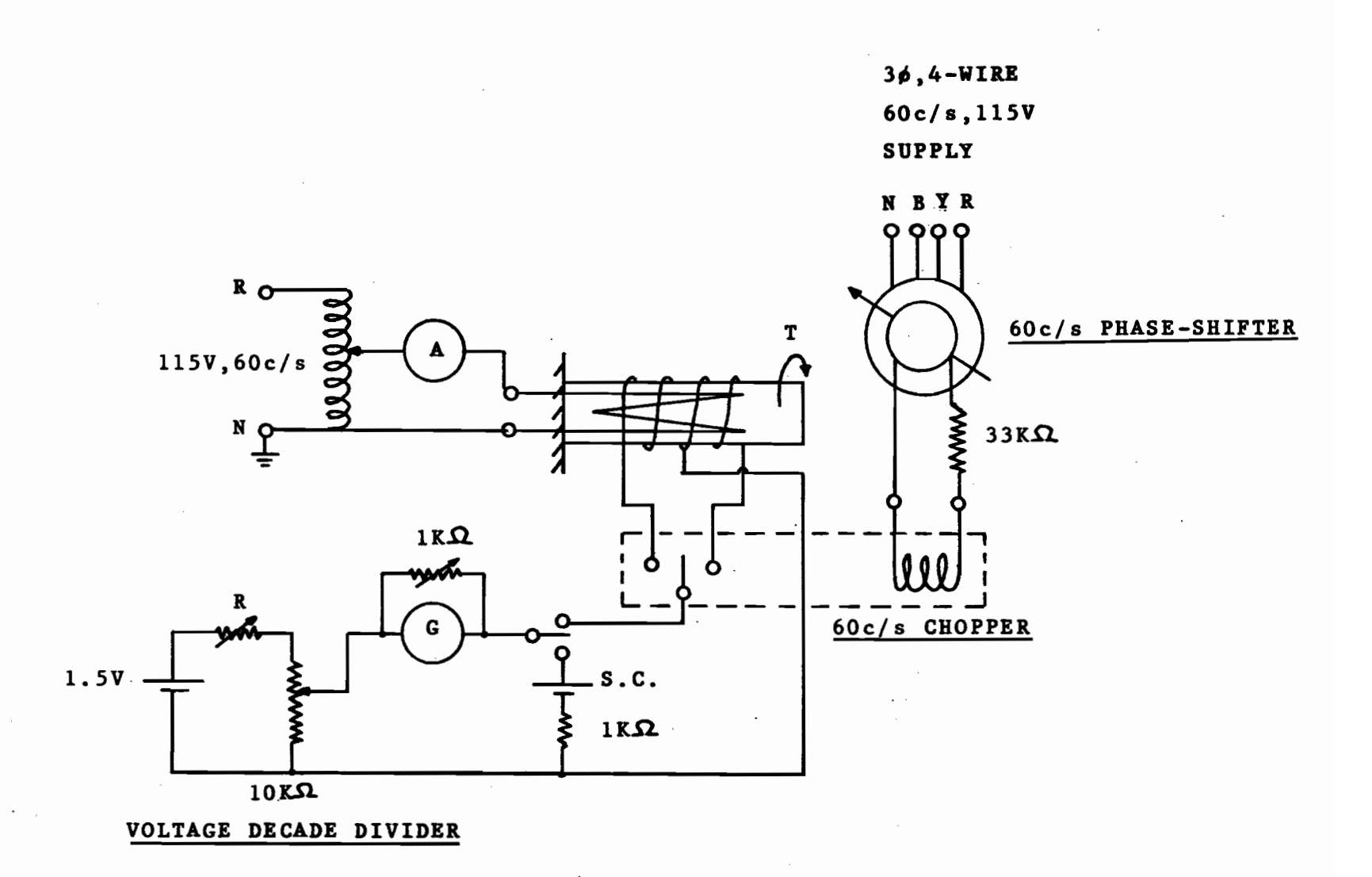
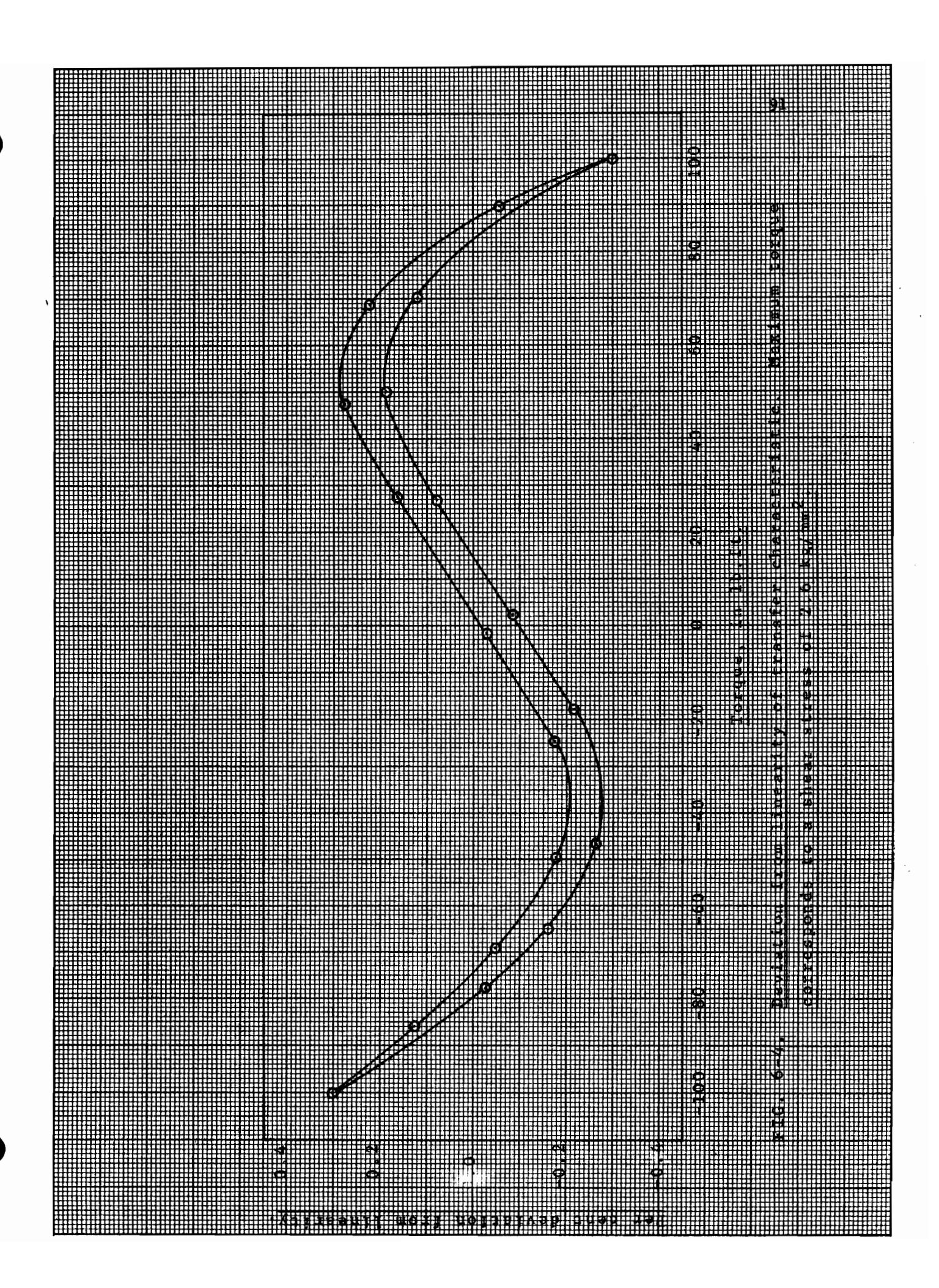


FIG. 6-3. Schematic diagram of circuit used for reproducibility test.



occurs at torques of ± 100 lb.ft., corresponding to a shear stress of 2.6 kg/mm², and is of the order of $\pm 0.3\%$; the hysteresis is less than 0.1%.

The linear portion of the curve extending up to ± 50 lb.ft. indicates that the linearity of the transfer characteristic is better than 0.1% within the above limits of torque. With the aid of a calibration curve, like the one of Fig. 6-4, the torque meter can be used as a 0.1% device for torques up to ± 100 lb.ft., the limit of 0.1% being imposed by the hysteresis present in the transfer characteristic.

The above experiment was repeated at regular intervals over a period of a month and the sensitivity of the device was compared for reproducibility. A random variation of sensitivity was observed, which, however, never exceeded $\pm 0.15\%$.

6.4.1 Possible Sources of Error

Although the reproducibility of the transfer characteristic was within +0.15%, it is the author's strong belief that the sources of error were not inherent in the torque meter, but were due to inadequate external circuitry.

No doubt the circuit used, was capable of better than 0.1% accuracy; this was proved by the ability to observe a 0.1% hysteresis. However, in the reproducibility tests, possible sources of error might have been the unreliable performance of the mechanical chopper, the imperfect setting of the phase-shifter, the inability to detect the position of the weight on the weighbeam within less than 0.01" and finally the difficulty in keeping settings unaltered for a period of a month.

The chopper was driven by a 6V sinusoidal voltage from the phase-shifter. It would have been preferable to drive it with a square pulse of fast rise time, ensuring as a result,

fast and positive triggering at a particular voltage level.

The precision measurements were carried out in the Power Laboratory and it was virtually impossible to keep settings unaltered. Any slight variation in the setting of the induction regulator, used as phase-shifter, affects its ability to suppress the quadrature component present in the signal and hence changes the slope of the transfer characteristic.

6.5 Conclusions

The steel torque meter, developed in this project, is a 0.15% precision measuring device. The deviation from linearity and hysteresis are less than 0.1% for shear stresses not exceeding 1.3 kg/mm². Temperature variations of $\pm 30^{\circ}$ C have an effect on the sensitivity of not more than 0.5%, while $\pm 10\%$ variations in the optimum exciting level result in a 0.1% effect.

CHAPTER VII

CONCLUSIONS

The aim of this project was to investigate the behaviour of the magnetic-anisotropy torque meter, determine the factors affecting its performance and attempt to develop a theory explaining its operation. In the light of theory and under optimum conditions of operation, the possibility of adopting the torque meter as a 0.1% precision measuring device was to be examined.

A general survey, carried out with nickel and steel torque tubes, revealed some interesting results, regarding the factors affecting the behaviour of the torque tubes. established that, although nickel is more stress-sensitive than steel, due to its high magnetostriction and fairly low crystal anisotropy, a linear transfer characteristic is obtained for shear stresses not exceeding 2.5 kg/mm². This high stresssensitivity of nickel is very temperature dependent, making it unsuitable for the construction of precision torque meters. This, however, is not the case for steel torque tubes. are less sensitive to stress, but at the same time, temperature variations of +30°C do not affect the sensitivity by more than 0.5%. The deviation from linearity of the transfer characteristic does not exceed 0.1% for stresses up to 1.3 kg/mm² and it is less than 0.3% up to 2.6 kg/mm², while for a 0.5% deviation, stresses up to 4 kg/mm² can be easily tolerated. Thus, steel is to be preferred in the construction of the torque tubes.

For each torque meter an optimum magnetizing level exists; it corresponds to saturation of the whole of the material at the particular frequency of operation. At this level, maximum sensitivity is attained, which may vary by not more than 0.1% for a $\pm 10\%$ change in exciting current. The linearity and

hysteresis are better than 0.1%, provided the optimum stress level is not exceeded. Thus, good saturation of the tube is a necessity.

Operating the torque meter at a frequency higher than 60 c/s, (400 c/s is recommended for future work), permits the detection of transient torques of higher frequency than 60 c/s.

Although only a static calibration of the torque meters has been performed in this project, the method of construction of the device indicates that the output signal should be independent of the speed of rotation.

The device is very inexpensive and an ideal transfer characteristic can be obtained with very simple external circuitry, namely a chopper and a "torque-zero" signal suppressor circuit.

The reproducibility of the transfer characteristic was of the order of 0.15%. However, the author believes, that with better measuring equipment and more experience in precision measurements, one could establish the fact that the magneticanisotropy torque meter is a 0.1% precision measuring device.

To the author's knowledge, the theory developed is original. It successfully explains both the qualitative and quantitative (within 15%) behaviour of the magnetic-anisotropy torque meter. The predictions made regarding crystal orientation, operating temperature and stress level, are a contribution to the design of better torque meters.

In conclusion, the author believes that the purpose of this project was fully met, and that the magnetic-anisotropy torque meter developed can favourably compete with any other type of torque transducer.

CHAPTER VIII

APPENDIX

DESCRIPTION OF EQUIPMENT

To facilitate the investigation into the behaviour of the torque meters and to reduce human effort, equipment was designed enabling the automatic recording of the transfer characteristic. The main items of the equipment are:

- (i) Weighbeam for applying torque to the torque meter,
- (ii) Weight-position detector,
- (iii) Phase-shifting network,
 - (iv) Phase-sensitive detector.

8.1 Beam Arrangement

A weighbeam, made of aluminum plates and supported at its centre on hardened steel knife-edges, thus minimizing the effect of friction, was designed and used for the static calibration of the torque tubes. It carried a leadscrew, 1" in diameter, ½" pitch, 5ft. long, accurately machined to give less than 0.01" overall error, and a travelling weight made of 50 lb. + ½ oz. of lead.

A d.c., separately excited, motor was coupled to one end of the leadscrew, while the other end carried a photocell arrangement, as shown in Fig. 8-1. The torque tube was placed into position, between two clamps; one of them was securely fixed on the weighbeam, consequently turning with it, while the other was held stationary.

Depending on the direction of rotation of the motor shaft, the weight could travel "forward" or "reverse", thus applying at the free end of the torque tube a "clockwise" or "anticlockwise" torque respectively, given by the product of

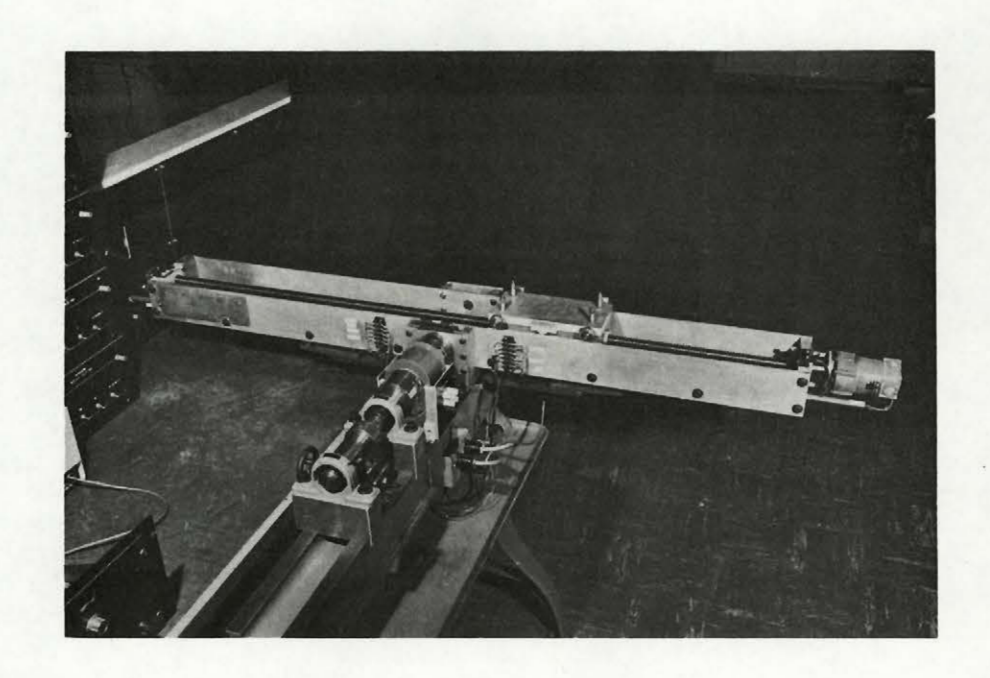


FIG. 8-1. The weighbeam arrangement.

the weight, its distance from the knife-edges and the cosine of the angle of inclination of the beam from the horizontal position.

Provisions were made at the fixed end of the torque tube, so that the whole weighbeam could be set at a horizontal position irrespective of the position of the weight, thus eliminating the necessity of determining the angle of inclination. As it was found that the error introduced in the torque calculation by neglecting the cosine term was extremely small, the above arrangement was only used during the precision measurement experiments.

Special precautions were taken to minimize any backlash in the leadscrew; on testing for backlash with a dial gauge, it was found to be less than 0.001". This was considered negligibly small and the matter was not pursued any further.

All electrical connections to circuits on the weighbeam, namely driving motor, photocell unit and limit microswitches, were made by flexible leads; at the design stage the centre of gravity of the weighbeam was set to rest on the knife-edges, with its stability increased as a result.

The weighbeam was found to be extremely sensitive and torques of the order of 0.001 lb.ft. could be easily detected. The maximum torque that could be applied to the torque tube by this arrangement was of the order of 120 lb.ft.

8.2 Weight-position Detector

The position of the travelling weight on the weighbeam was determined at each instant by a detector, consisting of a photocell unit arrangement and a digital-to-analogue converter.

8.2.1 Photocell Arrangement

For this, an RCA, type 7467 Germanium p-n alloy photojunction cell was chosen, on account of its fast response; a disk, having 25x3/32" holes on a 3" P.C.D., rotating with the leadscrew, was interposed between the photocell unit and an illuminating source. Fig. 8-2 shows the circuit used.

Whenever light falls on the photocell surface from the source through the disk holes, the photocell is activated, i.e. its resistance collapses, allowing current from the supply to flow towards the output terminals, while during the dark periods the resistance of the photocell builds up and acts practically as an open circuit. This results in the formation of pulses at the output, each pulse corresponding to 0.01" movement of the weight along the beam.

Calibration

At this stage, the ability of the device to detect the position of the weight within 0.01" was tested, by counting the photocell circuit pulses by means of a Beckman digital counter and comparing them against the actual position of the weight, as determined by means of a 5ft. precision scale bearing 0.01" divisions and attached to the weighbeam. Over a travel of 49", an error of 0.05" was introduced by the photocell circuit. This was attributed to small vibrations of the photocell in its base and accidental triggering of the counter by switching surges.

The photocell was firmly secured in its base, shielded cables were used in the photocell circuit and capacitors were connected at suitable places in the circuit to suppress switching surges. On retesting the error was entirely eliminated.

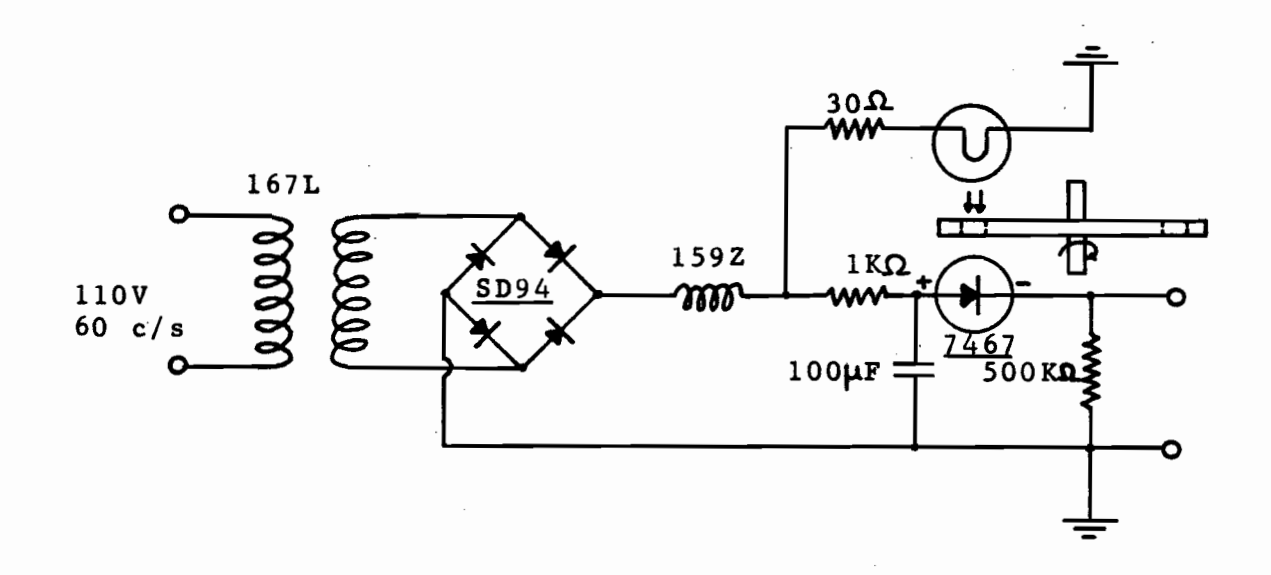


FIG. 8-2. Schematic diagram of photocell circuit.

8.2.2 Digital-to-analogue Converter

Various schemes to convert the photocell pulses into an analogue voltage output, were tried out, bearing in mind that in doing so, it was undesirable to add any extra weight on the weighbeam. Finally, a digital-to-analogue converter, consisting of a step motor, mechanical counter, helipot and gearbox, was designed.

The step motor, type AU5105/80, and its associated electronic switch, type 2P72743, recently manufactured by Philips Co., is a device whereby an incoming pulse turns the motor shaft by a certain angle, in this case 7.30'+20'; by means of the two-channel switch, the motor can turn in either direction. Its speed of response, as specified by the manufacturer, is 150 steps per second, well within the operating region of the photocell arrangement, namely 35 pulses per second.

The step motor was coupled through an appropriate gear ratio to a high speed Veeder-Root mechanical counter, type 1134, and to a ten-turn, $1K\Omega$ centre-tapped helipot, energized from a highly stabilized d.c. supply.

A Schmitt trigger circuit (Fig. 8-3) with a rise time of 1 μ sec, was designed to reshape the photocell pulses, before triggering the step motor electronic switch. A block diagram of the arrangement used, is shown in Fig. 8-4.

Calibration

The Beckman counter was connected at the output of the Schmitt trigger, while a meter, connected between the slider and the centre-tap of the helipot, was used to record the output voltage.

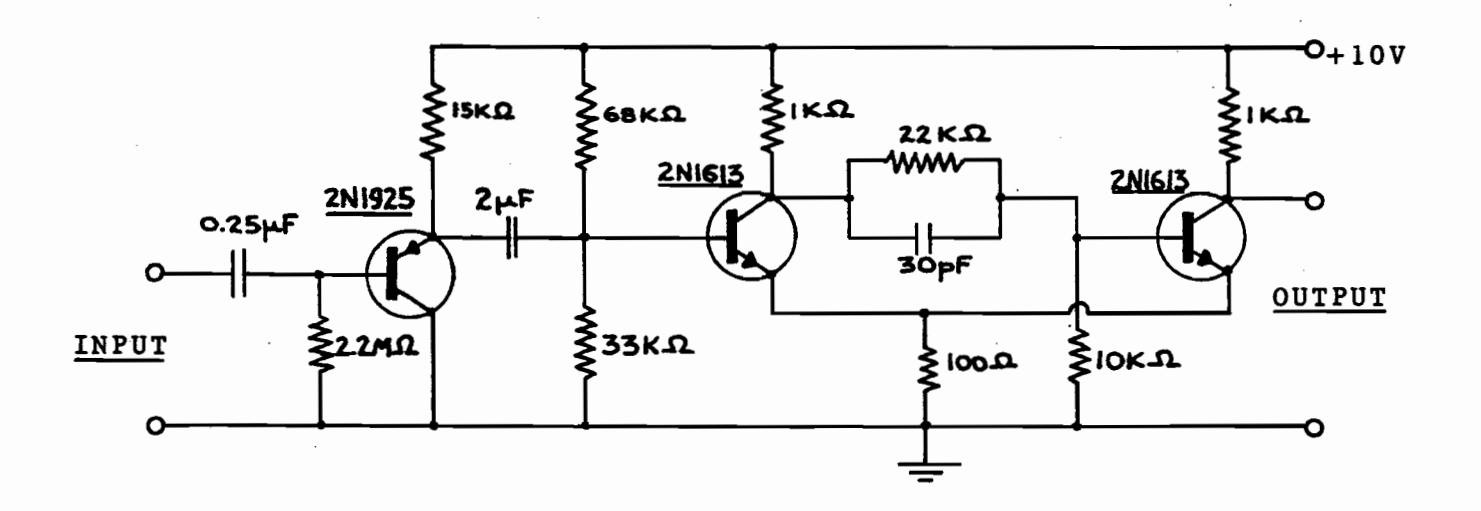


FIG. 8-3. The Schmitt trigger circuit and buffer amplifier.

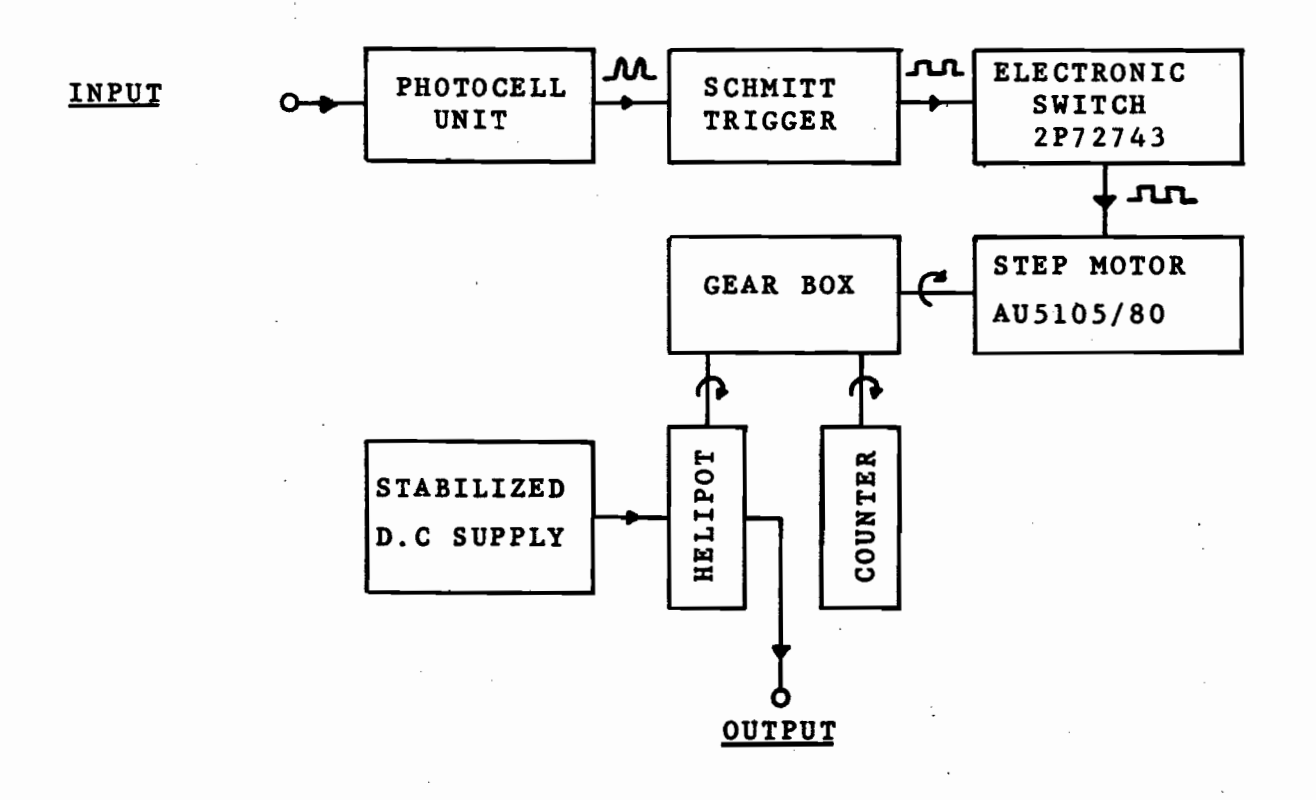


FIG. 8-4. Block diagram of digital-to- analogue converter.

Test runs of the weight were carried out at suitable intervals, during the period of the project, indicating that the position of the weight on the weighbeam could be detected within 0.01".

8.3 Phase-shifting Network

To eliminate the zero-torque signal present in the pick-up coil circuit of the torque meter, as mentioned in Chapter III, a two-stage phase-shifting network (Fig. 8-5) was used. By proper adjustment of the resistances and capacitances of the circuits, the output voltages of the helipots could be set at any desirable phase relationship.

8.4 Phase-sensitive Detector

The automatic plotting of the locus of the pick-up coil signal vector with respect to the magnetizing current was achieved through a phase-sensitive detector in conjunction with the X-Y recorder.

The phase-sensitive detector, transistorized in order to provide more flexibility with regard to amplitude and frequency of the signal, has the following basic principle:

Consider two sinusoidal voltages, a reference voltage, V_{REF} , and a signal voltage, V_{SIG} . If a chopper transistor, triggered by V_{REF} , as shown in Fig. 8-6, is used to select portion of the wave V_{SIG} , then the average value of the output signal V_{op} , is proportional to the in-phase component of V_{SIG} relative to V_{REF} , i.e. to $\cos \phi$, where ϕ is the phase angle of V_{REF} and V_{SIG} .

If a similar circuit, but now triggered by $jV_{\mbox{\scriptsize REF}}$, is used, the average value of the output signal will be proportional

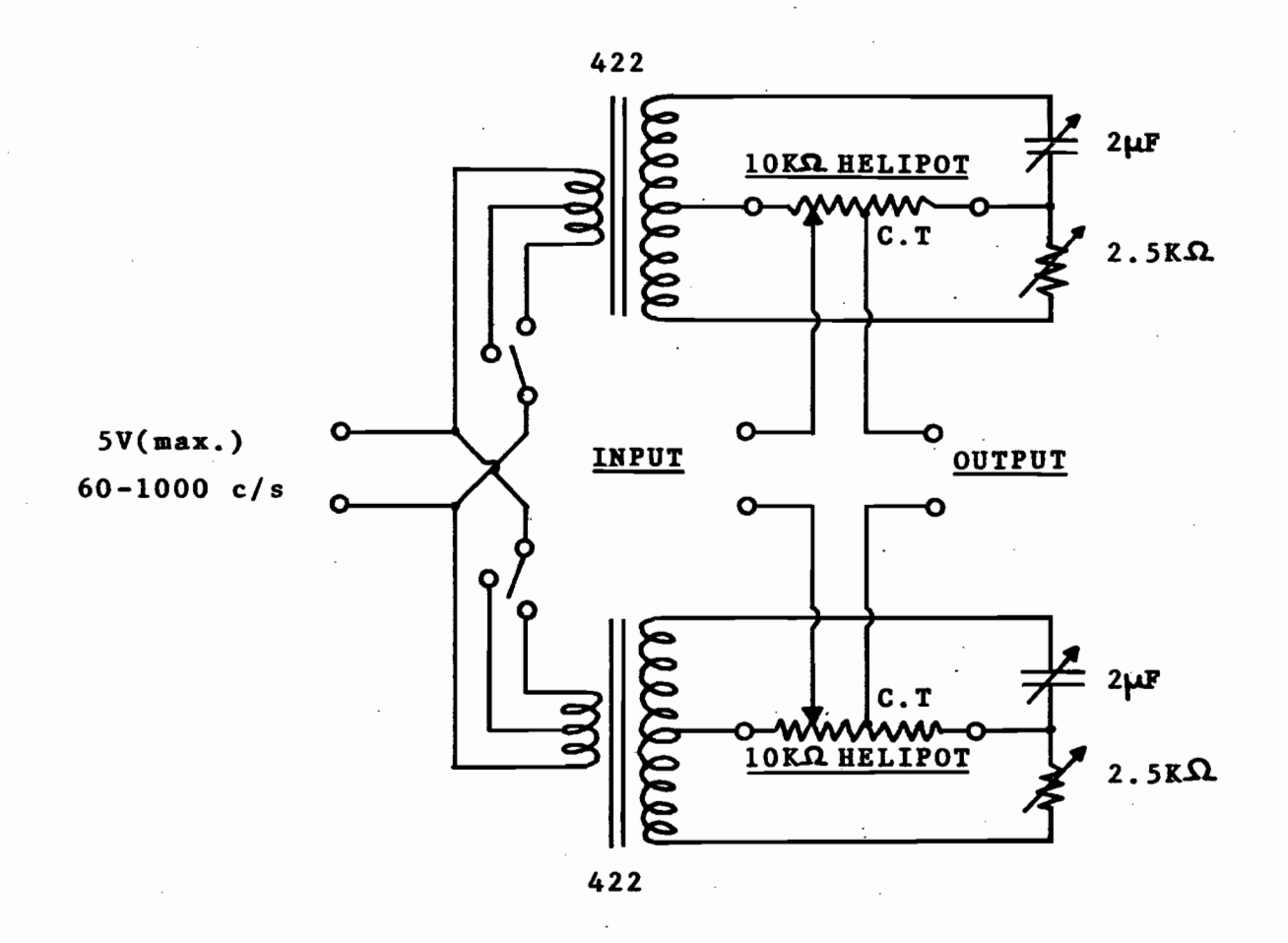


FIG. 8-5. The phase-shifting network.

to the quadrature component of $V_{\rm SIG}$, i.e. to $\sin \phi$. Hence, by means of a two-channel phase-sensitive detector and an X-Y recorder one is able to plot the locus of $V_{\rm SIG}$ relative to $V_{\rm REF}$.

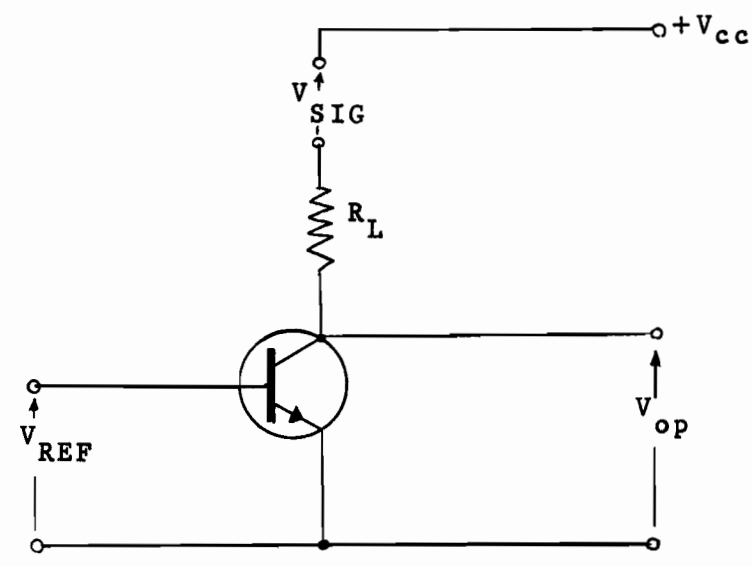


FIG. 8-6. Chopper circuit of phase-sensitive detector.

Certain modifications and additions to the above circuit are necessary for better accuracy and more reliable performance. Thus, to ensure positive operation of the transistor at a specified voltage level, the sinusoidal reference voltage was replaced by a square waveform of fast rise time. This was achieved by using the sine-to-square converter, shown in Fig. 8-7. This is merely an emitter-coupled limiter with the switching transistors driven out of a common collector stage. Very fast rise times can be obtained, independent of the magnitude of the input sine wave. With an input sine wave of 6 volts (peak-to-peak), a symmetrical square wave with a rise time of approximately 10 nsec was obtained at the output. This was used to drive the chopper transistor, as

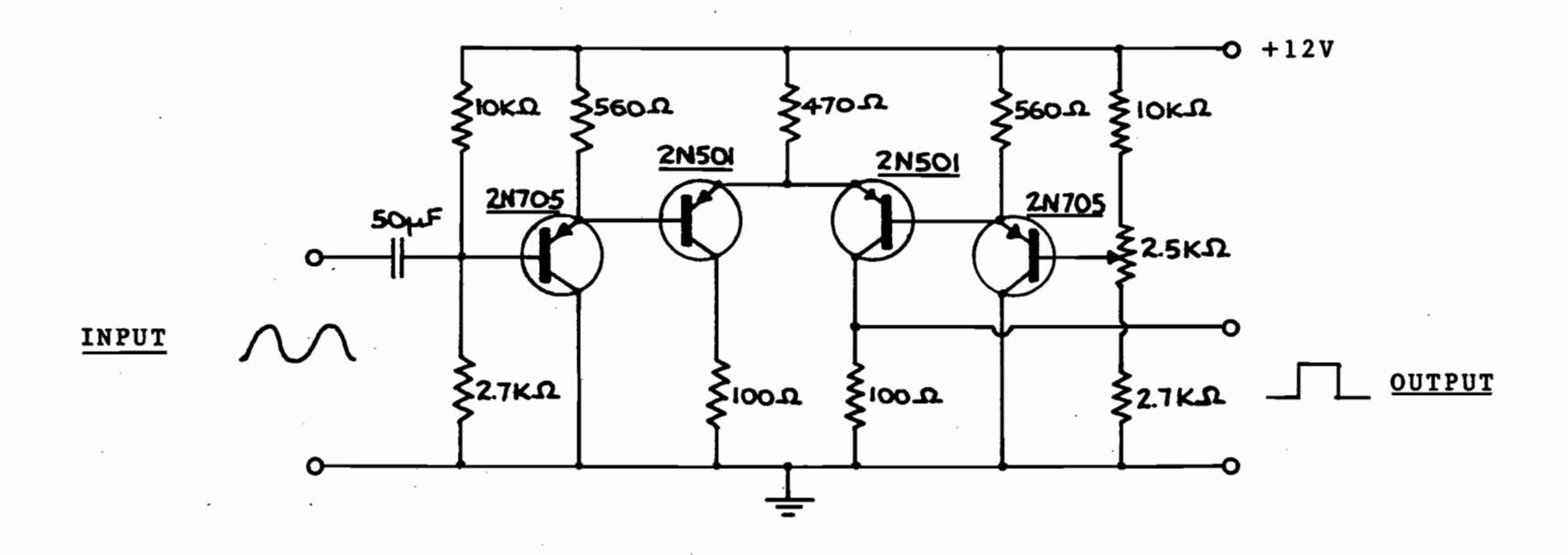


FIG. 8-7. The sine-to-square converter.

shown in Fig. 8-8.

The output voltage of each stage will include part of the d.c. supply voltage of the chopper transistor. This can be fed into a summer and nullified by a d.c. bias.

8.4.1 Effect of Harmonics

In general, the signal voltage will contain harmonics. Thus, consider a voltage comprising fundamental and harmonics as below:

$$v = \sum_{n=1}^{\infty} (V_{an} \sin n\theta + V_{bn} \cos n\theta)$$

If the chopper used, selects portion of the wave, from $\theta=\alpha$ to $\theta=\beta$, then the average value of the resultant output is given by:

$$\bar{v} = \frac{1}{2\pi} \int_{\alpha}^{\beta} \sum_{n=1}^{\infty} (V_{an} \sin n\theta + V_{bn} \cos n\theta) d\theta$$

$$= \frac{1}{2\pi} \sum_{n=1}^{\infty} \left[-\frac{V_{an}}{n} \cos n\theta + \frac{V_{bn}}{n} \sin n\theta \right]_{\alpha}^{\beta}$$

$$= \sum_{n=1}^{\infty} \frac{1}{n\pi} \sin \frac{n(\beta - V)}{2} \left[V_{an} \sin \frac{n(\alpha + \beta)}{2} + V_{bn} \cos \frac{n(\alpha + \beta)}{2} \right]$$

If $\alpha = -\beta$, i.e. chopping is symmetrical about origin, the sine components will not contribute to the result and hence:

$$\overline{v} = \sum_{n=1}^{\infty} \frac{v_{bn}}{n\pi} \sin n\beta$$

If $\beta=\frac{\pi}{2}$, as is usually the case, all even harmonics are eliminated. If $\beta=\frac{\pi}{3}$, all triple harmonics are eliminated, e.t.c. The remaining harmonics are attenuated by a factor at

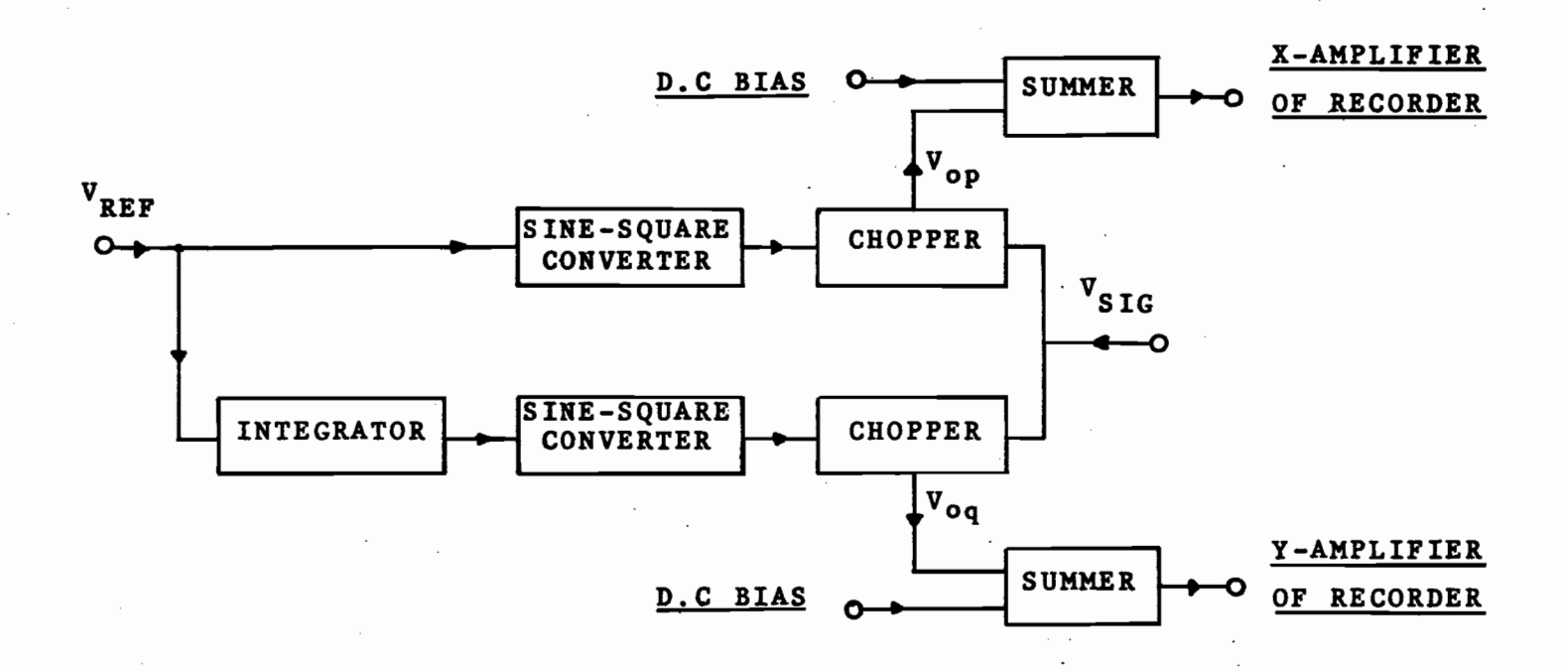


FIG. 8-8. Block diagram of phase-sensitive detector.

least equal to the order of the harmonic, i.e. fifth is attenuated at least five times.

In case of unsymmetrical chopping, a certain error is introduced. This, however, is extremely small and can be neglected, provided the unsymmetry is less than 1° .

8.4.2 Calibration of Detector

The calibration of the phase-sensitive detector was carried out at frequencies up to 1 kc/s. Only the 60 c/s method of calibration will be given here; similar techniques were applied for higher frequencies, with the exception that the phase-shifting network, previously described, was used in place of the 60 c/s induction regulator.

With the circuit set-up, shown in Fig. 8-9, the procedure was as follows:

By means of the auto-transformer, connected across, say R and N of a 3-phase, 4-wire supply, the voltage $V_{\rm SIG}$ was varied in amplitude and points with coordinates $V_{\rm op}$ and $V_{\rm oq}$, were recorded. The locus of the points was a straight line. The phase of $V_{\rm SIG}$ was changed by $\pm 120^{\circ}$, by simply connecting the auto-transformer to either the Y and N or B and N lines of the supply and the above was repeated.

It was found that the straight lines obtained were inclined at 120° to each other, as was expected. This was repeated at random settings of the phase-shifter with similar results, indicating that the phase-sensitive detector developed had an accuracy of better than 0.5% (this limit being imposed mainly by the X-Y recorder).

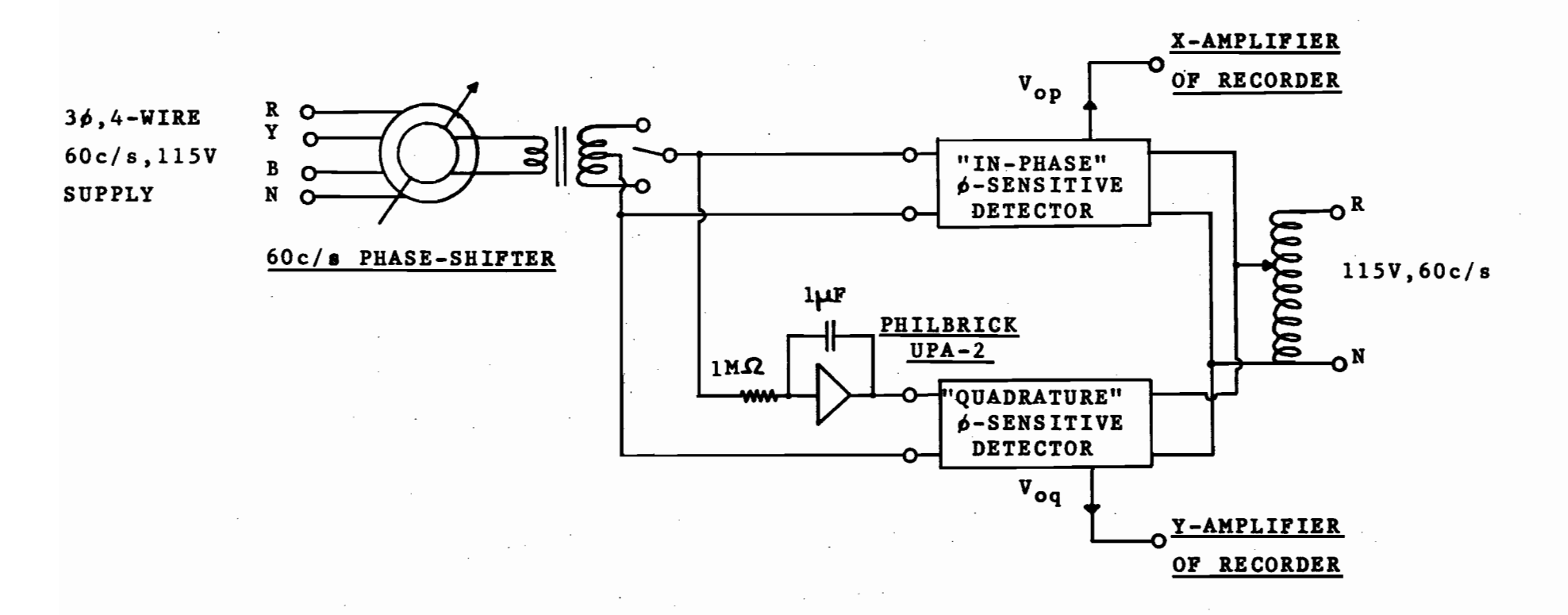


FIG. 8-9. Circuit set-up for the 60c/s calibration of phase-sensitive detector.

8.4.3 Suggestions for Future Work

Although the operation of the phase-sensitive detector was very reliable at low frequencies, certain difficulties were encountered at higher frequencies, originating from the coupling between the "in-phase" and "quadrature" stages. This can be eliminated by decoupling the two stages using R-C networks.

APPENDIX A

AUXILIARY EQUIPMENT

Moseley X-Y Recorder, Model 2D

	d.c. scales	a.c. scales
Linearity	0.1%	0.1% (20c/s to 20kc/s)
Accuracy	0.2%	0.5% (20c/s to 20kc/s)
Input Impedance	200K Ω /V (1 volt/inch	$2M\Omega$ shunted by $25ppF$
	and lower scales)	on all ranges
	$2 \mathtt{M} \mathfrak{Q}$ (higher scales)	(20c/s to 100kc/s).

Philbrick Operational Amplifier, Model UPA-2

Overall dc gain of amplifier 2 x 10⁷
before feedback

Effective resistance and capacitance 1 M \(\Omega\)
from summing point to ground 9 \(\mu\)F

Drift (referred to input) 50 μ V per day

Bristol Syncroverter Switch, C1417-3

Coil voltage 6.3 volts

Frequency of operation 0 - 120 c/s

Dissymmetry 15 $^{\circ}$ maximum

Dwell time 175 $^{\circ}$ + 15 $^{\circ}$

APPENDIX B

THEORETICAL ANALYSIS OF STEEL TORQUE METER

Consider a single crystallite, situated at some point in the torque tube wall, with a direction of easy magnetization making an angle θ_0 to the applied field \vec{H} , as shown in Fig.B.

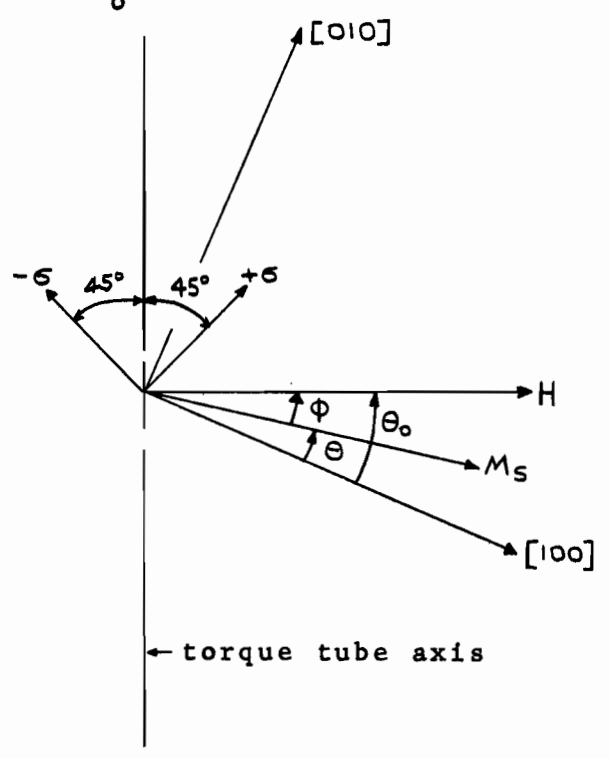


FIG. B. Vectors and angles used in calculating the axial component of magnetization.

The direction cosines of $\vec{M}_{_{\mbox{S}}}$ with respect to the crystallographic axes are given by:

$$\alpha_1 = \cos\theta$$

$$\alpha_2 = \sin \theta$$

$$\alpha_3 = 0$$

Substituting in equ. (4.1),

$$W_{K} = \frac{K_{1}}{8} (1 - \cos 4\theta)$$

Hence, the crystal anisotropy torque is

$$T_K = -\frac{\partial W_K}{\partial \theta} = -\frac{K_1}{2} \sin 4\theta$$

The direction cosines of the tensile stress, +o, are:

$$\begin{cases}
\gamma_1 = \cos(\theta_0 + \frac{\pi}{4}) \\
\gamma_2 = \sin(\theta_0 + \frac{\pi}{4})
\end{cases}$$

$$\gamma_3 = 0$$

while those of compressive stress, -G, are:

$$\begin{cases} \begin{cases} \frac{1}{1} = \cos(\theta_0 + 3 \frac{\pi}{4}) \\ \frac{1}{2} = \sin(\theta_0 + 3 \frac{\pi}{4}) \end{cases}$$

$$\begin{cases} \frac{1}{3} = 0 \end{cases}$$

Assuming that the stresses act independently, equ. (4.2) reduces to:

$$W_S = \frac{3}{2} \in \left[\lambda_{100} \sin 2\theta_0 \cos 2\theta - \lambda_{111} \cos 2\theta_0 \sin 2\theta \right]$$

and the corresponding rotational torque is:

$$T_S = -\frac{\partial w_S}{\partial \theta} = 3 \in \left[\lambda_{100} \sin 2\theta_0 \sin 2\theta + \lambda_{111} \cos 2\theta_0 \cos 2\theta \right]$$

Similarly, the magnetostatic energy is:

$$W_{H} = -HM_{S} \cos \phi$$

and the magnetostatic torque

$$T_{H} = -\frac{\partial W_{H}}{\partial \theta} = HM_{S} \sin(\theta_{o} - \theta)$$

The positions of equilibrium of \overrightarrow{M}_S are given by:

$$\frac{K_1}{2} \sin 4\theta - 36 \left[\lambda_{100} \sin 2\theta \sin 2\theta + \lambda_{111} \cos 2\theta \cos 2\theta \right] = HM_S \sin \theta$$

At this instant, the axial induction is given by:

$$B_a = B_S \sin \phi$$

Since, for steel, the anisotropy torque will be the dominating factor in aligning M_S , angle θ is very small. Thus an approximate solution can be obtained, by replacing the sine and cosine terms of angle θ by the first terms of the corresponding series expansion, as follows:

$$\sin \phi = \sin(\theta_0 - \theta) = \sin \theta_0 - \theta \cos \theta_0$$

Hence,

$$\frac{\kappa_1}{2} (4\theta) - 3\sigma \left[\lambda_{100} \sin 2\theta_0 (2\theta) + \lambda_{111} \cos 2\theta_0 \right] = HM_S \left[\sin \theta_0 - \theta \cos \theta_0 \right]$$

which gives

$$\theta = \frac{36\lambda_{111} \cos 2\theta_{o} + HM_{S} \sin \theta_{o}}{2K_{1} - 66\lambda_{100} \sin 2\theta_{o} + HM_{S} \cos \theta_{o}}$$

and, hence,

$$\sin \phi = \sin \theta_o - \frac{\cos \theta_o (36\lambda_{111}\cos 2\theta_o + HM_S \sin \theta_o)}{2K_1 - 66\lambda_{100}\sin 2\theta_o + HM_S \cos \theta_o}$$

For random crystal orientation,

$$\bar{B}_{a} = -\frac{1}{\pi} \int_{-\frac{\pi}{4}}^{\frac{\pi}{4}} \frac{HM_{S} \sin 2\theta_{o} + 66\lambda_{111} \cos 2\theta_{o} \cos \theta_{o}}{2K_{1} - 66\lambda_{100} \sin 2\theta_{o} + HM_{S} \cos \theta_{o}} d\theta_{o}$$

The integration was performed by a numerical method, namely Simpson's Rule.

APPENDIX C

THEORETICAL ANALYSIS OF NICKEL TORQUE METER

(i) Temperature of specimen below 80°C

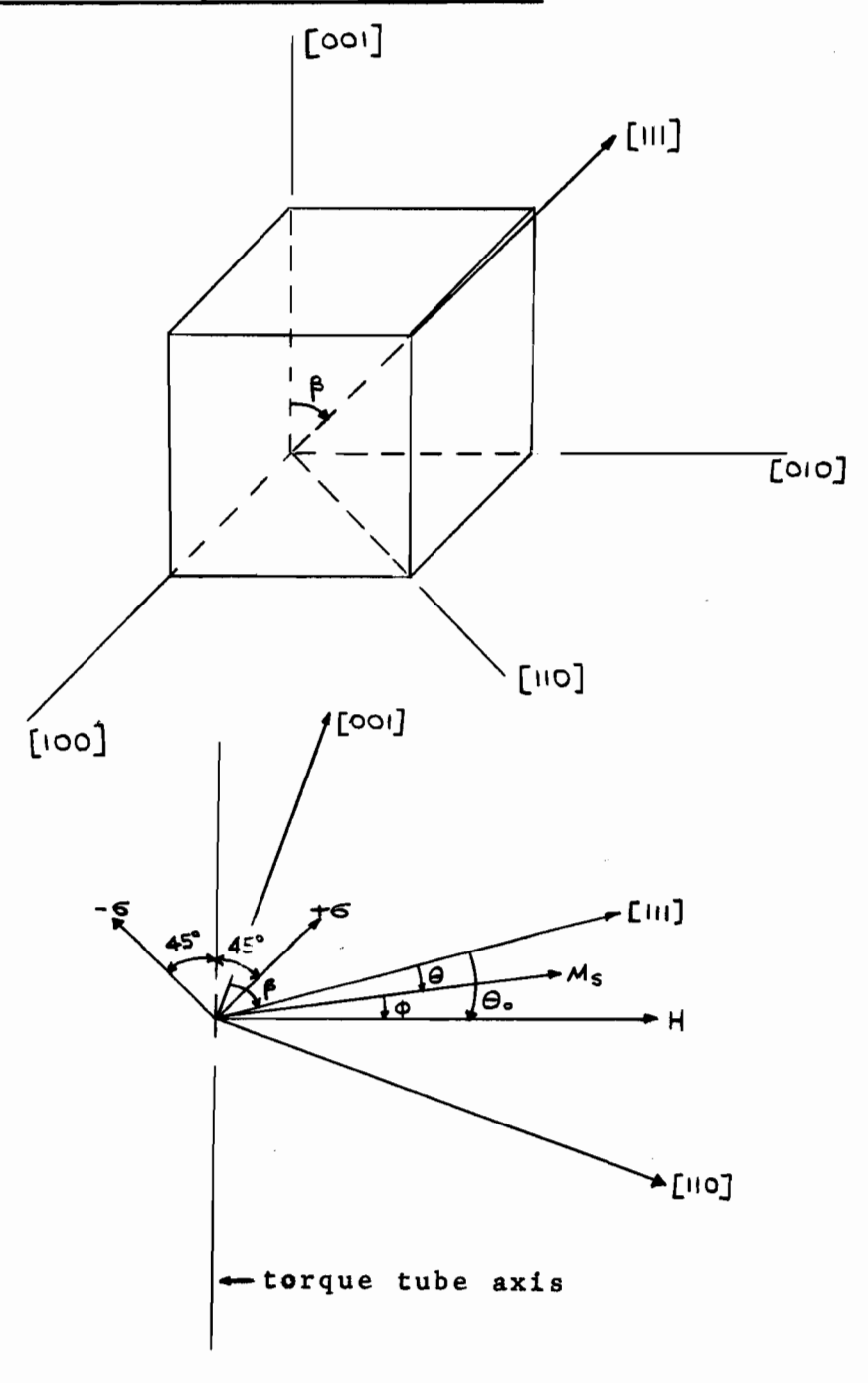


FIG. C.1.. Vectors and angles used in calculating the axial component of magnetization.

Assuming that \overrightarrow{M}_S lies in the plane of $\begin{bmatrix} 001 \end{bmatrix}$ - axis and \overrightarrow{H} , the direction cosines of \overrightarrow{M}_S are:

$$\alpha_1 = \frac{1}{\sqrt{2}}, \sin (\beta + \theta)$$

$$\alpha_2 = \frac{1}{\sqrt{2}} \sin (\beta + \theta)$$

$$\alpha_3 = \cos (\beta + \theta)$$

Substituting in equ. (4.1),

$$W_{K} = \frac{K_{1}}{32} \left[7 + \frac{4}{3} \cos 2\theta + \frac{8\sqrt{2}}{3} \sin 2\theta + \frac{7}{3} \cos 4\theta - \frac{4\sqrt{2}}{3} \sin 4\theta \right]$$

$$+ \frac{K_{2}}{128} \left[2 + \frac{1}{3} \cos 2\theta + \frac{2\sqrt{2}}{3} \sin 2\theta + \frac{14}{9} \cos 4\theta - \frac{8\sqrt{2}}{9} \sin 4\theta + \frac{23}{27} \cos 6\theta + \frac{10\sqrt{2}}{27} \sin 6\theta \right]$$

The direction cosines of the tensile stress, +6, are:

$$\begin{cases}
\chi_1 = \frac{1}{\sqrt{2}} \sin(\beta + \theta_0 - \frac{\pi}{4}) \\
\chi_2 = \frac{1}{\sqrt{2}} \sin(\beta + \theta_0 - \frac{\pi}{4})
\end{cases}$$

$$\begin{cases}
\chi_3 = \cos(\beta + \theta_0 - \frac{\pi}{4})
\end{cases}$$

and those of the compressive stress, - 6, are:

$$y_1^* = -\frac{1}{\sqrt{2}}\cos(\beta + \theta_0 - \frac{\pi}{4})$$

$$y_2^* = -\frac{1}{\sqrt{2}}\cos(\beta + \theta_0 - \frac{\pi}{4})$$

$$y_3^* = \sin(\beta + \theta_0 - \frac{\pi}{4})$$

Hence, equ. (4.2) reduces to:

$$\begin{aligned} \mathbf{w}_{S} &= -\frac{1}{16} \varepsilon \left[(\lambda_{100} - \lambda_{111}) \left\{ 4\sqrt{2} \cos 2\theta_{o} - 2\sin 2\theta_{o} + 4\sqrt{2} \cos 2(\theta_{o} + \theta) + 7\sin 2(\theta_{o} + \theta) \right\} + 3(3\lambda_{100} + 5\lambda_{111}) \sin 2(\theta_{o} - \theta) \right] \end{aligned}$$

Finally, the magnetostatic energy is:

$$W_H = - HM_S \cos \phi$$

Similar expressions can be obtained for the corresponding rotational torques.

The positions of equilibrium of \overrightarrow{M}_S are determined from:

$$\begin{split} &\frac{K_1}{48} \left[-4 \sin 2\theta + 8\sqrt{2} \cos 2\theta - 14 \sin 4\theta - 8\sqrt{2} \cos 4\theta \right] \\ &+ \frac{K_2}{576} \left[-3 \sin 2\theta + 6\sqrt{2} \cos 2\theta - 28 \sin 4\theta - 16\sqrt{2} \cos 4\theta \right] \\ &- 23 \sin 6\theta + 10\sqrt{2} \cos 6\theta \right] \\ &+ \frac{1}{8} 6 \left[(\lambda_{100} - \lambda_{111}) \left\{ 4\sqrt{2} \sin 2(\theta_0 + \theta) - 7 \cos 2(\theta_0 + \theta) \right\} \\ &+ 3(3\lambda_{100} + 5\lambda_{111}) \cos 2(\theta_0 - \theta) \right] = HM_S \sin(\theta_0 - \theta) \end{split}$$

This equation was solved on the IBM 7040 digital computer by a numerical method. The corresponding FORTRAN IV program is given in Appendix D.

(ii) Temperature of specimen between 80 and 100°C.

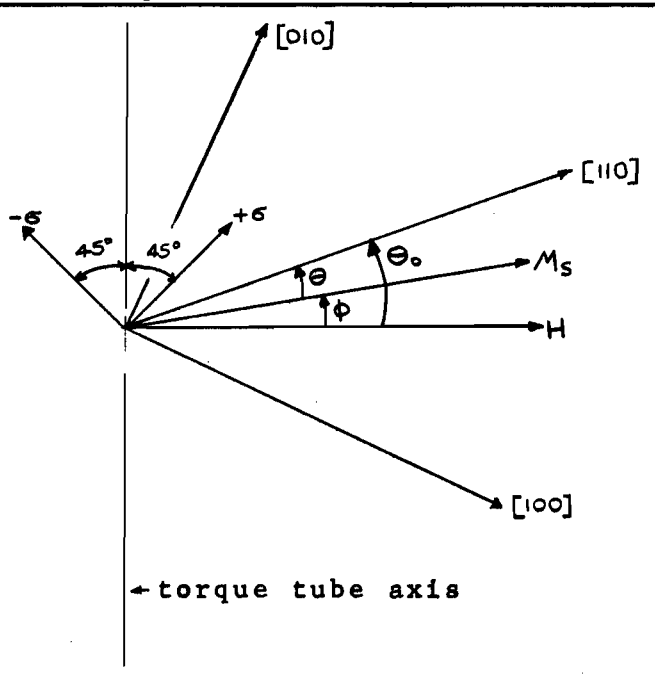


FIG. C.2. Vectors and angles used in calculating the axial component of magnetization.

The direction cosines of \overrightarrow{M}_S are:

$$\alpha_1 = \cos \left(\frac{\pi}{4} - \theta\right)$$

$$\alpha_2 = \cos \left(\frac{\pi}{4} + \theta\right)$$

$$\alpha_3 = 0$$

Hence, equ. (4.1) reduces to:

$$W_{K} = \frac{K_{1}}{8} (1 + \cos 4\theta)$$

The direction cosines of the tensile stress, +6, are:

and of the compressive stress, -6,

$$y_2^* = \sin\theta_0$$

$$\chi_3^* = 0$$

Thus, equ. (4.2) reduces to:

$$W_{S} = \frac{3}{2} \in \left[\lambda_{100} \cos 2\theta_{o} \sin 2\theta - \lambda_{111} \sin 2\theta_{o} \cos 2\theta \right]$$

The magnetostatic energy is given by:

At equilibrium,

$$-\frac{K_1}{2}\sin 4\theta + 36\left[\lambda_{100}\cos 2\theta_{o}\cos 2\theta + \lambda_{111}\sin 2\theta_{o}\sin 2\theta\right] = HM_{S}\sin \theta$$
and $B_a = B_{S}\sin \theta$

Above equation was solved on the IBM 7040 digital computer, using a numerical method. It should be noted that the effect of random crystal orientation can be simulated by rotating the single crystallite through 90° , i.e. by allowing 90° to vary from -45° to $+45^{\circ}$.

(iii) Temperature of specimen above 100°C

Above 100°C, nickel has a cube edge as the direction of easy magnetization. Hence the analysis becomes identical to the case of steel, as described in Appendix B.

APPENDIX D

FORTRAN COMPUTER PROGRAM FOR

EVALUATING THE AXIAL INDUCTION

A typical FORTRAN IV computer program, for the evaluation of the axial induction of nickel specimen, at temperatures below 80° C, is given in this Appendix. The output data are:

- (i) Angle of crystal orientation, θ_{α} ,
- (ii) Angle of magnetization vector, ϕ ,
- (iii) Crystal anisotropy energy and torque,
 - (iv) Magneto-elastic energy and torque,
 - (v) Magnetostatic energy and torque,
 - (vi) Average axial induction,

at a given stress and magnetic field H.

This program is to be read in conjunction with equations (5.2) and (5.3).

TABLE D.1

		H	
		CON	FORTRAN STATEMENTS
	1 5	6	7 72
1	190		PRINT 53
2	53		FORMAT (1H1,19H NICKEL TORQUE TUBE)
3			READ 50, AK1, AK2, AH, AM, AL1, AL2, AB
4	50		FORMAT (2E10.2,2F10.2,2E10.2,F10.2)
5			PRINT 54, AK1, AK2, AL1, AL2, AM, AB, AH
6	54		FORMAT (1HK, 4H K1=,F10.2,5X,4H K2=,F10.2,5X,6H
			L100=,E10.2,5X, 6H L111=,E10.2,5X,3H M=,F10.2,
			5X,3H B=,F10.2,5X,3H H=,F10.2)
7			STRESS=0.0
8			H=5.0*3.14/180.0
9			DO 2 I=1,13
10			PRINT 55
11	5.5		FORMAT (1HL, 1X, 6H ANGLE, 4X, 6H ANGLE, 4X, 5H SINE,
			5X,6H FIRST,3X,7H SECOND,2X,11H ANISOTROPY,2X,
			12H MAG-ELASTIC, 2X, 11H MAG-STATIC, 2X, 11H
			ANISOTROPY, 2X, 12H MAG-ELASTIC, 2X, 11H MAG-STATIC)
12			PRINT 222
13	222		FORMAT (1HJ,31X,6H DERIV, 4X,6H DERIV,4X,7H
			TORQUE, 6X, 7H TORQUE, 8X, 7H TORQUE, 4X, 7H ENERGY,
			7X,7H ENERGY,8X,7H ENERGY)
14			SUM=0.0
15	-		L= 1
16			A=-55.0
17	8		AA= A*3.14/180.0
18			X=-60.0
19			Y=120.0
20			N=0
21	6		CD = (X+Y)/2.0

			CONT	FORTRAN STATEMENTS
	1	5	6	7 72
22				N=N+1
23				CCD=CD*3.14/180.0
24				C=2.0*(AA-CCD)
25				D=C*2.0
26				E=C*3.0
27				G=2.0*(2.0*AA-CCD)
28				GG=2.0*CCD
29				B=SIN(C)
30				BB=COS(C)
31				P=SIN(D)
32				PP=COS(D)
33				Q=SIN(E)
34				QQ=COS(E)
35				R=SIN(G)
36				RR=COS(G)
37	 			WCA=(AK1/48.0)*(-4.0*B+8.0*1.414*BB-14.0*P-8.0*
				1.414*PP)+(AK2/576.0)*(-3.0*B+6.0*1.414*BB-28.0*
	1			P-16.0*1.414*PP-23.0*Q+10.0*1.414*QQ)
38				WME=-(0.981E+8/8.0)*STRESS*((AL1-AL2)*
				(-4.0*1.414*R+7.0*RR)-3.0*(3.0*AL1+5.0*AL2)*
	1			COS(GG))
3 9				WMS=-AH*AM*SIN(CCD)
40				C C= WCA+ WME+ WMS
41				IF (N-20) 7,7,4
42		7		IF (CC) 5,4,3
43		3		X=CD
44				GO TO 6
45		5		Y=CD
46				GO TO 6
47		4		DC=SIN(CCD)

			CONT	FORTRAN STATEMENTS	
	1	5	6	7	2
48				AE=(AK1/24.0)*(-4.0*BB-8.0*1.414*B-28.0*PP	
				+16.0*1.414*P)+(AK2/288.0)*(-3.0*BB-6.0*1.414*	
				B-56.0*PP+32.0*1.414*P-69.0*QQ-30.0*1.414*Q)-	
				(0.981E+8/4.0)*STRESS*((AL1-AL2)*(-4.0*1.414*	
				RR-7.0*R)-3.0*(3.0*AL1+5.0*AL2)*SIN(GG))+AH*AM* COS(CCD)	•
49				XCA=(AK1/32.0)*(7.0+1.333*BB+8.0*1.414*B/3.0+	
				2.333*PP-4.0*1.414*P/3.0)+(AK2/128.0)*(2.0+0.33	3*
				BB+2.0*1.414*B/3.0+14.0*PP/9.0-8.0*1.414*P/9.0	
				+23.0*QQ/27.0+10.0*1.414*Q/27.0)	
50				XMS=-AH*AM*COS(CCD)	
51				XME=-(0.981E+8*STRESS/16.0)*((AL1-AL2)*	
				(4.0*1.414*COS(2.0*CCD)-2.0*SIN(2.0*CCD)+	
				4.0*1.414*RR+7.0*R)+3.0*(3.0*AL1+5.0*AL2)*	
				SIN(2.0*CCD))	
52				WWCA=-WCA	
53				WWME=-WME	
54			}	WWMS=-WMS	
55				PRINT 80,A,CD,DC,CC,AE,WWCA,WWME,WWMS,XCA,XME, XMS	
56	8	0		FORMAT (1HJ,1X,F7.2,4X,F6.2,5X,F5.2,5X,F5.3,3X,	
				F8.1,3X,F8.1,4X,F8.1,8X,F8.1,4X,F8.1,5X,F8.1,	
				8X,F8.1)	
57				IF (A+55.0) 17,15,17	
58	1	7		IF (A-125.0) 16,15,16	
59	1	5		SUM=SUM+DC	
60				GO TO 18	
61	1	6		GO TO (19,20),L	
62	1	9		SUM=SUM+4.0*DC	
63				L= 2	
64				GO TO 18	

		CONT	FORTRAN STATEMENTS	
	1 5	6	7	72
65	20		SUM=SUM+2.0*DC	
66			L=1	
67			GO TO 18	
68	18		IF (A-125.0) 21,23,23	
69	23		SUM=H*SUM/(3.14*3.0)	
70			BIN=SUM*AB	
71			PRINT 92,STRESS,SUM,BIN	
72	92		FORMAT (1HK,8H STRESS=,F10.2,5X,14H AVERAGE	
			SINE=,F10.5,5X,17H AXIAL INDUCTION=,F10.3)	
73			GO TO 9	
74	21		A=A+5.0	
75			IF (A-125.0) 8,8,9	
76	9		IF (ABS(STRESS)-4.0) 300,400,400	
77	300		STRESS=STRESS+0.5	
78			GO TO 2	
79	400		STRESS=STRESS+2.0	
80	2		CONTINUE	
81			GO TO 190	
82			STOP	
83			END	

REFERENCES

- 1. Firth, D. "Electric dynamometer of high precision-Air-lubricated trunnion bearings employed", Engineering, Vol. 179, No. 4660, 1955, p. 628-30.
- 2. Potts, B.S. "Hydrostatic Bearings", Machine Design, Vol. 24, No. 10, 1952, p. 180-84.
- Leslie, W.H.P. "The precision driving and absorption dynamometer II, Torque measurement", Automatic and Remote Control Proceedings 1st International Congress of I.F.A.C., Moscow, Vol. 3, 1960, p. 376-80.
- 4. Emmerling, A.A. "A torque measurement transducer system", Electrical Engineering, A.I.E.E., Vol. 82, No. 10, 1963, p.621-25.
- 5. Kyowa Electronic Instr., Japan. "Kyowa torque meter", Cat. No. 369, 1958.
- 6. Westland Aircraft Ltd., England. "Technical data sheets SRT on torque transducers".
- 7. <u>Dahle, O.</u> "The Torductor and the Pressductor, two magnetic stress-gauges of new type", IVA (Periodical of the Royal Swedish Academy of Engineering Sciences), 25, No. 5, 1954, p.221-38, reprinted in ASEA Research 1, 1958, p.45-68.
 - <u>Dahle, O.</u> "The Pressductor, a high output load-cell for heavy industry", ASEA Journal 32, 1959, 9, p.115-23.
 - <u>Dahle, 0.</u> "The Ring Torductor, a torque-gauge without slip rings for industrial measurements and control", ASEA Journal 33, 1960, No. 3.

- 8. Westinghouse Co., U.S.A. "Generalised machine manual".
- 9. Lee, E.W. "Magnetostriction and magnetomechanical effects", Reports on Progress in Physics, Physical Society (London), Vol. 18, 1955, p.184-229.
- 10. McCorkle, P. "Magnetostriction and magneto-electric effects in Fe, Ni and Co", Physical Review, Vol. 22, 1923, p.271-78.
- 11. Bozorth, R.M. "Ferromagnetism", Van Nostrand.

 Bozorth, R.M. "Directional ferromagnetic properties of metals", Journal of Applied Physics, Vol. 8, 1937, p.575-88.
- 12. Scott, K.L. "Variation of inductance of coils, due to magnetic shielding effect of eddy currents in the cores", Proceedings I.R.E., Vol. 18, 1930, p.1750-64.
- 13. Kittel, C. "Domain theory", Solid State Physics, Vol. 3, p.437-564.
- Honda, K., Masumoto, H., Kaya, S. "Magnetization of single crystal of Fe at high temperatures", Science Reports, Tôhoku Imperial University, Vol. 17, 1928, p.111-30.
- 15. <u>Kaya, S.</u> "On the magnetization of single crystal of Ni", Science Reports, Tohoku Imperial University, Vol. 17, 1928, p.639-63.
- Honda, K., Masumoto, H., Shirakawa, Y. "On the magnetization of Ni at various temperatures", Science Reports, Tôhoku Imperial University, Vol. 24, 1935, p.391-410.

- 17. Takaki, H. "Uber die magnetostriktion der eisenkristalle bei hoher temperatur", Zeitschrift für Physik, Vol. 105, 1937, p.92-103.
- 18. Corner, W.D., Hunt, G.H. "The temperature dependence of magnetostriction in a nickel crystal", Proceedings, Physical Society (London), Vol. 68A, 1955, p.133-44.
- 19. <u>Carr, W.J., Jr.</u> "Magnetostriction", Magnetic Properties of Metals and Alloys, American Society for Metals, Chapter 10, 1958, p.200-50.
- Norton, J.T., Hiller, R.E. "Structure of cold-drawn tubing", Transactions of the American Institute of Mining and Metallurgical Engineers, Vol. 99, 1932, p.190-201.
- 21. Barrett, C.S. "Structure of metals", McGraw-Hill, N.Y., 1952.